A MODEL BASED FAULT DETECTION AND DIAGNOSIS STRATEGY FOR AUTOMOTIVE ALTERNATORS

A MODEL BASED FAULT DETECTION AND DIAGNOSIS STRATEGY FOR AUTOMOTIVE ALTERNATORS

By

Nicholas D'Aquila, B.Eng.

A THESIS SUBMITTED TO THE DEPARTMENT OF MECHANICAL ENGINEERING AND THE SCHOOL OF GRADUATE STUDIES OF MCMASTER UNIVERSITY IN PARTIAL FULFILMENT OF THE REQUIREMENTS FOR THE DEGREE OF MASTER OF APPLIED SCIENCE

Master of Applied Science (2018) McMaster University

(Mechanical Engineering) Hamilton, Ontario, Cananda

TITLE:	A Model Based Fault Detection and Diagnosis Strategy for Automotive Alternators
AUTHOR	Nicholas D'Aquila B.Eng., (Mechatronics Engineering) McMaster University, Ontario, Canada
SUPERVISOR	Professor Saeid Habibi
NUMBER OF PAGES	xiv,122

To My Family and Fiancé

For Their Love and Support Through My Studies

Abstract

Faulty manufactured alternators lead to commercial and safety concerns when installed in vehicles. Alternators have a major role in the Electrical Power Generation System (EPGS) of vehicles, and a defective alternator will lead to damaging of the battery and other important electric accessories. Therefore, fault detection and diagnosis of alternators can be implemented to quickly and accurately determine the health of an alternator during end of line testing, and not let faulty components leave the manufacturer.

The focus of this research is to develop a Model Based Fault Detection and Diagnosis (FDD) strategy for detecting alternator faults during end of line testing. The proposed solution uses Extended Kalman Smooth Variable Structure Filter (EK-SVSF) to detect common alternator faults. A solution using the Dual Extended Kalman Filter (DEKF) is also discussed. The alternator faults were programmatically simulated on alternator measurements. The experimental results prove that both the EK-SVSF and DEKF strategies were very effective in alternator modeling and detecting open diode faults, shorted diode faults, and stator imbalance faults.

Acknowledgements

I would like to thank my supervisor, Dr. Saeid Habibi, and CMHT lab coordinator, Cam Fisher, for their knowledge and support during my research for this thesis. I would also like to thank D&V Electronics Ltd. as access to their testing facilities was essential in gathering data for implementing and verifying the proposed strategy in this thesis. Special thanks to my colleagues Mahmoud Ismail and Rioch D'lyma for their support and friendship.

I would especially like to thank my family and fiancé for their unconditional love and support throughout my academics and everyday life.

Table of Contents

List of Figures

List of Tables

List of Nomenclature

θ_e	Electrical rotor angle
$P(\theta_e)$	Park's transformation matrix
A	Linear system matrix
B	Input gain matrix
C	Linear measurement matrix
u	Input matrix
$\lambda_a, \lambda_b, \lambda_c$	Flux linkage
I_a, I_b, I_c	Phase currents
R_a, R_b, R_c	Stator resistances
L_a, L_b, L_c	Stator inductances
I_f	Field current
R_f	Field resistance
L_f	Field inductance
M_a, M_b, M_c	Stator-rotor mutual inductances
φ	Phase angle between stators
g_a, g_b, g_c	Phase switching function
V_{dc}	Alternator output voltage
I_{dc}	Alternator output ripple current
V_f	Field voltage
E_a, E_b, E_c	Stator induced electromotive forces
E_f	Field induced electromotive force
V_a, V_b, V_c	Stator voltages
ω_e	Rotor angular velocity
H	linearized measurement matrix
w_k	Process noise
v_k	Measurement noise
$k+1\|k$	Subscript, a priori
$k+1\|k+1$	Subscript, a posteriori
z_{k+1}	Discrete system measurement
e_z	Error
K	Kalman gain
P_k	Error covariance

F_k	Partial derivative of non-linear function f
R_{k+1}	Measurement noise covariance
A^{-1}	Inverse of some matrix A
A^T	Transpose of some matrix A
$A^- \; or \; A^+$	Pseudo-inverse of some matrix A
I	Identity matrix
Υ	SVSF convergence rate between 0 and 1
ψ	SVSF boundary layer
$\widehat{w}_k$	DEKF parameter state vector
C_k^w	DEKF change rate of state for system parameter vector
$O(H, A)$	Observability matrix
$R_{a_{MN}}$	Artificial measurement

Chapter 1 Introduction

1.1 Overview

The automotive industry continues to reduce cost of mass production while increasing throughput and revenue. Although this practice is profitable, it yields a percentage of improperly manufactured products. Faulty parts are more expensive to replace once they are already installed and can potentially endanger lives. It is crucial for only properly manufactured parts to make their way into vehicles. In attempt to ensure this, manufactures acquire pass or fail algorithms for end of line testing on finished products. This rudimentary limit checking approach requires operators to discard failed parts as it would cost more to spend man hours trying to manually diagnose and resolve the issue. This is especially apparent in the area of automotive alternator production.

Alternator end of line testing could benefit from the advantages of Model Based Fault Detection and Diagnosis (FDD) strategies. Model based FDD is a process where the condition of a system can be monitored for potential faults by comparing experimental and simulated outputs. The result of the Model Based FDD has more sophisticated and comprehensive information about the detected fault. This powerful tool can detect and diagnose the fault to give the operator knowledge of how to fix the product. Faulty products that used to be discarded for loss can be fixed and remain within profit margins.

In general terms, FDD scheme should minimize additional sensors and when possible use existing signals from testers to determine and diagnose faults. It is important for the FDD algorithm to remain computationally feasible especially for end of line testing, to report faults in a timely manner (about 3-5 seconds, refer to Section 7.1). Additionally, it must be sophisticated enough to clearly differentiate between various types of alternator faults. In this study, a model based FDD approach was developed and implemented for end of line testing for a 12V, 140A three phase Lundell alternator using the D&V Electronics Ltd ALT-198 machine. A mathematical model of the alternator was developed and its parameters were determined through experimentation and by using Genetic algorithm optimization. Parameter estimation theory was introduced to track changes in a select set of system parameters. The residual evaluation and parameter estimation FDD methods were validated by simulating fault conditions on an alternator. The combination of the Extended Kalman Filter and Smooth Variable Structure Filter has not been previously attempted to estimate or perform fault detection and diagnosis on a Lundell alternator system.

1.2 Introduction to Alternators

The automotive industry uses Lundell alternators to charge the battery and to power the electrical system (radio, electric wipers, and other accessories) when the engine is running. Alternators were first used in vehicles during World War II to power radio equipment, it was not until the 1960s that alternators were in nearly all consumer cars. Alternators are a type of synchronous generator, meaning they

convert mechanical energy into electrical energy using principles of electromagnetic induction. Given rotation from the prime mover, the induced voltage follows a sinusoidal pattern depending on how the flux is aligned with the magnetic field. This cyclic phenomenon generates AC power as the alternator's output. This AC power must be converted to DC power, as the electronics within the vehicle need a constant power supply. A full-wave bridge rectifier, shown in Figure 1-1, is used to achieve this conversion.

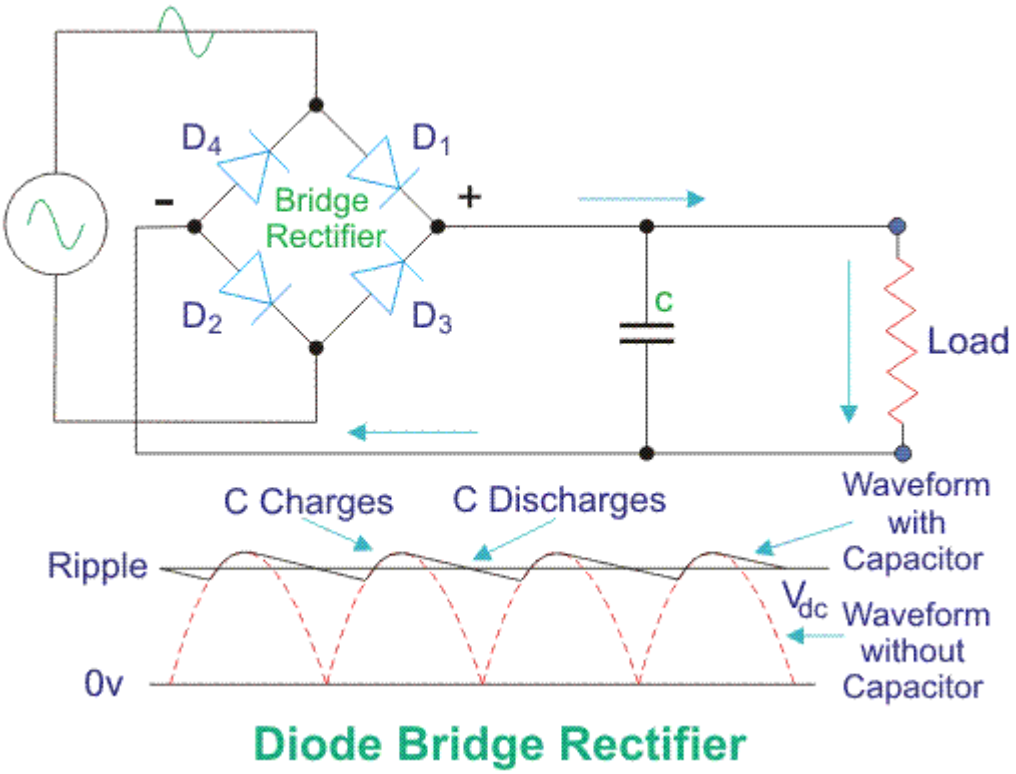

Figure 1-1 the effect of diode bridge rectifier [1]

The automotive alternator uses field windings to magnetize the rotor as opposed to the use of permanent magnets. This solution results in lower production cost

and ability to regulate the alternator's output. The alternator is equipped with an Automatic Voltage Regulator (AVR) to ensure that voltage output remains constant regardless of speed and load from vehicle accessories. The AVR maintains the output power by controlling the field current supplied to the rotor. An example of a modern automotive alternator is shown in Figure 1-2.

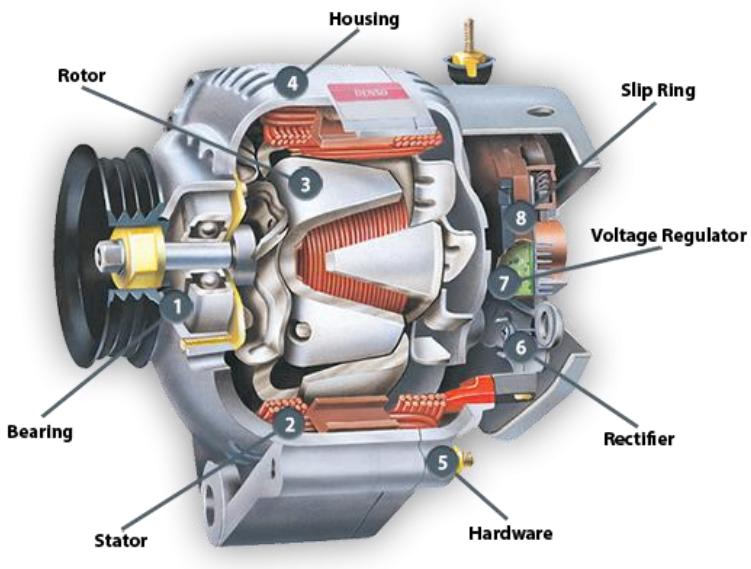

Figure 1-2: Diagram of the modern alternator [2]

1.3 Research Objectives

The objectives of this research is to develop a robust automotive alternator model for detecting and diagnosing faults in end-of-line testing using the D&V Electronics Ltd ALT-198 machine. These objectives are divided into two major categories, namely

(i) the development of an accurate model and

(ii) (ii) the development of a model based FDD strategy.

Each objective carries a collection of challenges and novel solutions.

1.3.1 Automotive Alternator Model Objectives

Synchronous generator modelling is usually done in Finite Element Analysis (FEA) programs, such as ANSYS. Although this method is very powerful, it is not computationally feasible for end-of-line testing. Furthermore, the alternator specifications needed for a successful FEA analysis is rarely available to the tester operator. Therefore, the difficult challenge is to create an alternator model that uses only measurements collected by the ALT-198 to generate an accurate simulation for any Lundell alternator in a timely manner. The proposed solution is to make assumptions on the governing equations for FEA of an alternator to reduce computational complexity of the model and simulate signals not measured by the tester.

This practice significantly affects the accuracy of the simulation. To eliminate this uncertainty nonlinear state estimation techniques such as the Extended Kalman Filter (EKF) and the Smooth Variable Structure Filter (SVSF) were used to increase accuracy and robustness of the proposed model. Important unknown signals, such as the alternator rotor angle and phase currents, were derived by innovative manipulation of existing sensor signals in the post-processing of experiments. As mentioned earlier in this section, each alternator has different specifications,

therefore the model parameters must be tuned accordingly. A genetic algorithm script was introduced to automatically find the best suited parameters for each individual alternator. The proposed solution yielded a +/-2.3% error between the simulated and experimental data.

1.3.2 Model Based Fault Detection and Diagnosis

This objective is to create a strategy that uses modern FDD methods to accurately diagnose faults in a timely manner. This strategy should have a high success rate with minimal false positives. The capability of the FDD strategy to detect and diagnose must be tested against common alternator faults.

An FDD strategy has been developed to detects alternator faults that are responsible for the bulk of alternator failures. Residual evaluation techniques are used to detect faults by monitoring error signals between experimental and simulated data. The faults are diagnosed by using parameter estimation, a novel approach that utilizes the EKF and the SVSF to track fault sensitive parameters as states within a Lundell alternator system. These “artificial states” change dramatically in the presence of a fault and give the operator a clear understanding of the fault’s origin. The proposed strategy is able to successfully diagnose stator imbalance faults, shorted diode faults, open diode faults, and improper rotor faults with the existing sensors on the D&V Electronics ALT-198.

1.4 Outline of Thesis

This thesis is organized as follows: Chapter 2 is the main literature review on synchronous generators, automotive alternator modelling. Chapter 3 is the literature review on estimation theory, and model based fault detection and diagnosis of alternators. Chapter 4 discusses methodologies used in the research including parameter tuning methods introduced to determine best model parameters for any Lundell alternator, innovative methods used to extract artificial measurements, and then estimation theories implemented to track system states. In Chapter 5, the experimental results and the performance of the proposed model based FDD approaches are analyzed and discussed. The successful diagnosis of the selected faults indicates the effectiveness of the proposed methods. Chapter 6 completes the thesis with conclusions and recommendations for future research. Chapter 7 is the appendix where the D&V Electronics ALT-198 and its use in this thesis is described.

Chapter 2 Fundamentals of Alternator and Modelling

2.1 AC Generator Background

It important to understand what an alternator is before modelling and applying fault detection methods. An electric machine is a device which converts mechanical energy to electrical energy (known as generators) or electrical energy into mechanical energy (known as motors). Alternators are a type of electric generator; therefore, the discussion of motors will be limited.

2.1.1 AC Generators

All generators are composed of two parts, the stator and the rotor. Mechanical energy is given to the rotor by a prime mover, while the stator remains still. The rotor is an electromagnet made by coiling wire around two or more poles [3]. The rotor generates the rotating magnetic field. The stator is the stationary coil in which electricity is produced [3].

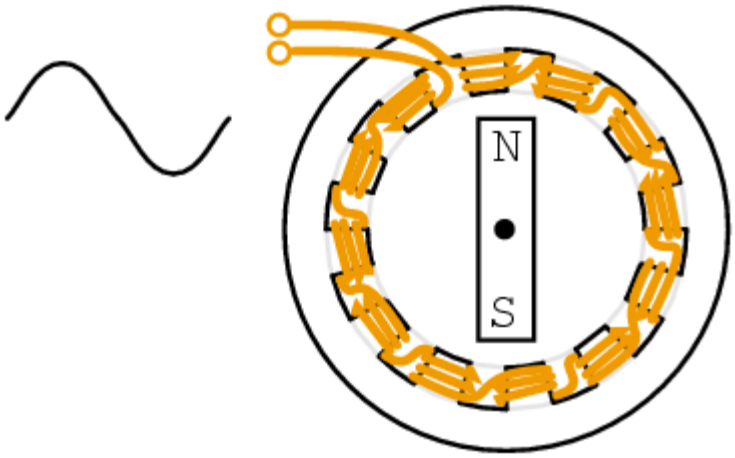

Figure 2-1 Generator with rotating magnet at rotor and fixed stator coils [4]

The induced currents that flow within electric machines can be either Alternating Current (AC) or Direct Current (DC) depending on commutator and winding design. In a DC generator, as shown in Figure 2-2, the coil that current flows through rotates in a fixed field. One end of the coil attaches to one half of a single rotating split ring and the other end of the coil attaches to the other half of the same split ring. Brushes connect the split rings (commutator) to an external circuit. With a fixed magnetic field, the current is always induced in the same direction [5].

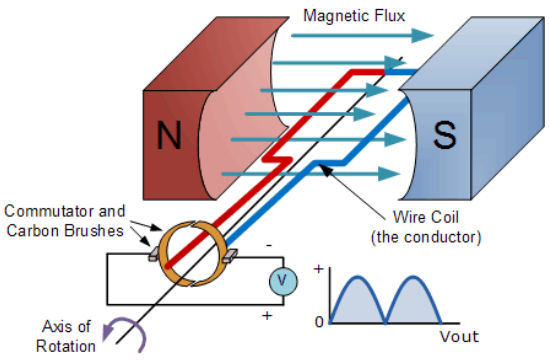

Figure 2-2 DC generator

In an AC generator, as shown in Figure 2-3, the armature coil is fixed, and the field exciters are moving [6]. AC generators have two slip rings, one for each end of the armature coil; brushes connect each slip ring to an external circuit. The design of the full slip rings results in the armature coil experiencing a rotating magnetic field. With a moving magnetic field, the direction of the magnetic field periodically changes due to the magnet's north and south poles, thus current will flow in opposite directions creating alternating current [5].

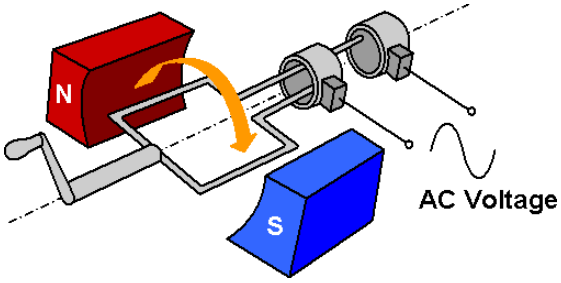

Figure 2-3 AC generator

Both AC and DC machines use principles of Faraday's law of electromagnetic induction. Faraday's law states, whenever a conductor moves in a magnetic field, an electromagnetic force (emf) gets induced in the conductor. The equation for Faraday's law of electromagnetic induction,

$$\varepsilon = -N\frac{\Delta\varphi}{\Delta t} \qquad \text{Equation 2.1.1.1}$$

demonstrates that the induced emf increases with the number of winding turns as well as the rate of change of magnetic flux [7]. The minus sign is to represent that the direction of the electromotive force opposes the change in the flux that produces the voltage. It is important to note that not all positions during rotation induces emf. When the flux is aligned with the magnetic field, then the flux is not cutting the field and therefore no emf is induced. When the flux is perpendicular to the field, as shown in Figure 2-1, then it cuts the field at a maximum, and therefore, the emf is at its highest peak [8].

2.1.2 Field Coils vs Permanent Magnets

In theory, having a magnet that never loses its magnetization properties (permanent magnet) in an electric generator seems very ideal. However, in some applications using a permanent magnet is not sustainable. For instance, if magnetic field is always constant the induced emf would vary directly with the rate of change in magnetic flux; in other words, the speed of the prime mover. This would be very difficult to manage in a system that needs a constant voltage at every speed. Likewise, permanent magnets are very expensive and can be more expensive than the rest of the electric device in some cases. This is why many electric machines use field coils instead. Field coils use the principles of Lenz's Law to create a magnetic field, as shown in Figure 2-4. Lenz's law describes that current flow in a loop of wire will generate a magnetic field perpendicular to the loop [8].

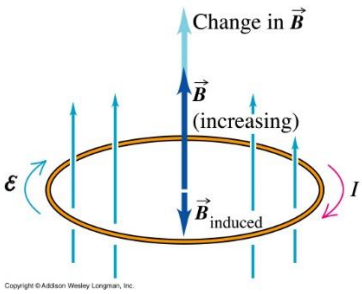

Figure 2-4 Lenz's Law

In order, to excite the field windings an external power source is used and when the windings are excited they work in the same manner as the permanent magnet shown in Figure 2-3. Using field coils allows for control of the generator's induced

voltage; varying the current in the field winding will vary the magnitude of the magnetic field [9]. There are a few drawbacks of using field coils. In order to use field coils there needs to be an available external power supply which isn't always possible. Likewise, there needs to be a commutator and brushes to constantly excite the field windings during rotation; these components are subject to wear and tear. Permanent magnets do not require excitation and do not suffer from this issue. Note, both systems still need a commutator and brushes to induce current in the external circuit. Lastly, field coils suffer from losses due to magnetizing, such as Eddy currents. The most useful advantage of the field coils is the ability to control the magnitude of magnetic field, as this is very useful in the automotive industry where vehicles are not always driving at constant speed [9].

2.1.3 Induction Generators and Synchronous Generators

Within the AC generator family there are induction generators and synchronous generators. Induction generators are also called asynchronous generators because the actual mechanical speed of the prime mover moves at a slightly smaller magnitude than the magnetic field. The speed at which the magnetic field rotates at is known as the synchronous speed. It is a function of electrical frequency (typically 50 or 60Hz) and the number of poles on the rotor. In induction generators a rotating magnetic field produced in the stator pulls the rotor to run behind it. If the rotor accelerates to the synchronous speed by the prime mover the "slip" (the difference between actual speed and synchronous speed) will become zero and

therefore the new torque will be zero [10]. If a rotor accelerates to be more than the synchronous speed, the slip becomes negative and a rotor current is generated in the opposite direction. This generated rotor current produces a rotating magnetic field which pushes onto the stator field. This causes a stator voltage which pushes current flowing out of the stator winding against the applied voltage. As shown in Figure 2-5, the induction generator needs a source of power to produce the rotating magnetic field. Reactive power is needed to produce this field; this power usually comes from an AC power line (grid) [10]. Then the generator supplies power back into the line through Active power.

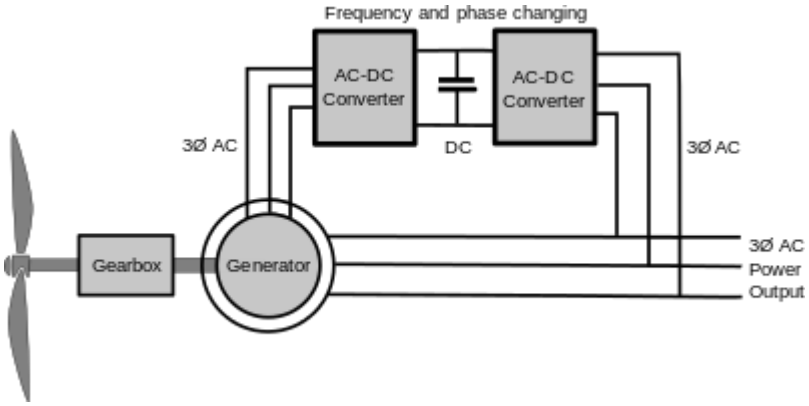

Figure 2-5 Induction Generator

Induction generators are mostly used in applications that have access to large amounts of reactive power such as wind turbines. They are also effectively used to supply additional power to a load in a remote area that is being supplied by a weak transmission line [11].

Synchronous machines work in the same manner as induction generators except the actual mechanical speed of the prime mover moves at the same magnitude as the magnetic field. The main difference between them is how they excite the armature windings. Synchronous generators can generate reactive power (to excite field windings) with the use of an external power supply and therefore have the capability to regulate the output voltage, while induction generators cannot [12]. However, this can be an advantage, as induction generators do not need an external DC excitation nor do they need commutators that break over time. Additionally, induction generators are cheaper and do not need to be synced to the supply line like synchronous generators do.

2.2 Structure of an Automotive Alternator

Considering the given information, it should be clearer what type of electric machine an automotive alternator is. The speed of a vehicle is not constant; however, the devices within the car need constant DC voltage in order to function properly when being powered by the alternator. The possibility of using an induction generator was ruled out as they cannot control the output voltage and there is no access to a large amount of reactive power within a vehicle. Permanent magnets could not be used because of their inability to regulate output voltage as well as their high costs. Therefore, permanent magnet synchronous machines could not be used for consumer vehicles. With these challenges, automotive engineers decided to make automotive alternators as an AC synchronous

generator with field windings and the vehicle engine as the prime mover, also called Lundell alternators.

2.2.1 The Three Phase Bridge Rectifier

Most alternators are 3 phase, meaning current and emf are induced in three sets of wires that have many loops (stator windings). This means the alternator runs as a 3 phase AC power supply to the accessories within the car. However, the accessories within the car need DC to function properly. Therefore, in order to use these AC supply components, a 3 phase bridge rectifier must be connected to the sets of stator windings to produce a DC output [5]. A bridge rectifier, as shown in Figure 2-6, is an array of semiconductor diodes. This is because semiconductor diodes are used to allow electrons to flow in one-way only. Thus by having each phase attached to two diodes, as shown in Figure 2-6, one diode will block the negative end of the wire from flowing while the other diode allows the positive end of the wire to flow to the load, creating direct current [13].

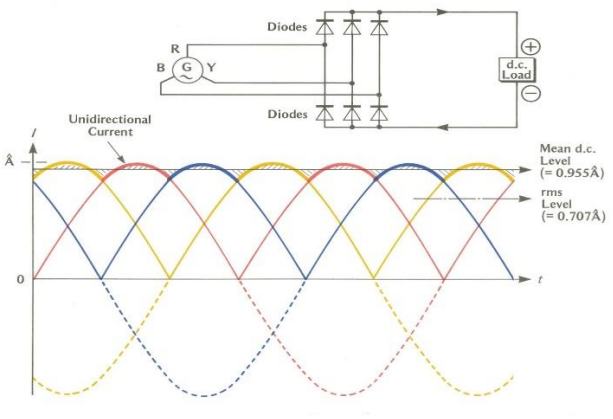

Figure 2-6 3 phase bridge rectifier and its corresponding output signal [14]

2.2.2 The Electric Power Generation System

For a consumer car the alternator voltage should always be around 14.4V (for bigger vehicles the alternator should usually be around 25.6V). This is very difficult to do in a regular drive cycle because that would require constant speed which is not possible when driving on suburban streets. As explained before the synchronous machine's induced emf is proportional to the speed of the prime mover, in this case the engine. Therefore, more voltage is induced when driving on the highway than when idling at a stoplight. If the voltage is too low the devices will not work properly and if the voltage is too high the devices are at risk of overvoltage. This is where the car battery becomes important to what is known as the Electric Power Generation System (EPGS). The car battery is used to excite the field windings of the alternator. As explained earlier in this section, the advantage of using field coils is the ability to control the magnitude of the magnetic field that is inducing the current in the stator windings. Therefore, to maintain a constant voltage, the excitation voltage (or field voltage) supplied to the alternator rotor by the car battery can be controlled to increase or decrease the output alternator voltage. The component is the automatic voltage regulator.

2.2.3 Automatic Voltage Regulator

The Automatic Voltage Regulator (AVR) controls the field current applied to the spinning rotor produced within the alternator. Some AVRs work like an electric switch. If no current is applied, then there is no voltage produced by the alternator.

So If the alternator voltage drops below a certain voltage (13.5V) the regulator will apply current to the field windings. Conversely, when the alternator voltage exceeds an upper limit voltage (14.4V) the AVR will stop supplying voltage to the field windings [5]. There are more sophisticated systems where a PID controller is adapted by the regulator to control the current to the field windings. In this system the change in current is smoother versus the system continuously turning on and off.

2.3 Alternator Modelling Techniques

In this section multiple alternator modelling techniques will be discussed including their strengths and caveats. The chosen alternator model must be sophisticated enough to capture useful information about the alternator and lightweight enough to be integrated into the D&V Electronics tester. The techniques studied include

1. Finite Element Analysis
2. 7^{th} order state space model
3. Non-linear model using flux-current relationships
4. The Linear Parameter Varying model

These are described in the following sections.

2.3.1 Finite Element Analysis

Finite Element Analysis (FEA) is one of the most accurate ways of modelling any complex engineering system. FEA is an applicable use of Finite Element

Method (FEM), a mathematical process of solving a problem by subdividing a whole domain into smaller elements [15]. As shown in Figure 2-7, FEA is based around Computer Aided Design (CAD) software and allows the user to graphically visualize components acting in/on their system. There are 3 stages to any FEA, the pre-process, the FEA calculations (either 2D or 3D), and the post-processing.

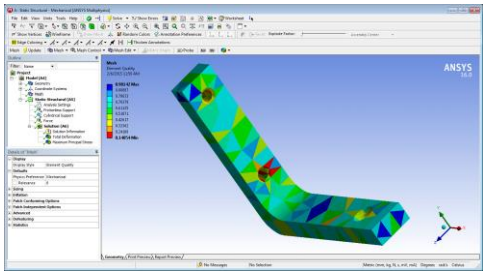

Figure 2-7 User interface of FEA application called ANSYS™

The pre-processing stage entails feeding the software as much detail as possible about the desired system, considering the CAD software does not have any information yet. Data about the geometry and physical properties of the machine's electrical and magnet circuits are needed. The user must start by drawing the machine's 2 or 3 dimensions within the software (see Figure 2-8). Afterward the user must provide specifics about the driving source for the simulation, the external coupled circuit it is a part of, which includes boundary conditions and fixed potentials [16]. Users must further the knowledge of the system by supplying material properties with BH curve data, and setting conductivities.

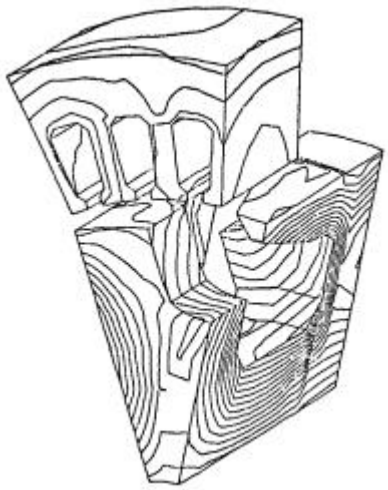

Figure 2-8 Part of synchronous machine drawn in an FEA software [1]

Finally, with the model built the user sets the solver type and simulation parameters. This includes the type of solution (linear or non-linear), the size of time step, and any geometric movements or specific variables that need to be addressed. The system is now prepped to be calculated.

The focus of this literature review is on synchronous machine, therefore, the FEA calculation stage will be discussed in terms of 2D synchronous machine modelling. The entire calculation step is automated by the CAD software, including the first phase of mesh generation. The meshing process is what gives the Finite Element Method its name. The CAD software works to divide the model into a series of smaller geometric regions such as triangles or quadrilateral elements in the 2D applications (see Figure 2-9). Although this is done by the software, the user must still specify options, in the pre-processing stage, including element size and number of elements in a region. These are important parameters as they may

determine the accuracy of the final solution. After the meshing process the solver is initiated.

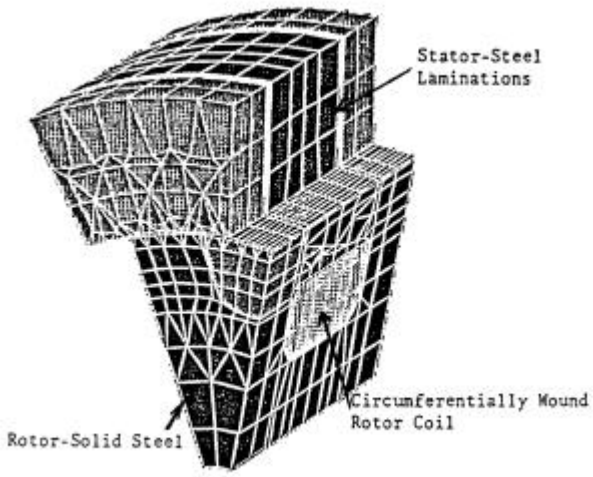

Figure 2-9 Mesh generation of Figure 2-8 [1]

The solver performs calculation with the defined system to acquire parameters requested for the application. FEM methods for synchronous machines originate from the low frequency limits of Maxwell's equations. The synchronous generator is treated as a quasi-static magnetic system, an infinitely slow process that is always approximately equilibrium, which is closed and bounded in 2D. It is important to understand that magnetic vector potential is usually used for magnetic field analysis, as scalar potential cannot include current as the source of the fields. To use this approach, the FEA must satisfy Gauss's law for magnetism and Ampere's circuital law [17]. In addition, electric machines' stator and rotor core are made from saturating iron and therefore the permeability μ is a function of magnetic

flux density. Therefore, while finding the solution the FEA must satisfy the following equations:

$\nabla \times H = J$, where H is magnetic field strength and J is free current density

$\nabla \cdot \mathrm{B} = 0$, where B is magnetic flux density

$B = \mu H$, where μ is permeability

From Maxwell's equations for potential field the relationship between magnetic flux density and magnetic vector potential is given by $B = \nabla \times A$, where A is magnetic vector potential. If we rearrange the equations the result is:

$\nabla \times \left(\frac{1}{\mu} \nabla \times A\right) = J$,

Assuming Coulomb gauge (a gauge field in which the vector potential has no divergence $\nabla \cdot A = 0$) for linear materials the equations reduces to

$-\frac{1}{\mu} \nabla^2 A = J$,

This is an example of what equations would be used by the FEA to generate a solution for a 2D synchronous generator system [17]. The time it takes to find the solution depends on the complexity of the model and mesh, varying anywhere between seconds to days to solve. The approach described could be used to solve the open circuit characteristic of the synchronous generator. For each value of the field current the flux linkage y is calculated from the finite element solution. The phase voltage E is calculated by $E = 4.44 N k_w f \psi$, where N is the number of turns

per phase winding, k_w is a winding coefficient and f is the frequency. With this data a relationship between field current vs open circuit voltage can be produced, as seen in Figure 2-10.

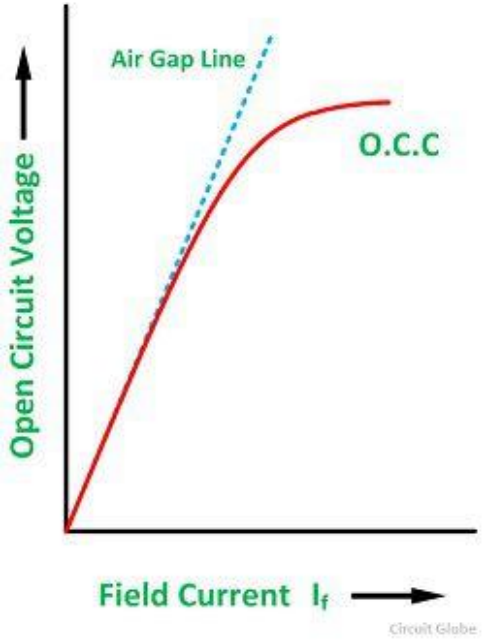

Figure 2-10 Example of Open Circuit Characteristic Graph

The FE solution can also be used to find other values such as the characteristic of the flux in the air gap, the distribution of the flux density in the air gap, and the electromagnetic torque to name a few. Data like this can be extracted by the user in the post-processing stage. The solution is displayed in a GUI allowing objects in the system to be selected for further calculation. Fields can be evaluated at points, along lines, and over areas for 2D configurations. All calculations, such as integral fields, use the data stored by the solver from the previous stage.

FEA is a very efficient tool when modelling complicated geometries and is used by almost all manufacturers to simulate tests that can potentially be harmful to the machine. Likewise, FEA programs like ANSYS™ allow embedding of the solver within a script inside MATLAB or Simulink. In contrast, the integration setup can be slow as for every step MATLAB would have to call the Finite Element solver. For instance, in a simulation of a synchronous machine the emf at a phase winding changes with every increment in the rotor. Therefore, for every increment in the rotor MATLAB must recalculate the solver and process the new data collected. This makes it almost impossible to use in real-time. There are methods that allow the use of only one solution such as pseudo-rotating superposition where the reference point for the conductor is moved in the post-processing stage, instead of incrementally rotating the rotor and recalculating a solution. However, in most cases a solution like this does not exist or the solution loses accuracy due to extrapolation. This is one of the drawbacks of modelling with FEA software. Another drawback is the need for a detailed explanation of the system. Only the manufacturer has a complete list of all the materials of the machine including their properties and BH curve data. In most cases, the manufacturer will not make this information public. This makes it very difficult to create an accurate system from the perspective of a third party company interested in modelling the machine.

2.3.2 7^{th} order state space model

This approach uses state space modelling of synchronous generators to calculate the output values of the system. As shown in Figure 2-11, the input to the model

would be the field voltage and the output of the model would be the phase currents as well as the phase voltages. In Figure 2-11, the current on each line can be written as,$i_a = i_{r_1} + i_{l_1}$where i_{r_1} is the current through the resistor and $i_{l_1}$is the current through the inductor.

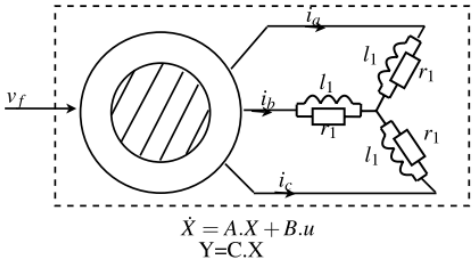

Figure 2-11 Synchronous generator with inside load [15]

Working with AC waveforms to calculate the outputs will be very complicated, instead it is useful to convert these waveforms to DC signals. To accomplish this, Park's transformation can be applied to the system. As shown in Figure 2-12, Park's transformation converts a three-phase reference frame to a rotating two-phase reference frame in order to simplify analysis. The two-phase values (on d and q axes on Figure 2-12) are achieved by taking the product of the three phase values (on a, b and c axes shown on Figure 2-12) and the Park's transformation equation,

$$P(\theta_e) = \sqrt{\frac{2}{3}}\begin{pmatrix} \cos(\theta_e) & \cos\left(\theta_e - \frac{2\pi}{3}\right) & cos(\theta_e + \frac{2\pi}{3}) \\ -\sin(\theta_e) & -\sin\left(\theta_e - \frac{2\pi}{3}\right) & -sin(\theta_e + \frac{2\pi}{3}) \end{pmatrix}, \qquad \text{Equation 2.3.2.1}$$

Where θ_e is electrical angle of the rotor [18].

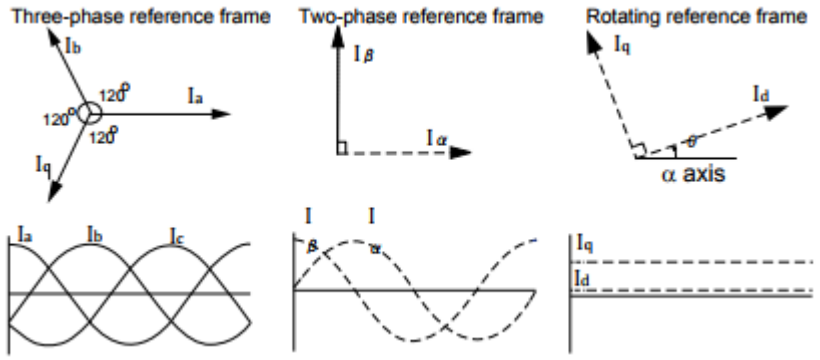

Figure 2-12 Park's transformation reference frames and corresponding current values during rotation

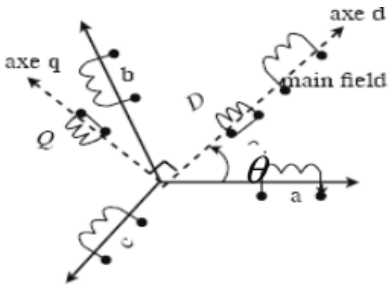

Figure 2-13 Synchronous machine winding with Park's transformation axes and corresponding dampers

Therefore, to get d-q axis voltage and current the following equations are used,

$$\begin{pmatrix} v_d \\ v_q \end{pmatrix} = P(\theta_e) \cdot \begin{pmatrix} v_a \\ v_b \\ v_c \end{pmatrix}$$ Equation 2.3.2.1

$$\begin{pmatrix} i_{d_1} \\ i_{q_1} \end{pmatrix} = P(\theta_e) \cdot \begin{pmatrix} i_{a_1} \\ i_{b_1} \\ i_{c_1} \end{pmatrix}, \qquad \text{Equation 2.3.2.3}$$

This gives us the relationship,

$$\begin{pmatrix} v_d \\ v_q \end{pmatrix} = \begin{pmatrix} r_1 & 0 \\ 0 & r_1 \end{pmatrix} \cdot \begin{pmatrix} i_{d_1} \\ i_{q_1} \end{pmatrix}, \qquad \text{Equation 2.3.2.4}$$

The combination of the previous relationship and the Park's transformation equations leads to the global equation of the synchronous machine in the Park's frame [19],

$$\begin{pmatrix} 0 \\ 0 \\ 0 \\ 0 \\ v_f \\ 0 \\ 0 \end{pmatrix} = \begin{pmatrix} r_1 & -l_1\omega_e & -r_1 & 0 \\ l_1\omega_e & r_1 & 0 & -r_1 \\ r_1 & 0 & -(r_s+r_1) & l_q\omega_e \\ 0 & r_1 & -l_d\omega_e & -(r_s+r_1) \\ 0 & 0 & 0 & 0 \\ 0 & 0 & 0 & 0 \\ 0 & 0 & 0 & 0 \end{pmatrix} \cdot \begin{pmatrix} i_{d2} \\ i_{q2} \\ i_d \\ i_q \\ i_f \\ i_D \\ i_Q \end{pmatrix} + \begin{pmatrix} l_1 & 0 \\ 0 & l_1 \\ 0 & 0 \\ 0 & 0 \\ 0 & 0 \\ 0 & 0 \\ 0 & 0 \end{pmatrix} \cdot \begin{pmatrix} 0 & 0 & 0 \\ 0 & 0 & 0 \\ 0 & 0 & -\omega_e m_{sQ} \\ \omega_e m_{sf} & \omega_e m_{sD} & 0 \\ r_f & 0 & 0 \\ 0 & r_D & 0 \\ 0 & 0 & r_Q \end{pmatrix} \cdot \begin{pmatrix} i_{d2} \\ i_{q2} \\ i_d \\ i_q \\ i_f \\ i_D \\ i_Q \end{pmatrix} + \begin{pmatrix} 0 & 0 & 0 & 0 & 0 \\ 0 & 0 & 0 & 0 & 0 \\ -l_d & 0 & m_{sf} & m_{sD} & 0 \\ 0 & -l_q & 0 & 0 & m_{sQ} \\ -m_{sf} & 0 & l_f & m_{fD} & 0 \\ -m_{sD} & 0 & m_{fD} & l_D & 0 \\ 0 & -m_{sQ} & 0 & 0 & l_Q \end{pmatrix} \cdot \frac{d}{dt} \begin{pmatrix} i_{d2} \\ i_{q2} \\ i_d \\ i_q \\ i_f \\ i_D \\ i_Q \end{pmatrix}$$

$$= R \cdot \begin{pmatrix} i_{d2} \\ i_{q2} \\ i_d \\ i_q \\ i_f \\ i_D \\ i_Q \end{pmatrix} + M \cdot \frac{d}{dt} \begin{pmatrix} i_{d2} \\ i_{q2} \\ i_d \\ i_q \\ i_f \\ i_D \\ i_Q \end{pmatrix}, \qquad \text{Equation 2.3.2.5}$$

where m_{ab} is the mutual induction between "a" (first component in subscript) and "b" (second component in subscript), r_a is the resistance of component "a", l_a is the inductance of component "a", and w_e is the electrical speed of the rotor, R is the resistance matrix and M is the mutual inductance matrix [19]. This equation is then rearranged into a state space representation,

$$\dot{X} = A.X + B.u,$$ Equation 2.3.2.6

$$Y = C.X$$, where Equation 2.3.2.7

$$A = -M^{-1}.R,$$ Equation 2.3.2.8

$$B = M^{-1},$$ Equation 2.3.2.9

$$C = \begin{pmatrix} -r_1 & 0 & r_1 & 0 & 0 & 0 & 0 \\ 0 & -r_1 & 0 & r_1 & 0 & 0 & 0 \end{pmatrix},$$ Equation 2.3.2.10

$$X = (i_{d_2} \quad i_{q_2} \quad i_d \quad i_q \quad i_f \quad i_D \quad i_Q)^T ,$$ Equation 2.3.2.11

$$Y = (v_d \quad v_q)^T ,$$ Equation 2.3.2.12

$$u = (0 \quad 0 \quad 0 \quad 0 \quad v_f \quad 0 \quad 0)^T$$ Equation 2.3.2.13

This solution proposes quite a few problems for its application in the testing industry. Similar to the issues of FEA modelling, this model requires knowledge of the mutual inductances that must be provided by the supplier. Likewise, the alternator phase currents cannot be directly measure in industry due to limitations of the tester and the closed casing of the alternator. These signals would have to be derived from another measurable value such as ripple current. In addition, the electrical rotor angle must be very accurate to properly use the Park's transformation; any inaccuracy will cascade throughout the other calculations. It should be noted that the resistance matrix, R, changes with the electrical speed, thus this model is non-linear. Unless the speed is constant throughout the entire simulation, there would need to be multiple state space models to represent the synchronous machine.

2.3.3 Non-Linear Model Using Flux-Current Relationships

The following model encompasses the entire Electric Power Generation System (EPGS) as shown in Figure 2-14. EPGS is composed of an alternator, battery, and the electronics of the automobile (shown as a current sink in Figure 2-14). The governing equations of this model use the same IEEE standard for modelling synchronous generators in FEM analysis [20].

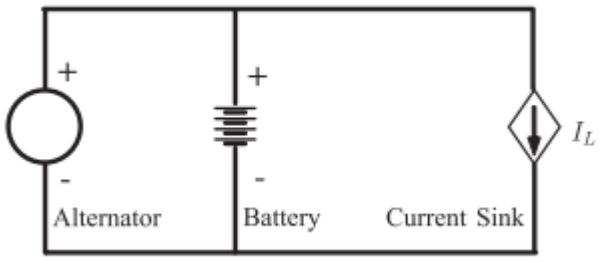

Figure 2-14 EPGS model

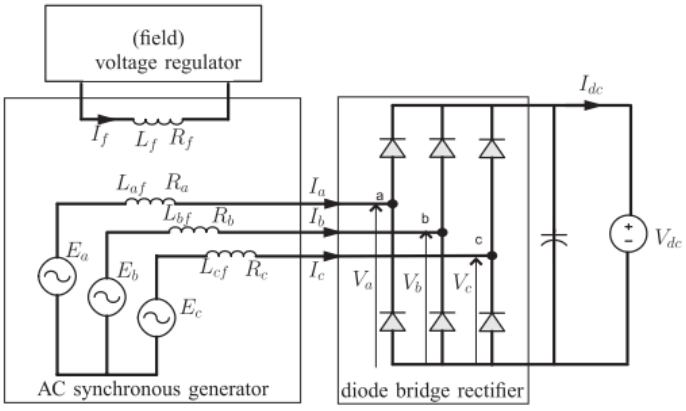

Figure 2-15. Alternator model with all subsystems

The common alternator (seen in Figure 2-15) is composed of multiple systems including a 3 phase AC synchronous generator, a 3 phase diode bridge rectifier and a voltage regulator. E_a, E_b, E_c are induced electromotive forces (EMF) of the individual phases and E_f is the induced EMF of the excitation field. $E_a = \frac{d\lambda_a}{dt}$, for all individual phases and field induced voltages where λ is flux linkage of the phase. Flux linkage is defined as

$$\lambda_a = -L_a I_a - L_{ab} I_b - L_{ac} I_c + L_{af}(\theta_e) I_f \quad \text{Equation 2.3.3.1}$$

$$\lambda_b = -L_{ba} I_a - L_b I_b - L_{bc} I_c + L_{bf}(\theta_e) I_f \quad \text{Equation 2.3.3.2}$$

$$\lambda_c = -L_{ca} I_a - L_{cb} I_b - L_c I_c + L_{cf}(\theta_e) I_f \quad \text{Equation 2.3.3.3}$$

$$\lambda_f = L_f I_f - L_{fa}(\theta_e) I_f - L_{fb}(\theta_e) I_f - L_{fc}(\theta_e) I_f \quad \text{Equation 2.3.3.4}$$

Where L_a is a self-inductance of the stator related to the three phases, and L_{ab}, L_{ba}, etc are the stator to stator mutual inductances [21]. The stator-rotor mutual inductances are described as

$$L_{af}(\theta_e) = L_{fa}(\theta_e) I_f = M\cos(\theta_e) \quad \text{Equation 2.3.3.5}$$

$$L_{bf}(\theta_e) = L_{fb}(\theta_e) I_f = M\cos(\theta_e + \varphi) \quad \text{Equation 2.3.3.6}$$

$$L_{cf}(\theta_e) = L_{fc}(\theta_e) I_f = M\cos(\theta_e - \varphi) \quad \text{Equation 2.3.3.7}$$

Where M is the peak stator-rotor mutual inductance, ϕ is the angle between stator windings, and θ_e is the phase angle of the alternator. It should be noted that relationship between the alternator's electrical angle and mechanical angular displacement, θ_m, is $\theta_e = \frac{p}{2}\theta_m$, where p is the number of poles of the alternator's

rotor. Assuming a balanced machine, the balance equation for three phase current is,

$$I_a + I_b + I_c = 0 \qquad \text{Equation 2.3.3.8}$$

The three phase diode bridge rectifier model associates a switching function (g_a, g_b, g_c) with each of the bridge branches representing the conduction state of the diode present in the branch. If the diode is active the switching function is equal to 1, otherwise the switching function is equal to 0. With this, the phase voltage can be calculated from the alternator output voltage, V_{dc} :

$$f_a = \frac{2g_a - g_b - g_c}{3}, \qquad \text{Equation 2.3.3.8}$$

$$V_a = f_a V_{dc} \qquad \text{Equation 2.3.3.9}$$

$$I_{dc} = g_a I_a + g_b I_b + g_c I_c \qquad \text{Equation 2.3.3.10}$$

The automatic voltage regulator (AVR) maintains the alternator output voltage across the engine's operating range. The regulator can be modelled in two unique ways. As shown in Figure 2-16, it can be measured as a switch that turns on if the alternator output voltage does not exceed the predetermined reference level, V_{ref}, or turns off when the voltage does exceed this level:

$$If\ V_{dc} < V_{ref}: V_f = V_{dc}, Else: V_f = 0 \qquad \text{Equation 2.3.3.11}$$

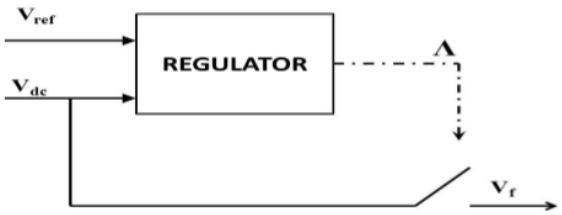

Figure 2-16 AVR model as a switch

Where V_f is field voltage. The second method is to model the AVR as a PI controller:

$$V_f = K_p\left(V_{ref} - V_{dc}\right) + K_I \int_{t_0}^{t}\left(V_{ref} - V_{dc}\right) dt \qquad \text{Equation 2.3.3.12}$$

Where K_p is position gain and K_i is integral gain [22].

With all the information presented, a model for the alternator as a whole can be expressed. Assuming all stator windings are equal, all self-inductances are equal and all mutual inductances are equal, the model can be simplified:

For The Phase Windings:

$$E = RI + V \qquad \text{Equation 2.3.3.13}$$

$$E = \frac{d}{dt}\lambda \qquad \text{Equation 2.3.3.14}$$

$$\lambda = -LI + L_f(\theta_e)I_f \qquad \text{Equation 2.3.3.15}$$

$$V = \mathrm{f}V_{dc} \qquad \text{Equation 2.3.3.16}$$

For the Excitation Winding:

$$E_f = R_f I_f + V_f$$ Equation 2.3.3.17

$$E_f = -\frac{d}{dt}\lambda$$ Equation 2.3.3.18

$$\lambda_f = -{L_f}^T(\theta_e)I + L_f I_f$$ Equation 2.3.3.19

$V_f = \forall V_{dc}$, where $\forall$ is the PI Controller Equation 2.3.3.20

Where $L_f(\theta_e) = \begin{bmatrix} L_{af}(\theta_e) \\ L_{bf}(\theta_e) \\ L_{cf}(\theta_e) \end{bmatrix}$, $I = \begin{bmatrix} I_a \\ I_b \\ I_c \end{bmatrix}$, $V = \begin{bmatrix} V_a \\ V_b \\ V_c \end{bmatrix}$, $\mathrm{f} = \begin{bmatrix} \mathrm{f}_a \\ \mathrm{f}_b \\ \mathrm{f}_c \end{bmatrix}$, $\lambda = \begin{bmatrix} \lambda_a \\ \lambda_b \\ \lambda_c \end{bmatrix}$, $R = \begin{bmatrix} R_{ss} & 0 & 0 \\ 0 & R_{ss} & 0 \\ 0 & 0 & R_{ss} \end{bmatrix}$, and $L = \begin{bmatrix} L_s & 0 & 0 \\ 0 & L_s & 0 \\ 0 & 0 & L_s \end{bmatrix}$

Finally combining the above equations:

$$\dot{I} = -L^{-1}(RI + V) + L^{-1}(\frac{d}{d\theta_e}L_f(\theta_e)\omega_e I_f + L_f(\theta_e)\,\dot{I}_f)$$ Equation 2.3.3.21

Similarly, the following can describe the dynamics of the field current

$$\dot{I}_f = -\frac{R_f}{L_f}I_f - \frac{1}{L_f}V_f + \frac{1}{L_f}(\frac{d}{d\theta_e}{L_f}^T(\theta_e)\omega_e I + {L_f}^T(\theta_e)\dot{I})$$ Equation 2.3.3.22

A battery model must also be provided to complete the EPGS model [22]. The model can be described by a simple electrical model known as the R-RC circuit shown in Figure 2-17.

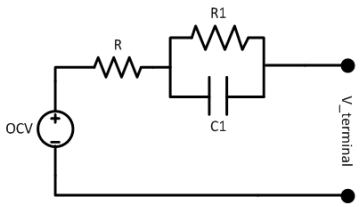

Figure 2-17 Example of Simple R-RC Circuit Battery Model

The equations for this model are:

$$V_B = E_0 - RI_B - V_{C_0} \quad \text{Equation 2.3.3.23}$$

$$\dot{V}_{C_0} = -\frac{V_{C_0}}{R_0 C_0} \quad \text{Equation 2.3.3.24}$$

Where I_B is the battery current that is positive during charging and negative during discharging, V_B is the battery voltage, R is the battery internal ohmic resistance, R_0 is the overvoltage resistance, C_0 is the capacitance and E_0 is the open-circuit voltage. It should be noted that the D&V Electronics LTD tester simulate a car battery with an infinite DC voltage, and therefore, the SoC is always 100%.

The block diagram representing the EPGS model can be seen in Figure 2-14. Unfortunately, the proposed equations are very complex. The combination of nonlinear dynamics from all three subsystems of the alternator makes the design of a fault diagnosis scheme very difficult. Linearization is also not a feasible option due to the complexity.

2.3.4 Linear Parameter Varying Model (DC Generator Equivalent Model)

The model presented in 2.3.3 can be simplified to an equivalent mathematical linear time-invariant model. Through research, Dr. Scacchioli discovered that the AC synchronous generator and diode bridge rectifier could be replaced with an equivalent DC generator [21]. An equivalent excitation field and a first-order

linearized model based on a DC generation equation demonstrate the input-output behaviour of the new system

$$\dot{I}_f = -\alpha I_f + \beta V_f \qquad \text{Equation 2.3.4.1}$$

$$\dot{I}_{dc} = -\gamma I_{dc} + \eta \omega_e + \kappa I_f - \lambda V_{dc} \qquad \text{Equation 2.3.4.2}$$

Where the input signals are engine speed, ω_e, field voltage, V_f, and alternator voltage, V_{dc} [22]. The output signal is the battery current, I_{dc}. The six parameters α, β, γ, η, κ, and λ are determined through system identification. A dataset of tested inputs and outputs must be provided for the parameter estimation. The dataset must be subdivided into regions based on speed, each region will get a unique parameter set [23], [24]. These parameter sets will be stored in a lookup table that will be dynamically selected by the engine speed. This method allows the equivalent model to successfully reproduce behavior of the nonlinear model.

Chapter 3 Fault Detection and Diagnosis

3.1 Estimation Theory

With an accurate model in place, the next step is to create a fault detection and diagnosis schematic. The faults should be detected during the testing procedure; therefore, batch estimation techniques would not be suitable. The estimator for this thesis should not need a history of values to be sufficient in detecting and diagnosing faults in real time systems. Recursive estimation techniques with predictor-corrector functionality are highly regarded for condition monitoring. The Kalman Filter (KF), the Extended Kalman Filter (EKF), and the Smooth Variable Structure Filter (SVSF) are explored to satisfy these criteria.

3.1.1 Kalman Filter (KF)

Published by R.E Kalman in 1960, the Kalman Filter (KF) is a set of equations that estimate the states of a process in a two phase method of predicting and updating [25]. Applying this process within every time step, the filter attempts to make a prediction about what the system will do next. The Kalman Filter is structured as a mean squared error minimizer which is very useful for noisy systems especially when there is uncertainty about the complete dynamics. Consider a discrete time system with noise:

$$x_{k+1} = Ax_k + Bu_k + w_k \qquad \text{Equation 3.1.1.1}$$

$$z_{k+1} = Hx_{k+1} + v_k \qquad \text{Equation 3.1.1.2}$$

Where x_{k+1} is the states of the system, u_k is the input, w_k is the process noise and v_k is the measurement noise [26]. The noise is considered to be zero mean Gaussian distribution

$$p(w) \sim N(0, Q) \qquad \text{Equation 3.1.1.3}$$

$$p(v) \sim N(0, R) \qquad \text{Equation 3.1.1.4}$$

Where the process noise covariance Q and measurement noise covariance R are assumed to be constant during the process.

There are two states vectors of the Kalman Filter. The first is the a priori and the a posteriori state estimate, $\hat{x}_{k+1|k}$ and $\hat{x}_{k|k}$ respectively. The second is the a priori and posteriori error covariance matrix, $P_{k+1|k}$ and $P_{k|k}$ respectively. The a posteriori state estimate is computed as a linear combination of the a priori estimate, $\hat{x}_{k+1|k}$, and a weighted difference between an actual measurement z_{k+1}, and a measurement prediction, $H\hat{x}_{k+1|k}$,

$$\hat{x}_{(k+1|k+1)} = \hat{x}_{k+1|k} + K_{k+1}(z_{k+1} - H\hat{x}_{k+1|k}) \qquad \text{Equation 3.1.1.5}$$

Where K_{k+1} is a calculated gain (known as the Kalman gain) and is updated at every time step. The a posteriori error covariance is defined as

$$P_{k+1|k+1} = E(e_{k+1|k+1} {e_{k+1|k+1}}^T) \qquad \text{Equation 3.1.1.6}$$

Where $\boldsymbol{e_{k+1|k+1}}$ is the error of the previous estimate. As mentioned before, the Kalman Filter works in a predictor-corrector fashion. Time update equations project forward (in time) the current state and error covariance estimates to obtain the a

priori estimates for the next time step. The measurement updates equations are for the feedback and incorporate a new measurement into the a priori estimate to obtain a better a posteriori estimate. The time update equations are the predictor equations while the measurement update equations are the corrector, or update, equations; together creating the predictor-corrector algorithm as summarized in Figure 3-1. R and Q are system and measurement noise covariance matrices. These variables are tuning parameters that are commonly determined manually through trial and error, but can be calculated in certain situations [27].

Time Update (Predict)

$$\hat{x}_{k+1|k} = A\hat{x}_{k|k} + Bu_k$$

$$P_{k+1|k} = AP_{k|k}A^T + Q$$

Measurement Update (Correct)

$$K_{k+1} = P_{k+1|k}H^T(HP_{k+1|k}H^T + R)^{-1}$$

$$\hat{x}_{(k+1|k+1)} = \hat{x}_{k+1|k} + K_{k+1}(z_{k+1} - C\hat{x}_{k+1|k})$$

$$P_{k+1|k+1} = (I - K_{k+1}H)P_{k+1|k}$$

Figure 3-1 Complete set of equations for the Kalman Filter

3.1.2 Extended Kalman Filter (EKF)

Although the Kalman Filter solves the general issue of trying to estimate the state of a linear discrete-time controlled process, it does not have the ability to estimate states in a nonlinear process. Non-linear estimates can be computed by linearizing the estimation around the current estimate using the partial derivatives of the process and measurement functions. A Kalman Filter that linearizes about the current mean and covariance is referred to as an Extended Kalman Filter or EKF.

Adjustments must be made to the Kalman Filter in order to achieve EKF. The EKF is a state estimator that only approximates the optimality of Bayes' rule by linearization [28]. The process can no longer be considered a discrete time system with noise; instead the process is now governed by the non-linear stochastic difference equation (Equation 3.1.2.1), where the current state (k) is computed as a non-linear function (f) of the state at the previous time step ($k-1$):

$$x_{k+1} = f(x_k, u_k, w_k) \qquad \text{Equation 3.1.2.1}$$

And the measurement equation is computed as

$$z_{k+1} = h(x_{k+1}) + v_k \qquad \text{Equation 3.1.2.2}$$

Where h is a nonlinear measurement model. With this modification to the governing equation and measurement equation, the predictor-corrector equations of the filter must be adjusted as well [25]. The a priori state estimation becomes a function of the a posteriori states and the inputs:

$$\hat{x}_{k+1|k} = f\left(\hat{x}_{k|k}, u_k\right) \qquad \text{Equation 3.1.2.3}$$

The a priori estimated error covariance becomes:

$$P_{k+1|k} = F_k P_{k|k} {F_k}^T + Q_k \qquad \text{Equation 3.1.2.4}$$

Where Q_k is the process noise covariance matrix and F_k is a Jacobian matrix derived from the partial derivatives of the non-linear function f:

$$F_k = \left.\frac{\partial f(x)}{\partial x}\right|_{x=\hat{x}_{k+1|k}} \qquad \text{Equation 3.1.2.5}$$

The measurement error covariance needed to compute the Kalman gain is defined as:

$$S_{k+1} = H_{k+1} P_{k+1|k} {H_{k+1}}^T + R_{k+1} \quad \text{Equation 3.1.2.6}$$

where R_{k+1} is the measurement noise covariance matrix and H_{k+1} is a Jacobian matrix derived from the partial derivatives of the nonlinear measurement model, h:

$$H_{k+1} = \left. \frac{\partial h(x)}{\partial x} \right|_{x=\hat{x}_{k+1|k}} \quad \text{Equation 3.1.2.7}$$

The next step is to compute the Kalman gain:

$$K_{k+1} = P_{k+1} {H_{k+1}}^T {S^{-1}}_{k+1} \quad \text{Equation 3.1.2.8}$$

and update the a priori estimates to the a posteriori estimates with the EKF gain:

$$\hat{x}_{k+1|k+1} = \hat{x}_{k+1|k} + K_{k+1} \tilde{y}_{k+1} \quad \text{Equation 3.1.2.9}$$

Where $\tilde{y}_{k+1}$ is the measurement error. Finally the a posteriori estimation error covariance is computed:

$$P_{k+1|k+1} = (I - K_{k+1} H_{k+1}) P_{k+1|k} \quad \text{Equation 3.1.2.10}$$

Where I is the identity matrix. The complete set of EKF's predictor-corrector equations are displayed in Figure 3-2. An important feature of the EKF is that the Jacobian H_{k+1} in the equation for the Kalman gain servers to correctly magnify only the relevant components of measurement information. Only portions of the residual $(z_k - h(x_k, 0)$ that affect the state will contribute to the Kalman gain [28]. Other

drawbacks to the EKF include sensitivity to computer precision and computational complexity due to matrix inversions.

Time Update (Predict)

$$\hat{x}_{k+1|k} = f(\hat{x}_{k|k}, u_k)$$

$$P_{k+1|k} = F_k P_{k|k} {F_k}^T + Q_k$$

Measurement Update (Correct)

$$S_{k+1} = H_{k+1} P_{k+1|k} {H_{k+1}}^T + R_{k+1}$$

$$K_{k+1} = P_{k+1|k} {H_{k+1}}^T {S^{-1}}_{k+1}$$

$$\tilde{y}_{k+1} = z_{k+1} - h(\hat{x}_{k+1|k})$$

$$\hat{x}_{k+1|k+1} = \hat{x}_{k+1|k} + K_{k+1}\tilde{y}_{k+1}$$

$$P_{k+1|k+1} = (I - K_{k+1}H_{k+1})P_{k+1|k}$$

Figure 3-2 Complete set of equations for the Extended Kalman Filter

Measurements are susceptible to noise in mechanical systems, making it very difficult to track trajectories or system states. This is especially true when derivatives are used to estimate system states (such as attempting to retrieve acceleration from velocity) and when non-linearity is involved. Applying EKF to a non-linear mechanical system would result in better accuracy of estimation. The EKF is known for being able to accurately estimate states better than other predictor-corrector algorithms [29]. For example, in [30] the author uses an EKF to improve the signal to noise ratio from ECG readings. In this thesis, noisy signals and modelling error will be fixed with the use of EKF in the same manner.

3.1.3 Smooth Variable Structure Filter (SVSF)

The Smooth Variable Structure Filter or SVSF is another useful predictor-corrector system. It was presented in 2007 and follows the same principles as the sliding model control (SMC) [31]. SVSF uses a discontinuous switching plane along the desired state trajectory, or the sliding surface, to keep the state values along this surface and minimize trajectory errors. With this switching action, SVSF can provide stability and convergence of estimate to a neighborhood of the actual states, given bounded uncertainties and disturbances. SVSF has a quite a few unique features that separate it from other filtering strategies. For instance, SVSF can be setup to explicitly identify the source of uncertainty within a system [25]. Furthermore, instead of implicitly considering the uncertainty, the SVSF uses this uncertainty information in its design. This reduces the trial and error required to manually tune the uncertainty. These features make SVSF an exceptional tool for fault detection and condition monitoring.

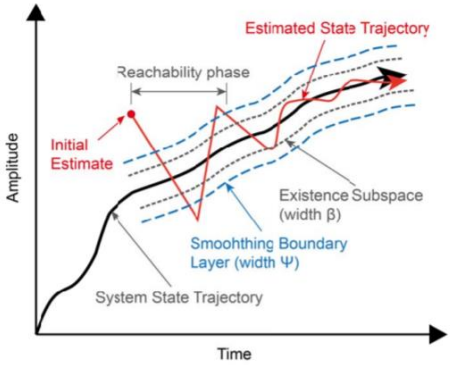

Figure 3-3 SVSF diagram [26]

As shown in Figure 3-3, there is the actual and estimated trajectory of a single state being estimated. The estimated state starts with an initial state value and is adjusted by the SVSF predictions until the existence subspace is reached. The width of the existence subspace, β, is recalculated at every time step based on the state trajectory, uncertainties, noise, and disturbances [29]. Once the estimated state reaches the existence subspace, known as the "reachability phase", it will continuously switch back and forth around the true state trajectory within this region. The estimation will successfully converge to the existence subspace if the a posteriori error decreases with time:

$$|e_{z,k+1|k+1}| < |e_{z,k|k}| \qquad \text{Equation 3.1.3.1}$$

Like SMC, the SVSF is subject to high frequency switching from pushing the system too hard toward the sliding hyperplane. To fix this problematic "chattering", a smoothing approximation must be introduced (shown in Figure 3-3). The smoothing boundary layer width,ψ, is a tuning parameter that must enclose the existence subspace such that $\psi > \beta$. Similar to the EKF estimation theory, a nonlinear process with a linear measurement equation is considered, where the a priori state estimate is expressed as

$$\hat{x}_{k+1|k} = f\left(\hat{x}_{k|k}, u_k\right) \qquad \text{Equation 3.1.3.2}$$

The a posteriori state estimate is computed as

$$\hat{x}_{k+1|k+1} = \hat{x}_{k+1|k} + K_{k+1}{}^{SVSF} \qquad \text{Equation 3.1.3.3}$$

Where $K_{k+1}{}^{SVSF}$ is the SVSF gain, similar to the Kalman gain, and is represented as:

$$K_{k+1}{}^{SVSF} = H^{-}\left(\left|e_{z,k+1|k}\right| + \Upsilon * \left|e_{z,k|k}\right|\right) * sat\left(\frac{e_{z,k+1|k}}{\psi}\right) \qquad \text{Equation 3.1.3.4}$$

Where $\left|e_{k+1|k}\right|$ and $\left|e_{k|k}\right|$ are the absolute values of the priori and the a posteriori state estimate error respectively [31]. Υ is a tuning parameter for the SVSF convergence rate that must be between 0 and 1. H^{-} is the pseudo-inverse of the measurement matrix. The SVSF strategy is summarized in Figure 3-4.

Time Update (Predict)

$$\hat{x}_{k+1|k} = f\left(\hat{x}_{k|k}, u_k\right)$$

$$e_{z,k+1|k} = z_{k+1} - H_{k+1}\hat{x}_{k+1|k}$$

Measurement Update (Correct)

$$K_{k+1}{}^{SVSF} = H^{-}\left(\left|e_{z,k+1|k}\right| + \Upsilon * \left|e_{z,k|k}\right|\right) * sat\left(\frac{e_{z,k+1|k}}{\psi}\right)$$

$$\hat{x}_{k+1|k+1} = \hat{x}_{k+1|k} + K_{k+1}{}^{SVSF}$$

$$e_{z,k+1|k+1} = z_{k+1} - H\hat{x}_{k+1|k+1}$$

Figure 3-4 Complete set of equations for SVSF

In [31], Dr. Habibi uses SVSF in an aerospace application. A mathematical model is derived for an electrohydraulic actuator for the purpose of performing health monitoring. For most predictor-corrector filters (such as EKF), health monitoring is very challenging. When a fault occurs, it causes abrupt changes in the system effecting its dynamic characteristics that cannot accurately be tracked by other methods. Engineers try to account for these abrupt changes in other methods by

relying heavily on guess and check work [31]. On the other hand, SVSF is robust to modelling uncertainty and can guarantee numerical stability further to the specification of upper bounds on parametric variations [31]. Although, the SVSF is very robust, it lacks in accuracy compared to the EKF. In this thesis, the EKF and SVSF are combined together to obtain the accuracy of the EKF and the robustness of the SVSF.

3.2 Fault Detection and Diagnosis Overview

Estimation of system states is very useful for model based fault detection and diagnosis. Faults are deviations in acceptable behavior from at least one characteristic property of a system. Estimation theory can be used to detect deviations in acceptable behavior as the measurements begin to drift from the predicted values of the model. Faults lead to malfunctions or failures of a system. Faults are inevitable in assembly line production which is why it is important to scan a new part for faults after it is built to make sure it is viable to use. This is especially true in the automotive industry where untested faulty alternators and starters are placed in cars. D&V Electronics Ltd solves this issue with their automotive system testers that have the ability to run and test parts in End-Of-Line testing. Their testers solve the issue before the part is sent out of the assembly line, reducing expenses and resources wasted. Traditionally testers, such as the ones built by D&V Electronics Ltd, accomplished fault detection through the rudimentary practice of limit checking. Through advancements in technology and computer processing power, more intelligent fault detection systems were created. Now,

through model and signal based approaches, faults within a system can be detected and diagnosed. D&V Electronics Ltd's Sound and Vibration Pro uses a signal based approach to pinpoint where the fault is occurring in alternator and starter systems.

3.2.1 Model Based Fault Detection and Diagnosis

As mentioned in the previous section, fault detection was originally done through limit checking. This is a practice where upper and lower limits are manually generated for important signals within a system. A part is then considered faulty if a signal deviates from these bounds during the test (shown in Figure 3-5). This method was adequate for detecting faults, but gave no instruction on where or why the fault was occurring. A more sophisticated way would be to express the system with mathematical process models and compare the estimated and experimental features. This is known as Model Based Fault Detection and Diagnosis (FDD) [32]. This method leads to higher diagnosis performance with more fault detection success over a larger operating range than limit checking. Likewise, with more knowledge about the system there is potential for more types of faults to be detected with a quicker detection time. The model based approach does have caveats. The knowledge required to build, tune and implement a reliable and accurate model of the dynamic system is time consuming. Moreover, the computational intensity increases with complexity of the model rendering it infeasible for certain applications. Even with this drawback the Model Based FDD approach is very effective for the scope of this thesis. Thus, the residual view and

parameter estimation approach are studied and implemented as two model based FDD methods.

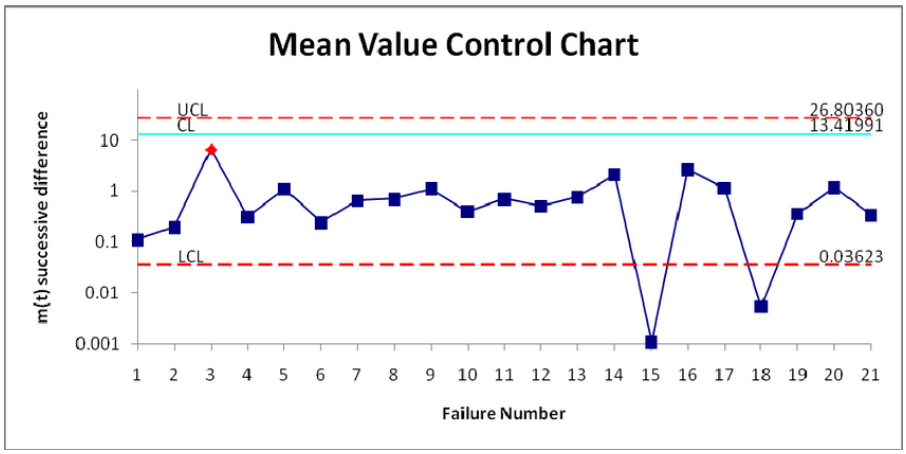

Figure 3-5 Limit checking fault detection

3.2.1.1 Residual View

A residual is a signal generated by the comparison between experimental and estimated features [32]. Consider the residual, $f(t)$:

If $f(t) \approx 0$, then the residual is given a value of 0 (not triggered)

If $f(t) \neq 0$ then the residual is given a value of 1 (triggered)

Every residual view system is composed of two parts, the residual generation and the residual evaluation. Residual generation is the process of determining the effect of a fault on each measured signal of the system. Residuals are created from the signals that are sensitive to the faults [33]. There must be a sufficient amount of residuals such that every fault is identified by a unique combination of triggered

residuals. For example, an overvoltage fault is described as a significantly larger alternator voltage. To anticipate this fault a residual is created that compares the experimental alternator voltage signal to the model's estimated signal. Then within the fault detection schematic the residual is set to trigger in the event of an overvoltage fault; this becomes important in the second stage of the residual view method. In the first stage known non-faulty and faulty parts, in this case alternators, are used to generate the residuals for the system. In the second stage new unknown parts are tested to determine their health; their residual is calculated and then evaluated against the FDD schematic. If the residuals do not trigger then the part is considered healthy. Conversely, if a fault's unique combination of triggered residuals is discovered then the part is considered unhealthy and is diagnosed as the fault that was triggered. Consider the structured residual model presented in [22] shown in Figure 3-6.

$$r_1 = (I_{\mathrm{dc}} - I_{\mathrm{dc}}^{\mathrm{eq}})/I_{\mathrm{dc}}^{\mathrm{nom}}$$
$$r_2 = (V_f - V_f^{\mathrm{eq}})/V_{\mathrm{ref}}^{\mathrm{nom}}$$
$$r_3 = (V_{\mathrm{dc}} - V_{\mathrm{dc}}^{\mathrm{eq}})/V_{\mathrm{ref}}^{\mathrm{nom}}$$

r_1	r_2	r_3	*Fault Type*
0	1	0/-1	Belt slippage
0	x	1	Voltage regulator (increased V_{ref})
0	0	-1	Voltage regulator (drop V_{ref})
1	x	x	Power Electronics (diode fault)
0	0	0	None

Figure 3-6 Fault Detection Diagnosis Schematic and corresponding residuals [22]

3.2.1.2 Parameter Estimation

The parameter estimation technique detects and diagnosis faults based on deviations in constant parameters of the system. The method requires adaptive

filtering such as Kalman Filtering for robustness and accuracy in the presence of modelling uncertainty. Essentially, the governing equations of the dynamic model are rearranged to compute the value of parameters instead. These “artificial states” become a part of the estimation process using measured signals to be computed [25]. An estimate of a constant, $\hat{k}$, can be compared to that of the correct constant,k, value. A fault has occurred if the deviation is above a determined threshold. The fault is diagnosed based on which unique set of constant parameters deviate. In [25], the resistance of each stator winding becomes an artificial measurement for parameter estimation (Equation 3.2.1.2.1). Under normal condition the parameters remain relatively constant as seen in Figure 3-7. In Figure 3-8, a fault is injected in the phase C resistance and the value drastically changes. The injected fault is detected and diagnosed once the parameter estimated value is above a pre-determined threshold.

$$r_{MN_a} = \frac{u_{MN_a} - L\frac{dI_{a_{MN}}}{dt} - K_{e2}\omega_{MN}}{I_{MN_a}} \qquad \text{Equation 3.2.1.2.1}$$

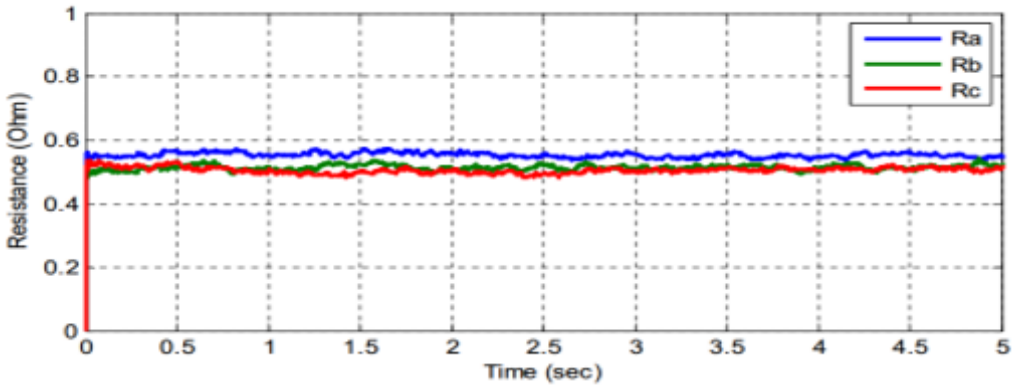

Figure 3-7 Parameters at normal operating conditions [25]

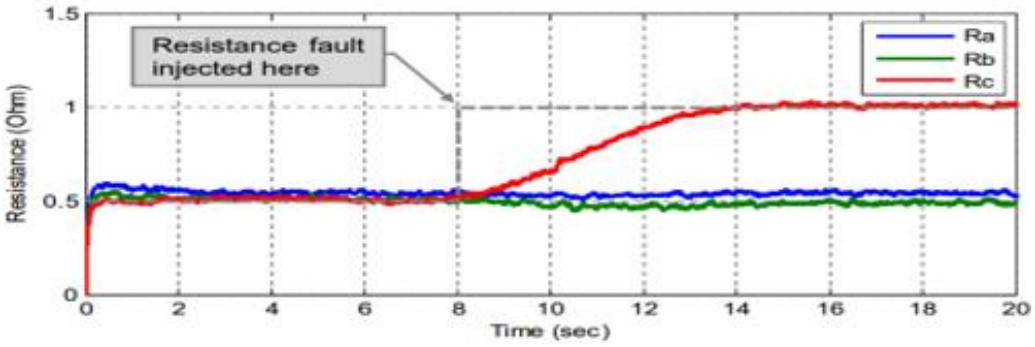

Figure 3-8 Parameters in the presence of a fault [25]

3.3 Parameter Tuning

Ideally, the work of this thesis will be used for fault detection and diagnosis of any Lundell alternator that is placed in the tester. However, no alternator is made the same. Thus, for an accurate simulation every alternator's parameters must be

loaded into the tester. As explained previously, this type of alternator specifications is very difficult to obtain from the manufacturer. A parameter tuning approach is introduced in order to eliminate the tedious process of contacting the manufacturer and manually storing this information. Parameter tuning is an iterative procedure that attempts estimating unknown values of a model by manipulating them until the error between the model output and experimental output is significantly low. With the use of genetic algorithms, new alternator's parameters can be automatically solved and stored within the tester for future simulations.

3.3.1 Genetic Algorithms

A genetic algorithm is a method for solving both constrained and unconstrained optimizations problems inspired by Charles Darwin's theory of natural evolution. The method imitates the process of natural selection where the fittest individuals are selected for reproduction in order to produce offspring of the next generation. Very useful to solve problems that are not well suited to standard optimization algorithms, including problems in which the objective function is discontinuous, non-differentiable, stochastic or highly nonlinear [34]. Essentially, natural selection starts with an initial population of an organism. The fittest individuals from the population are selected for reproduction and produce then next generation of offspring that inherit their parents' characteristics. Offspring with more fit parents will be better than their parents and have a better chance of survival [35]. This process iterates and eventually a generation with the fittest individuals will be discovered.

The process begins with a set of individuals called a population. Each individual within the population is a solution to the problem needed to be solved. An individual is characterized by a set of parameters known as genes. Genes are joined together to create a chromosome, which is a potential solution. Usually binary values are used to represent gene values. The hierarchy of the population is shown in Figure 3-9. The fitness function determines the ability of an individual to compete with other individuals.

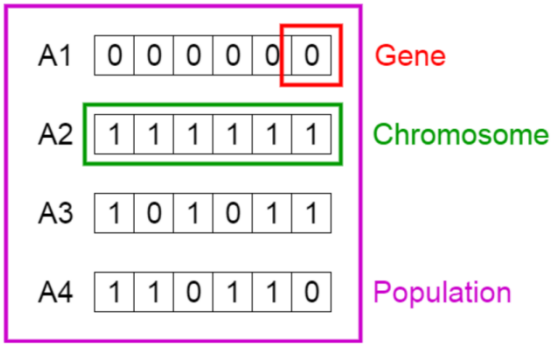

Figure 3-9: Population, Chromosome, and Genes as defined by [35]

The fitness function varies per application of the genetic algorithm and must be defined by the user. The fitness score is computed for each individual. An individual's fitness score determines how probable it will be reproducing during the selection phase. In the selection phase, pairs of individuals are chosen, based on their fitness scores, to pass their genes to the next generation's offspring. This segues nicely into the most significant stage of the genetic algorithm, the crossover. The crossover point is an integer value that corresponds to a gene index within the chromosome. For parents to mate a crossover point is chosen at random

from within the genes. Splitting the parent's chromosome at the specified gene index and exchanging their segments leads to the creation of two new offspring for the next generation (refer to Figure 3-10). Offspring replace low fitness individuals from the current population and become potential parents for the next generation [36]. An optional phase in genetic algorithms is the introduction of mutation into the genes of new offspring.

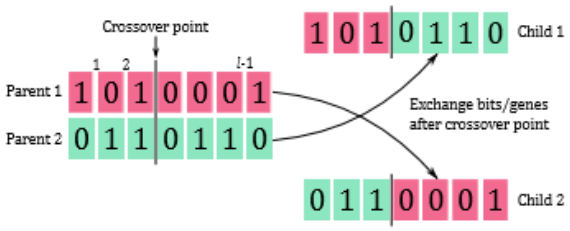

Figure 3-10 Creation of offspring by exchange of parent genes around crossover point [37].

This process randomly flips bits in the chromosome to maintain diversity within the population and prevent premature convergence [38]. Once the new population is completed, the next generations of individuals experience the same process. The genetic algorithm only terminates in two conditions. If the population no longer produces offspring which are significantly different in terms of cost function evaluation from the previous generation then the population converges and the algorithm has provided a set of solutions to the user's search problem. This convergence becomes apparent during the procedure as the average fitness of the

chromosomes increases. The algorithm also terminates when it reaches the max amount of allocated generations.

Chapter 4 Modelling of Alternators

4.1 Alternator Modelling Components

The Complex Nonlinear (CN) Model consists of many equations with unknown parameters and states. Multiple assumptions must be made in attempt to simplify the system. The equations are derived from the principles of electromagnetic induction such as Faraday's law and Lenz's law. From equation (Equation 2.1.1.1) the electromagnetic force is defined as the change in flux linkage. The equations (Equation 2.3.3.1) that relate flux linkage and corresponding current consists of 3 unknown parameters self-inductance, L_s, stator-stator mutual inductance, L_{ss}, and the peak stator-rotor mutual inductance M. To simplify the complex system it is assumed L_{ss} is negligible, self-inductances are equivalent, stator resistance are equivalent, the three stator phases are exactly 120^o separated from each other, field voltage (V_f) stays constant and field current (I_f) throughout the duration of the test. The inputs to the model are rotor angular speed (ω_e) and regulated field voltage. The unknown parameters to tune include: L_f, L_s, M. Unlike the equivalent LPV model, the parameters of the CN model stay constant throughout the entire speed spectrum of the alternator. This model assumes access to all phase voltages (V) and rotor angular displacement ($\emptyset_m$) of the alternator. This is not the case due to the closed casing of the alternator and limitations from the tester. Therefore, the states to estimate within the system are phase currents (I), diode switching states of bridge rectifier (G), phase voltages (V) and rotor angular displacement ($\emptyset_m$). The

output of the system is I_{dc} which is the dot product of the phase current and the diode switching state vectors.

4.1.1 Electrical Rotor Angle Artificial Measurement

The electrical rotor angular displacement is the most critical to estimate correctly because it affects the values of every other state in this model. A slight deviation will cause a phase shift in the ripple effect, leading to a large error signal with the experimental data even if their averaged signals are equivalent.

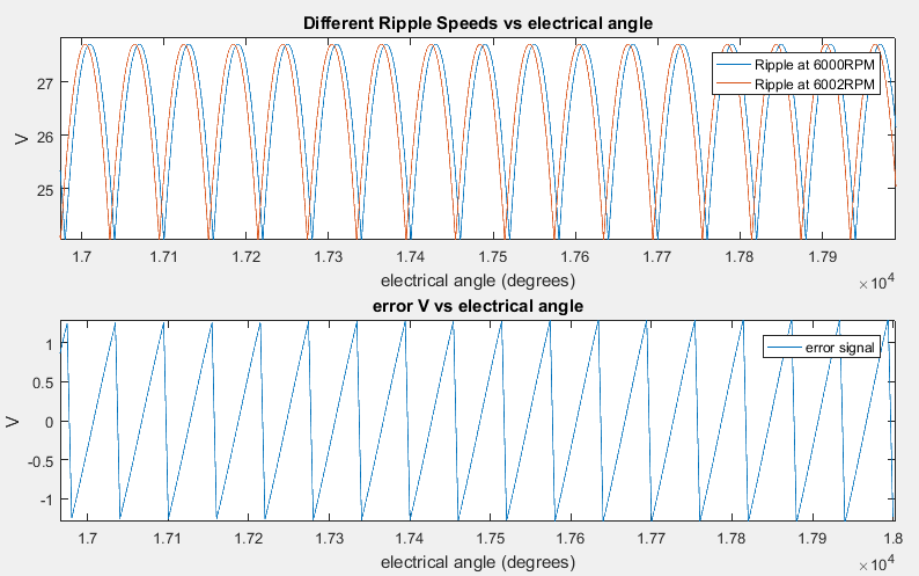

Figure 4-1 An offset of 2RPM leads to an error of +/- 1.4V in under 30 seconds of simulation

Electrical angular speed can be calculated with the input mechanical rotor angular speed using Equation 4.1.1.1.

$$\omega_e = \omega_m \frac{2\pi * num\_of\_pole\_pairs}{60}$$ Equation 4.1.1.1

Where $num\_of\_pole\_pairs$ is the number of pole pairs on the alternator's rotor. The electrical rotor angle is then calculated by integrating electrical angular speed over the time step.

$$\theta_e{}^{k+1} = \theta_e{}^{k} + \omega_m dt$$ Equation 4.1.1.2

Where dt is the sampling rate of the alternator tester. As mentioned before, the tester is not able to calculate rotor angle or phase values; this leads to complications when determining the initial angular displacement of the rotor. The initial angular displacement of the rotor cannot be assumed as zero because that would require a rotor pole to be perfectly aligned with the phase A stator when the test starts. This cannot be guaranteed due to the closed casing of the alternator. The alternator current samples at 200 KHz and the angular speed is sampled at 1200Hz, which means for every 160 samples of current there is only one sample of speed. As mentioned before, any slight deviation of angular displacement can cause large error. Hypothetically, if the speed changed abruptly the alternator current would be affected and the result would be captured by the current measurement. However, it is possible the speed measurement would not capture this abrupt change. Figure 4-1 demonstrates how a deviation of 2RPM can lead to increasing error in a short period of time. A solution must be presented that can accurately predict the initial rotor angle and produce a higher sampling speed measurement.

After careful analysis, a solution was derived from the stator voltage signal measured by the tester. As shown in Figure 4-2, the Stator Voltage signal oscillates between 0V and 14.2V. This is intriguing because the stator voltage should be a cosine wave with an amplitude of 14.2V. Notice how at certain instances, the voltage undergoes a great change in magnitude from 0V to 14.2V almost instantly.

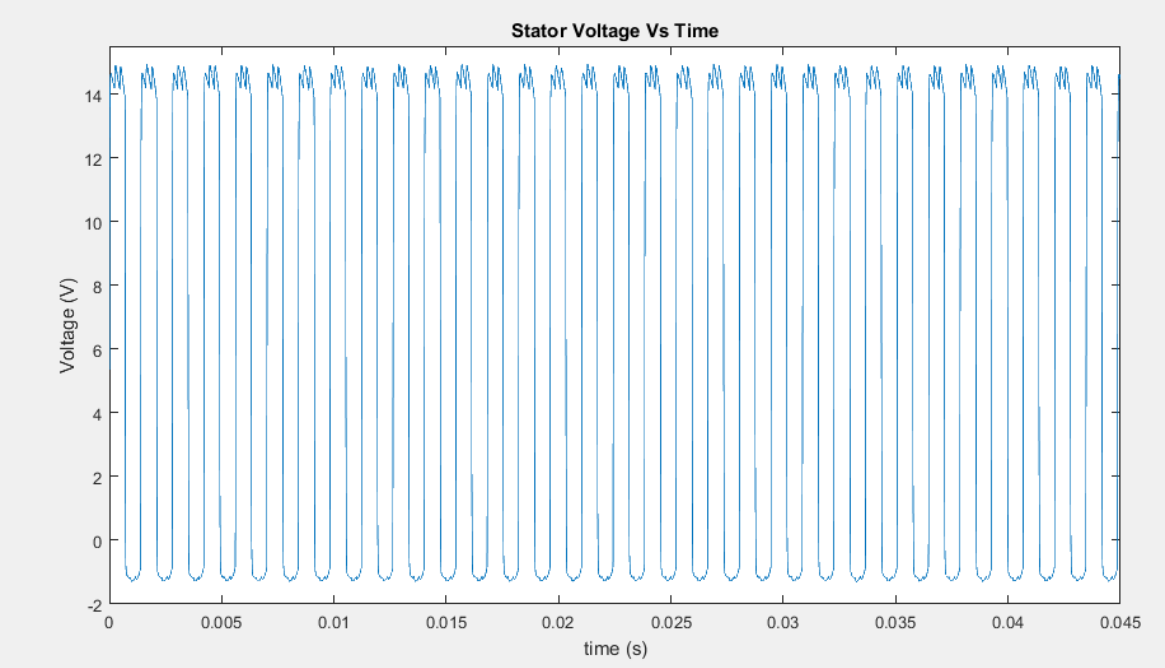

Figure 4-2 Stator Voltage measurement from ALT-198 tester

Through further analysis it was determined that this signal was actually the stator voltage with the effect of the diode bridge rectifier. Figure 4-3 demonstrates the

instances the phase A turns on in the time domain.

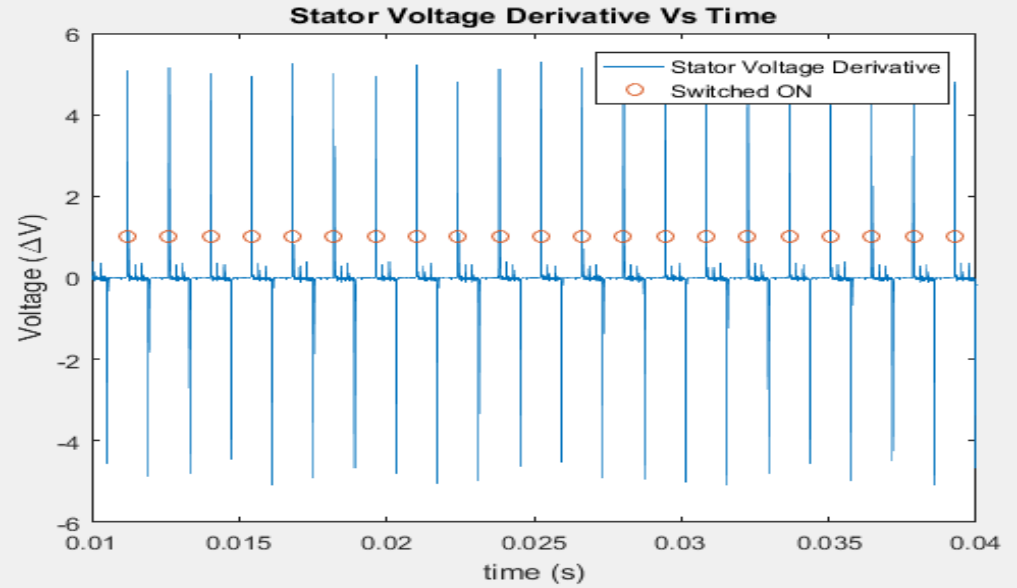

Figure 4-3 derivative of the stator voltage signal demonstrates the instances the phase turns on.

With knowledge of cosine waves, extracting the initial state of θ_e became possible. The phase's diode bridge turns on once every revolution when the phase vector goes from negative to positive. Cosine waves first go from negative to positive at 270º. Therefore, by shifting the sampled data to the first determined phase conduction switch, marked in Figure 4-3 as circles, then the initial electrical rotor angle can be assumed as 270º. The stator voltage derivative is also used to produce a more accurate speed signal. As mentioned previously, the phase's diode bridge only turns on once every revolution, therefore, the distance between each conduction switch is approximately 360º. The electrical speed for each revolution can be calculated as follows:

$$\omega_e = \frac{360^o}{(t_{conduction\ switch_{next}} - t_{conduction\ switch_{current}})}$$ Equation 4.1.1.3

Where $t_{conduction\ switch_{next}}$ and $t_{conduction\ switch_{current}}$ are the times the phase's diode turns on at the next and current electrical revolution respectively. To understand the results of the proposed method, the experimental ripple current is plotted against the ideal ripple current produced by calculating 3 phase cosine waves (section 4.4) using the new angle measurement and summing them with Equation 2.3.3.10. Figure 4-4 shows an experimental ripple current and an ideal ripple current by combining speed and angle equations (Equation 4.1.1.2) and (Equation 4.1.1.3) with the speed signal from the D&V tester. At a constant speed, the method yields an RMS error of +/-7.35A or +/-5.29% and a max error of 18.9A or 13.60%. This is less than satisfactory results.

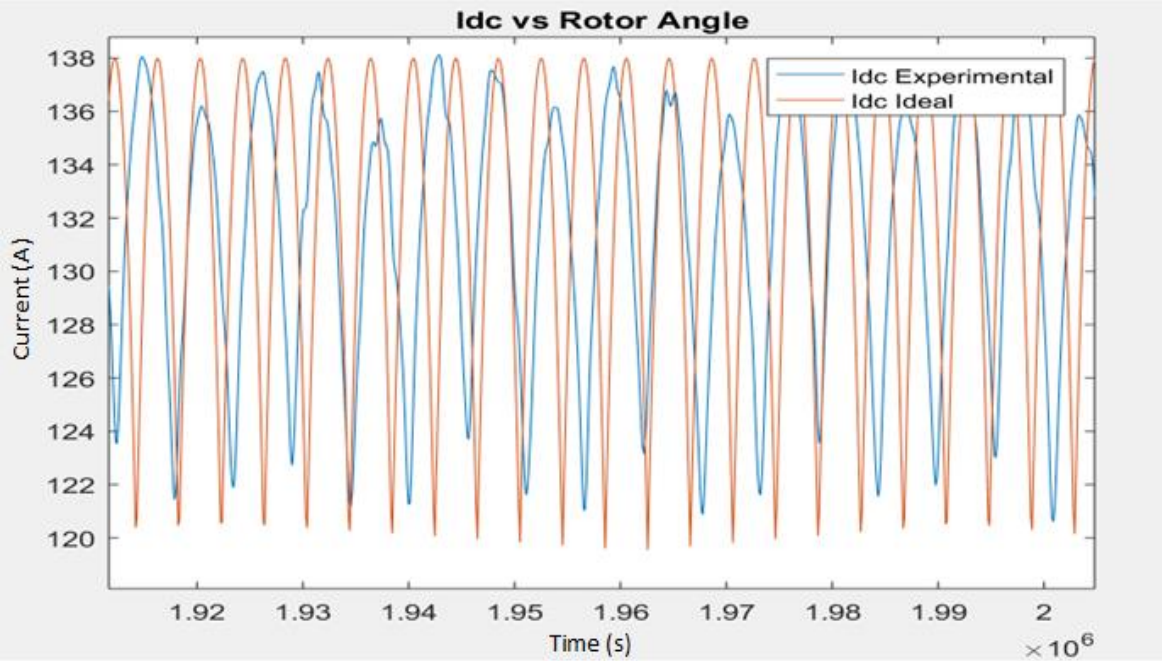

Figure 4-4 Experimental Idc vs Ideal Ripple Current using the speed signal from the D&V tester.

Figure 4-5 compares an experimental ripple current and an ideal ripple current (section 4.4) by combining speed and angle equations (Equation 4.1.1.2) and (Equation 4.1.1.3). At a constant speed, the method yields an RMS error of +/-2.08A or +/-1.49% and a max error of 8.16A or 5.87%. This introduced method produces very good results, more than doubling the accuracy of the ideal ripple current output.

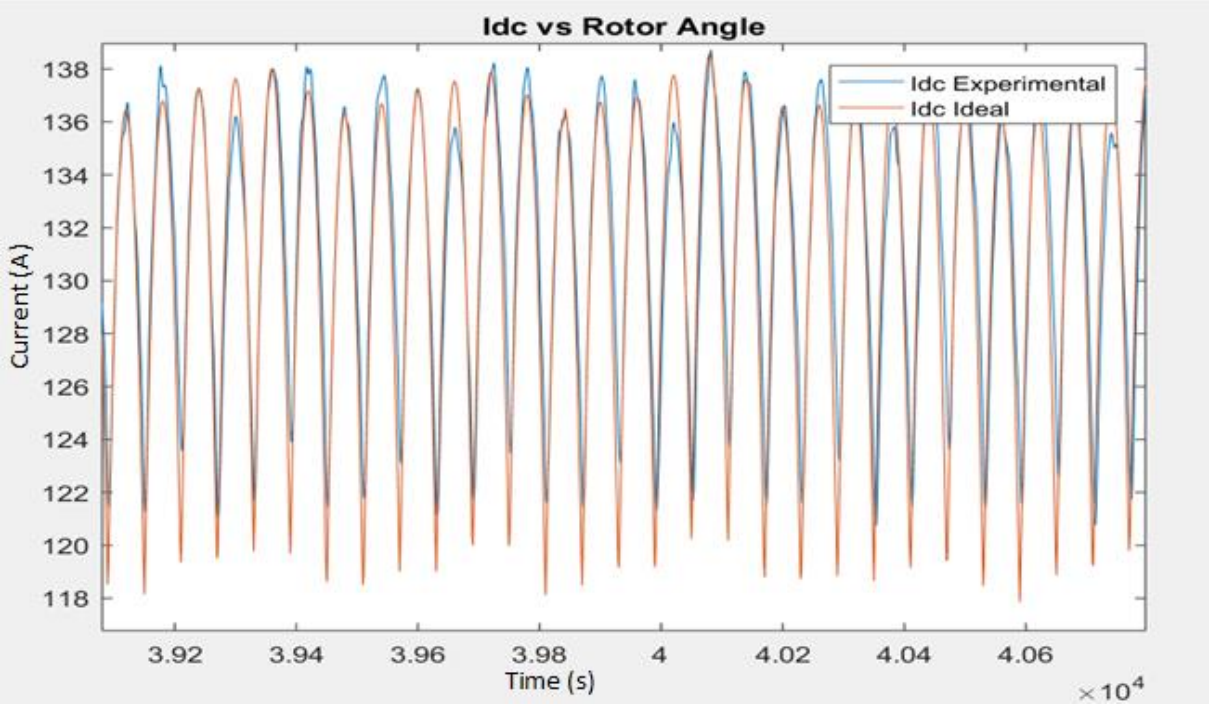

Figure 4-5 Idc Experimental vs Idc Ideal using new initial rotor angle and electrical speed

To further improve the proposed method, a syncing pulse was introduced to recalibrate the rotor angle value every revolution. This is easily implemented by shifting the rotor angle artificial measurement to a multiple of 360^{o} offset by 270^{o} on every instance that the phase conduction state turned on. At a constant speed, the method yields an RMS error of +/-1.56A or +/-1.12% and a max error of 5.24A or 3.77%, shown in Figure 4-6. The results of comparison at constant speed are summarized in Table 1.

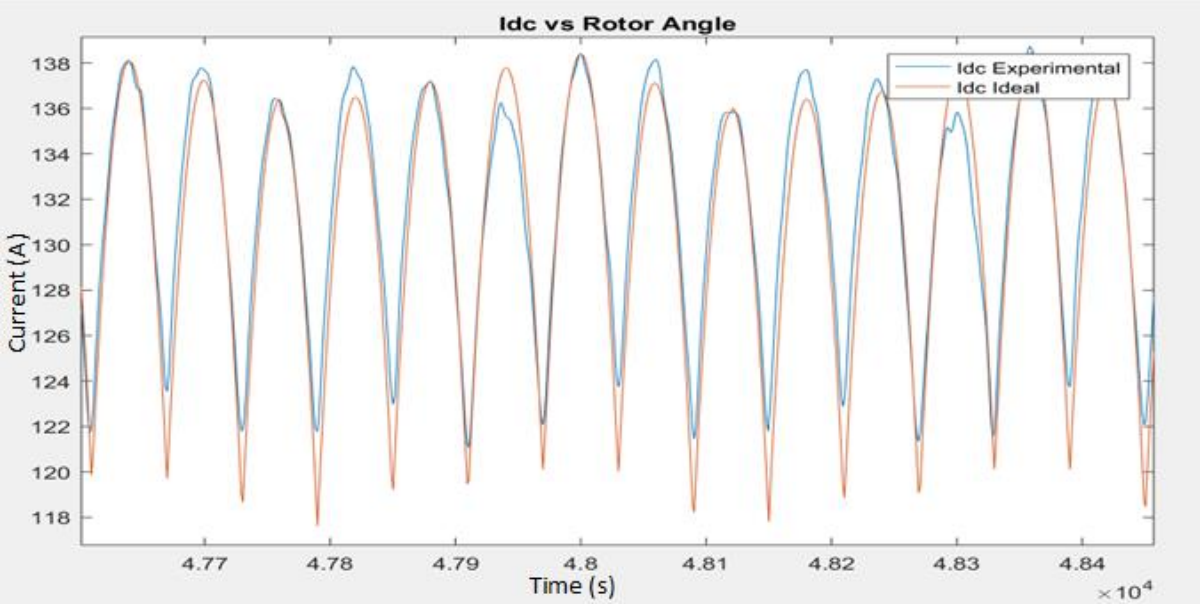

Figure 4-6 Experimental Idc vs Ideal Idc using new speed and syncing angle every revolution

At constant speed, the addition of the syncing pulse seems unnecessary as the improvement is negligible.

Table 1 Error at Constant Speed

	D&V Speed Signal	***Stator Derivative Speed Signal***	***Stator Derivative Speed Signal with Syncing***
RMS Error %	**5.29**	**1.49**	**1.12**
Max Error %	**13.26**	**5.87**	**3.77**

The syncing pulse plays an important role during larger changes in speed when the calculation of speed loses accuracy. Without any type of feedback, the rotor angle measurement has trouble returning to its true value even when the speed becomes constant again. Figure 4-7 demonstrates the difficulty the proposed non-synced method experiences under inconsistent speed, resulting in an RMS error of 7.01% and max error of 23.58%.

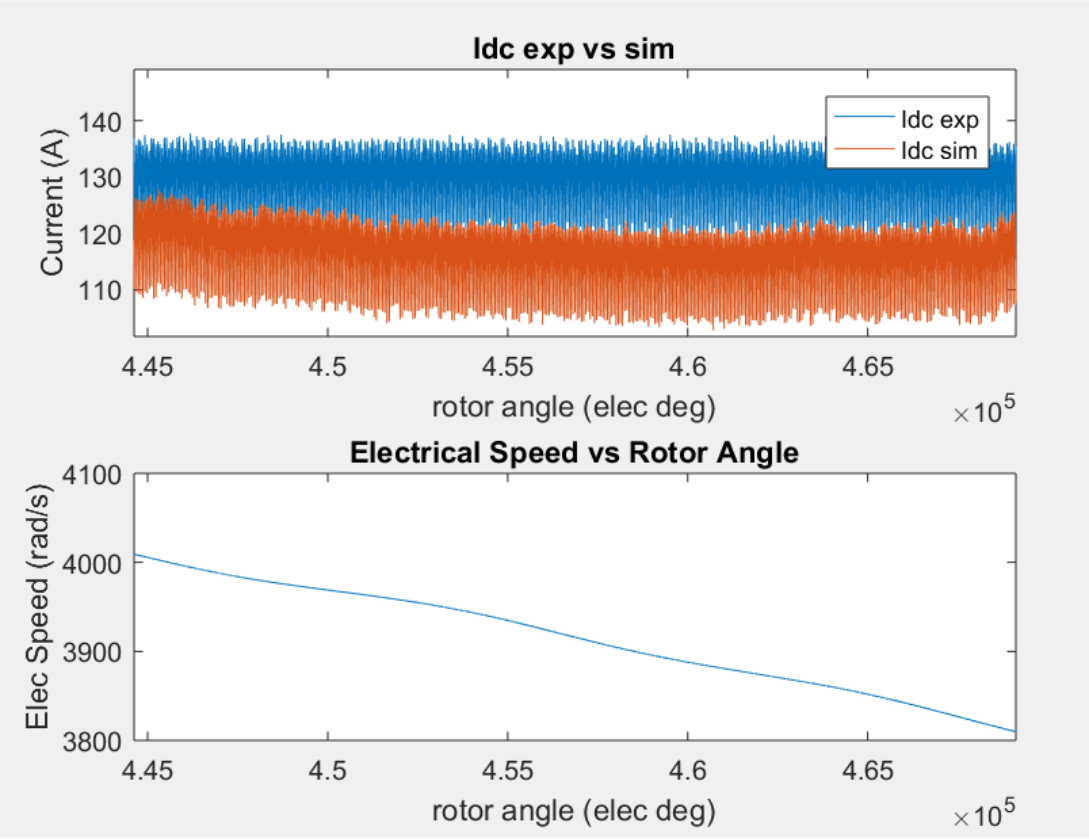

Figure 4-7 Experimental Idc vs Ideal Idc at inconsistent speed without syncing.

By resyncing the angle every revolution, the estimation of the rotor angle becomes a closed loop control with the ability to converge to its true value without introducing

any advanced control techniques. Figure 4-8 demonstrates the robustness of the proposed synced method under inconsistent speed, resulting in an RMS error of 1.05% and max error of 4.18%. The results of the inconsistent speed test are summarized in Table 2.

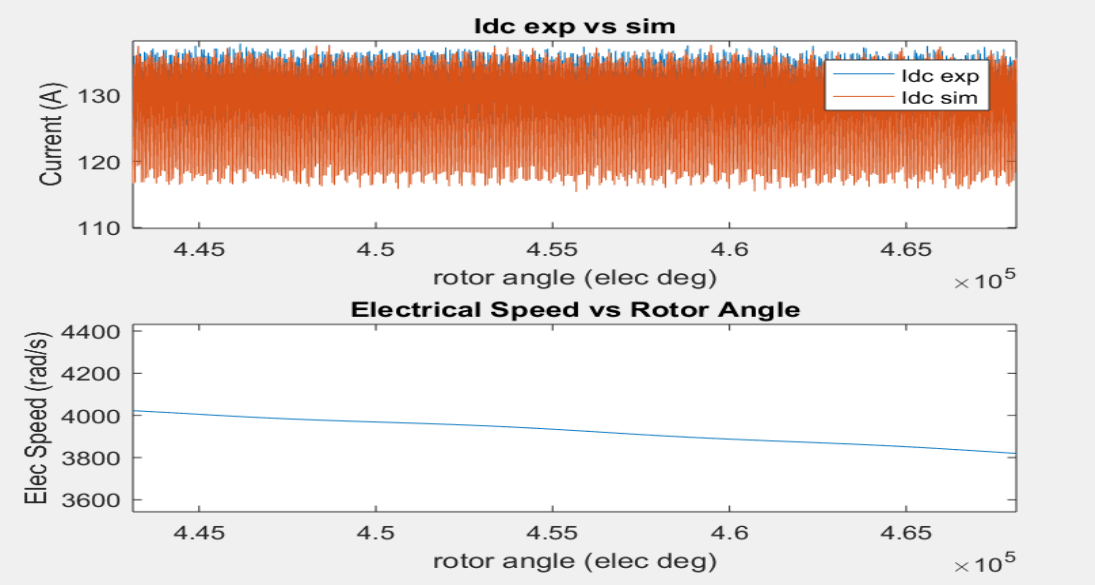

Figure 4-8 Experimental Idc vs Ideal Idc at inconsistent with syncing

Table 2 Error at Inconsistent Speed

	Stator Derivative Speed Signal	***Stator Derivative Speed Signal with Syncing***
RMS Error %	**7.01**	**1.05**
Max Error %	**23.58**	**4.18**

The improved speed and synced rotor angle measurements are used as inputs to other components of the alternator model.

4.1.2 3 Phase Voltages

The phase voltage is assumed to be sinusoidal with amplitude of $V_{p_{max}}$ and no DC offset. $V_{p_{max}}$is the largest phase voltage magnitude and varies depending on the alternator's DC voltage (V_{dc}). The D&V Tester, with aide from the alternator's AVR, keeps $V_{p_{max}}$ at the alternator's rated voltage throughout the entire operating region. The states of the phase voltages are calculated using the electrical rotor angle (section 4.1.1). Similar to other phase related states, phase A is considered to be shifted by 0º, phase B is considered to be shifted by -120º, and phase C is considered to be shifted by -240º. Equations 4.1.2.1, 4.1.2.2, and 4.1.2.3 lead to the waveform described in Figure 4-9.

$$V_a = V_{p_{max}} * \cos(\emptyset_e) \qquad \text{Equation 4.1.2.1}$$

$$V_b = V_{p_{max}} * \cos(\emptyset_e - 120) \qquad \text{Equation 4.1.2.2}$$

$$V_c = V_{p_{max}} * \cos(\emptyset_e - 240) \qquad \text{Equation 4.1.2.3}$$

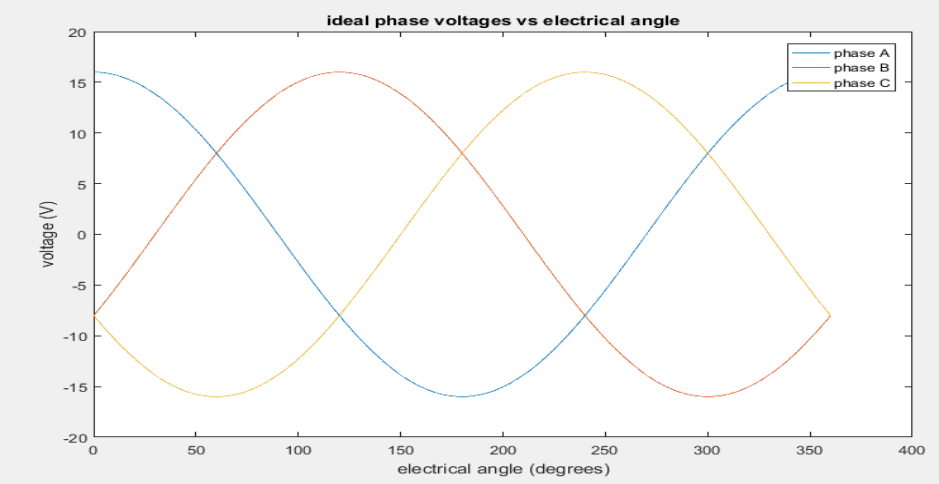

Figure 4-9 ideal phase voltages of a synchronous generator, where $V_{p_{max}} = 16$

4.1.3 The Three Phase Diode Rectifier Bridge

Within every three phase alternator there is a three phase full bridge rectifier. The diode bridge consists of 6 diodes; there is a pair of diodes for each phase, refer to Figure 2-6. The diode bridge works to keep the output current positive. To accomplish this, a phase's diode pair must be able to open and close the phase signal circuitry. There are complex models that describe how the rectifier manipulates the phase currents to produce a DC output. Instead, a Heaviside function is utilized to generally satisfy all alternators by reducing computational complexity and eliminating the need to tune more model parameters. As shown in Figure 4-10, A Heaviside function refers to a piecewise function that has a value of zero when negative and a value one when positive [39].

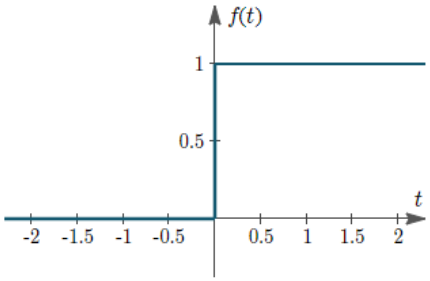

Figure 4-10 The Heaviside function, also known as Unit Step Function [39]

In [40], the conduction state of a diode pair becomes "on" or 1 when $I \geq 0$, where I is the phase current vector and "off" or 0 when $I < 0$. The conduction state Heaviside function becomes

$$G_n = \begin{bmatrix} I_n \geq 0, & 1 \\ I_n < 0, & 0 \end{bmatrix} \qquad \text{Equation 4.1.3.1}$$

Where G is the phase conduction state and n is the phase index (either A,B,C). A normalized phase current vs the phase conduction state is shown in Figure 4-11 for visualization of on and off switching.

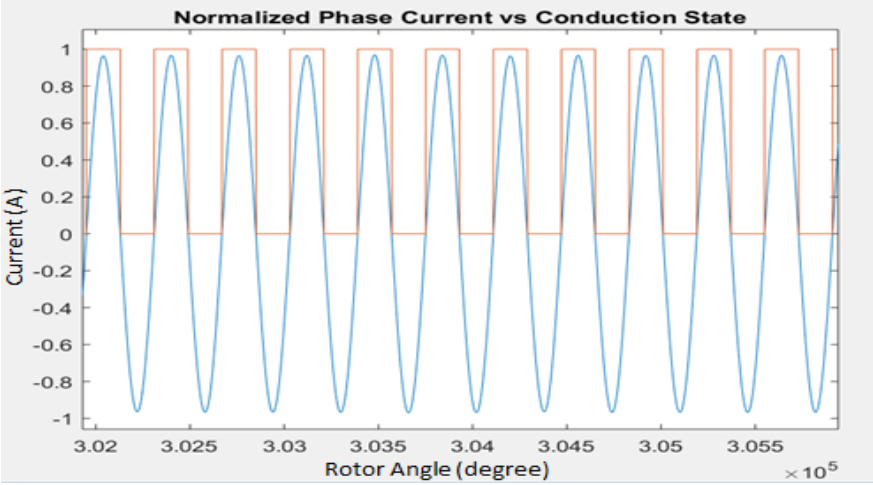

Figure 4-11 phase A voltages and its corresponding conduction state switching

The conduction states are a critical component to the measurement equation of the ripple current model. The simulated ripple current is the dot product of the diode conduction states and the phase currents as shown in Equation 4.1.3.1.

$$I_{DC} = G_A I_A + G_B I_B + G_C I_C \qquad \text{Equation 4.1.3.1}$$

4.1.4 Field Current

The governing equations (Equation 2.3.3.21 and Equation 2.3.3.22) for the chosen alternator model hold a fundamental problem. The equations are coupled together, requiring numerical analysis, such as Newton's method, to acquire the system's

state values at every iteration. This practice is too computationally demanding and is not feasible for the scope of this project. A simplified model of $\dot{I}_f$ is introduced that removes the governing equations dependencies on each other [21]. Dr. Scacchioli implements this technique in the Linear Parameter Varying model introduced in Section 2.3.4 [21]. Comparing Equation 4.1.4.1 and Equation 2.3.4.1, Dr. Scacchioli replaced coefficients $\frac{1}{L_f}$ and $-\frac{R_f}{L_f}$ with parameters β and $-\alpha$ respectively [21]. As shown in Figure 4-12, the armature winding circuit is often expressed as an equivalent circuit with an inductance, resistance, and adjustable resistance controlled by the AVR [41],[42]. In the equivalent circuit model the effect of the stator-rotor mutual inductance is eliminated [42]. When the AVR is on the adjustable resistance value is zero and the adjustable resistance is an open circuit, essentially infinite, when the AVR is off. Therefore, by performing Kirchhoff's mesh analysis on the equivalent circuit the field current reduces to the following equation:

$$\dot{I}_f = \frac{1}{L_f} V_f - \frac{R_f}{L_f} I_f \qquad \text{Equation 4.1.4.1}$$

Similar to the alternator phase voltage, the field voltage of the system remains constant throughout the alternator's operating region from collaborating efforts of the D&V Tester machine and the alternator's AVR. The tester has the capability to

detect overvoltage faults, making it safe to apply these assumptions.

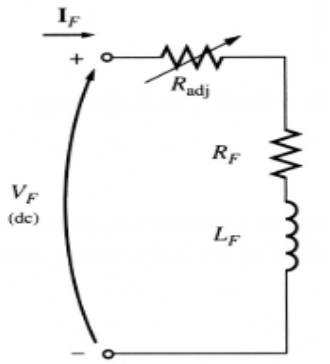

Figure 4-12 Field Voltage Equivalent circuit [41]

The equivalent circuit model was compared to experimental field current data to prove its feasibility. As shown in Figure 4-13, the model is able to model the field current transient well as the alternator accelerates from 0 RPM to 6000 RPM. The model accuracy increases during steady state performance of the alternator. Estimation theory could be applied to increase accuracy and robustness of the model.

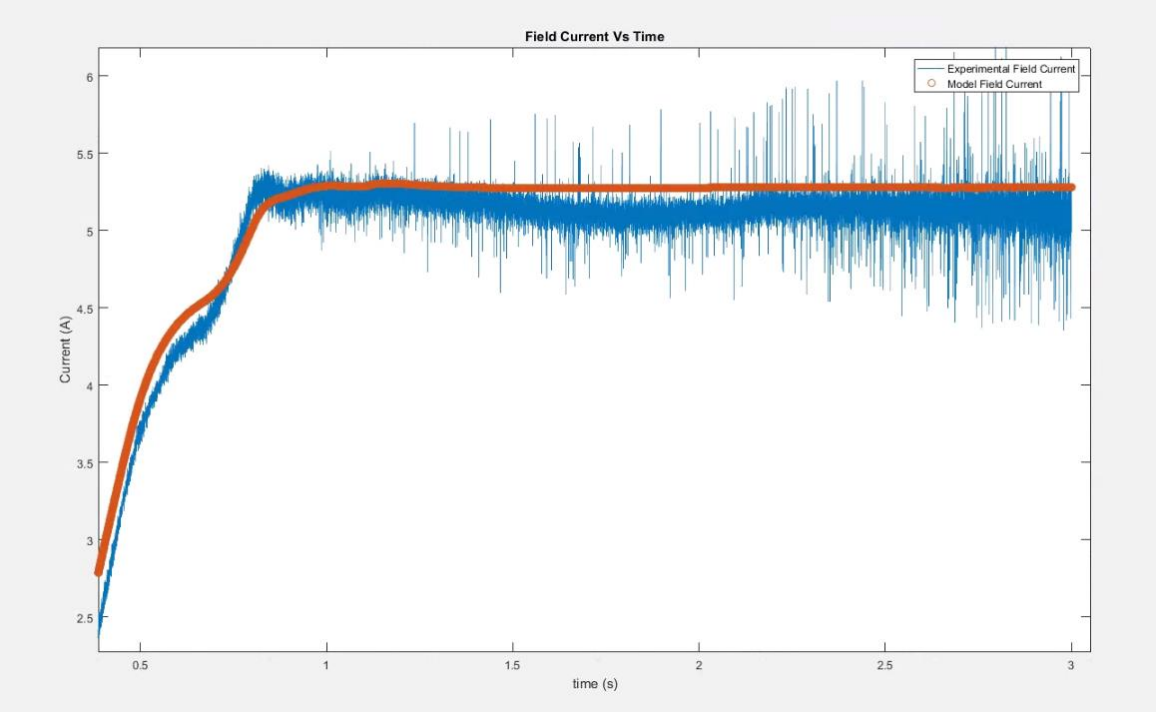

Figure 4-13 Equivalent Circuit Model Field Current Vs Experimental Field Current as the alternator accelerates from 0RPM to 6000 RPM

4.1.5 Summary

In this Section 4.1, each component's contribution to the alternator model is explained. Due to the capability of the tester and the closed casing of the alternator, it is very difficult to extract all needed measurements to implement and tune a complete alternator model. To overcome these issues, assumptions were defined on model inputs such as phase voltages, field voltage, conduction state of rectifier bridge diodes, etc. Likewise, the artificial measurements for electrical rotor angle and individual phase currents were derived from existing sensors. Unfortunately, the introduction of these solutions has produced uncertainty. A novel approach is discussed in Section 4.2 that uses existing advanced estimation theory to eliminate modelling error.

4.2 Advanced Estimation Theory

Simplifying the governing equations (Equation 2.3.3.21 and Equation 2.3.3.22) for the alternator FEM model has allowed modelling uncertainty to enter the system. Thus, a nonlinear state estimation approach must be applied to the model. This section describes estimation methods that combine nonlinear filters to maintain both accuracy and robustness.

4.2.1 EK-SVSF

Extended Kalman Smooth Variable Structure Filter (EK-SVSF) combines the estimation accuracy of EKF while using the robustness of SVSF [25]. It is similar to the process of EKF and SVSF except the smoothing boundary layer varies (VBL). The VBL is calculated by taking the partial derivative of the a posteriori error covariance matrix (from EKF) with respect to the smooth boundary layer term [29]. VBL is a function of covariance, S_{k+1}, and a combined error vector, A_{k+1} as follows:

$$\psi_{k+1} = (A_{k+1}H_{k+1}P_{k+1|k}{H_{k+1}}^{T}{S^{-1}}_{k+1})^{-1} \qquad \text{Equation 4.2.1.1}$$

Where $P_{k+1|k}$ is a priori error covariance and H_{k+1} is the measurement matrix. The new boundary layer is recalculated at every iteration and compared to a user defined boundary limit, ψ_{lim}. As depicted in Figure 4-14, within the boundary limit the EKF gain is used to correct the state estimates, conversely, outside the boundary limit the SVSF gain is applied instead [29]. This is beneficial as EKF is desirable within the existence subspace for its estimation accuracy. Otherwise, SVSF must be used to maintain robustness within the system.

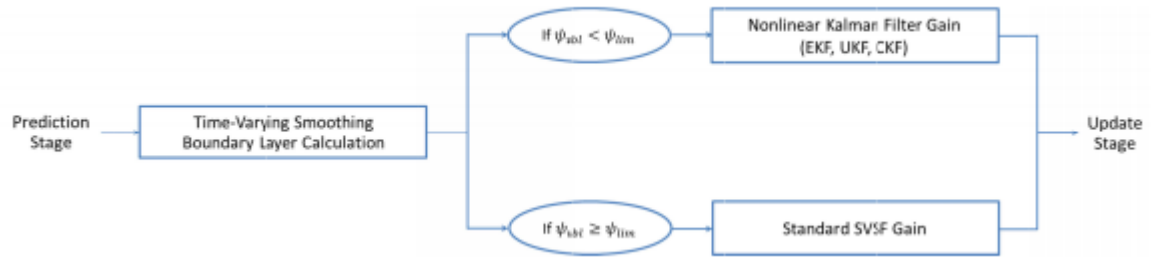

Figure 4-14 Method of combining Nonlinear Filtering Strategies [29]

The complete set of EK-SVSF's predictor-corrector equations are displayed in Figure 4-15.

Time Update (Predict)

$$\hat{x}_{k+1|k} = f(\hat{x}_{k|k}, u_k)$$

$$P_{k+1|k} = F_k P_{k|k} {F_k}^T + Q_k$$

$$e_{z,k+1|k} = z_{k+1} - H_{k+1}\hat{x}_{k+1|k}$$

Measurement Update (Correct)

$$S_{k+1} = H_{k+1} P_{k+1|k} {H_{k+1}}^T + R_{k+1}$$

$$A_{k+1} = \left(\left|e_{z,k+1|k}\right| + \Upsilon * \left|e_{z,k|k}\right|\right)$$

$$\psi_{k+1} = (A_{k+1} H_{k+1} P_{k+1|k} {H_{k+1}}^T {S^{-1}}_{k+1})^{-1}$$

$$\begin{cases} K_{k+1} = P_{k+1} {H_{k+1}}^T {S^{-1}}_{k+1}, if\ \psi_{k+1} < \psi_{lim} \\ K_{k+1} = H^{-1} diag\left[(A_{k+1}) * sat\left(\frac{e_{z,k+1|k}}{\psi}\right)\right]\left[diag(e_{z,k+1|k})\right], if\ \psi_{k+1} \geq \psi_{lim} \end{cases}$$

$$\tilde{y}_{k+1} = z_{k+1} - h(\hat{x}_{k+1|k})$$

$$\hat{x}_{k+1|k+1} = \hat{x}_{k+1|k} + K_{k+1}\tilde{y}_{k+1}$$

$$P_{k+1|k+1} = (I - K_{k+1}H_{k+1}) P_{k+1|k} (I - K_{k+1}H_{k+1})^T + K_{k+1} R_{k+1} {K_{k+1}}^T$$

$$e_{z,k+1|k+1} = z_{k+1} - H\hat{x}_{k+1|k+1}$$

Figure 4-15 Summary of EKSVSF equations

In the scope of this thesis, the three phase currents are the system states to estimate. The sampling rate of the ALT-198 is 200KHz for alternator output values, thus, the time step is 5e-6 seconds for the estimation theory.

4.2.2 Dual Extended Kalman Filter

The Dual Extended Kalman Filter (DEKF) is a sophisticated estimation method that combines to Extended Kalman Filters. One of the filters is in charge of estimating the system states, as usual, and the other is used for weight estimation. Note, weights refer to the constant parameters within a model. For example, in $y = mx + b$, m and b would be considered weights. Every time step, the two filters work together and use the previous system states, weights and measurements to compute the next step's system states and weights. A depiction of this process is shown in Figure 4-16.

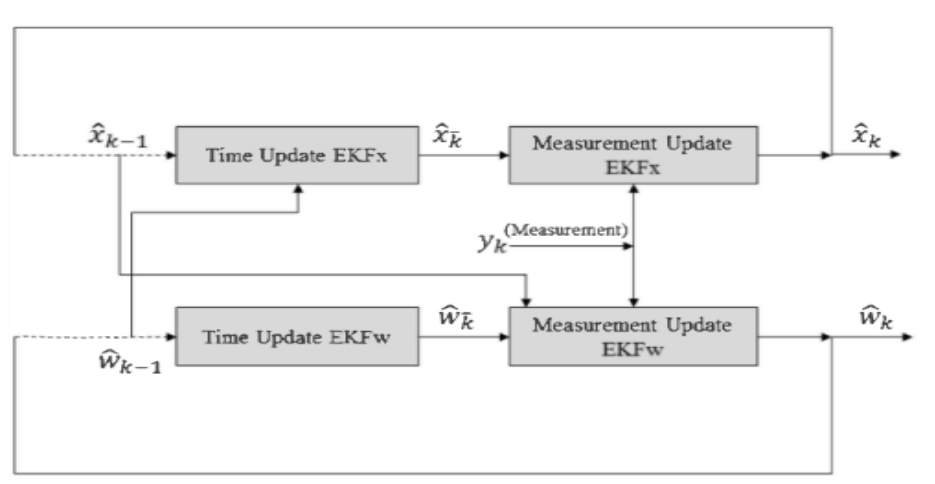

Figure 4-16 Visual Depiction of DEKF [43]

This method is very computationally expensive as the filters mutually give and take data to estimate unknown states and parameters [44]. However, this computational complexity leads to the incredible accuracy achievable by the

algorithm. The system state estimation is done with a regular EKF approach as summarized in Figure 3-2. It is the estimation of the system parameters that increases the complexity. Consider the discrete time dynamic system:

$$x_k = f(x_{k-1}, w) + p_k \quad \text{Equation 4.2.2.1}$$

$$y_k = h(x_k, w) + m_k \quad \text{Equation 4.2.2.2}$$

Where w is the system parameter vector, p_k is process noise, and m_k is measurement noise. The first step it to set the parameter prediction a priori value and error covariance priori value:

$$\widehat{w}_{k+1|k} = \widehat{w}_{k|k} \quad \text{Equation 4.2.2.3}$$

$$\hat{P}_{w_{k+1|k}} = \hat{P}_{w_{k|k}} + R_{k-1}^r \quad \text{Equation 4.2.2.4}$$

Where R_{k-1}^r is a tunable parameter similar to parameter Q for regular EKF. The EKF gain is calculated as follows:

$$K_k^w = \hat{P}_{w_{k+1|k}} (C_k^w)^T [C_k^w \hat{P}_{w_{k+1|k}} (C_k^w)^T + R^e]^{-1} \quad \text{Equation 4.2.2.5}$$

Where R^e is a tunable parameter and $C_k^w$is calculated through a Jacobian Matrix:

$$C_k^w \triangleq C \frac{\partial \hat{x}_{k+1|k}}{\partial w}\bigg|_{w=\widehat{w}_{k+1|k}} \quad \text{Equation 4.2.2.6}$$

Where C_k^w is the change rate of state for system parameter vector at the current time step [43]. The gain and priori state error are then used to compute the parameter prediction posteriori:

$$\hat{w}_{k+1|k+1} = \hat{w}_{k+1|k} + K_k^w(y_k - C\hat{x}_{k+1|k})$$ Equation 4.2.2.7

Concluding the DEKF procedure for that time step. A summary of DEKF is shown in Figure 4-17.

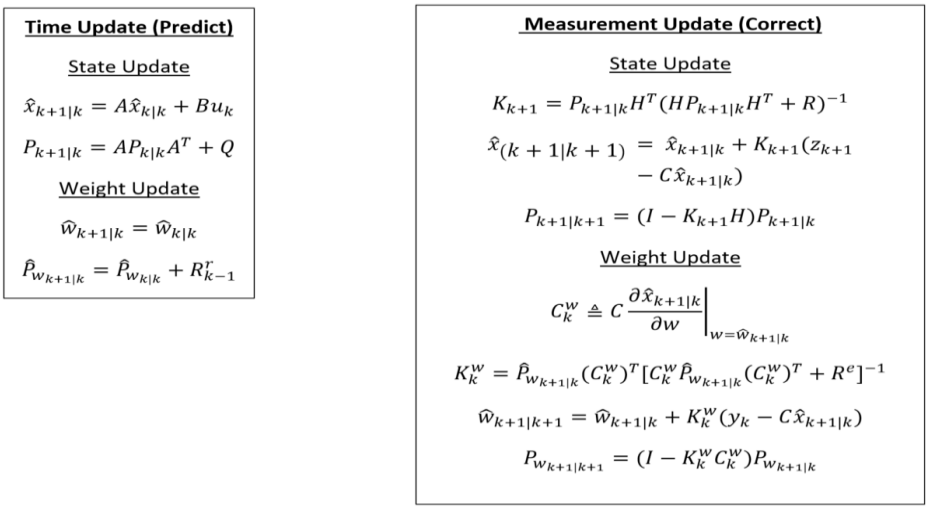

Figure 4-17 Summary of DEKF Equations

In the scope of this thesis, the three phase currents are states handled by the state estimator, and parameters *R*, *L*, and *M* are the parameters handled by the parameter estimator .

4.3 Observability

Observability is required to monitor states of a system. Sensors are used in an attempt to measure/monitor system states. In certain situations, the states are not directly accessible and therefore, the output of the system must be observed in an effort to estimate the states that are not directly measured. A system is considered completely observable if the states can be uniquely extracted from measured signals. An observability matrix can be obtained from the state space model. The

system is observable if this matrix is of full rank. The rank of a matrix is defined as either the maximum number of linearly independent column or row vectors, depending which value is smaller. If the system is not completely observable, then the unobservable states cannot be monitored and this implies that certain state cannot be uniquely extracted from measurements[45]. Consider a linear discrete time system with a description in state space:

$$x_{k+1} = Ax_k + Bu_k \quad \text{Equation 4.3.1}$$

$$z_{k+1} = Cx_{k+1} + Du_k \quad \text{Equation 4.3.2}$$

The observability matrix can be computed as

$$O(H, A) = \begin{bmatrix} H \\ HA \\ \vdots \\ HA^{-1} \end{bmatrix} \quad \text{Equation 4.3.3}$$

Where H is the measurement matrix. Complete Observability can be concluded if the difference of the rank of the observability matrix and the largest dimension of matrix A is equivalent to 0:

$$Complete\ Observability = \begin{cases} True, & if\ length(A) - rank(O) = 0 \\ False, & if\ length(A) - rank(O) \neq 0 \end{cases} \quad \text{Equation 4.3.4}$$

In certain conditions, partial observability can be acceptable, however, for this project it was important to ensure complete observability.

4.3.1 Nonlinear Observability

Estimating states within a system requires a completely observable model. This becomes more difficult in nonlinear systems when state space matrices are not

readily available. The Extended Kalman Filter can be used to overcome this. EKF works to compute non-linear estimates by linearizing the estimation around the current estimate at every time step (Section 3.1.2) [46]. At each iteration the system matrix A and the measurement matrix C are generated by computing the linearized Jacobian matrix of the process, $f(x)$, and measurement functions, $h(x)$:

$$A_k = \frac{\partial f(x)}{\partial x}\Big|_{x=\hat{x}_{k+1|k}} \quad \text{Equation 4.3.1.1}$$

$$C_{k+1} = \frac{\partial h(x)}{\partial x}\Big|_{x=\hat{x}_{k+1|k}} \quad \text{Equation 4.3.1.2}$$

Where the observability of the system can now be computed at each time step using equations (Equation 4.3.4).

4.3.2 Observability of System with Ripple Current as Measurement

Using Equation 2.3.3.21, the linearized system matrix for a single phase at every time step becomes

$$f(x) = I_{k+1} = I_k + \Delta t \dot{I}_k = I + -L^{-1}(RI + V) + L^{-1}(\frac{d}{d\theta_e} L_f(\theta_e)\omega_e I_f + L_f(\theta_e)\, \dot{I}_f) \quad \text{Equation 4.3.2.1}$$

Where Δt is the sampling rate. Therefore,

$$A_k = \frac{\partial f(x)}{\partial x}\Big|_{x=\hat{x}_{k+1|k}} = \frac{\partial I_{k+1}}{\partial I} = 1 - \Delta t(L^{-1}R) \quad \text{Equation 4.3.2.2}$$

The complete system matrix becomes identity,

$$A_k = \begin{bmatrix} 1-\Delta t(L^{-1}R) & 0 & 0 \\ 0 & 1-\Delta t(L^{-1}R) & 0 \\ 0 & 0 & 1-\Delta t(L^{-1}R) \end{bmatrix} \quad \text{Equation 4.3.2.3}$$

With all phase currents included. Using Equation 4.1.3.1, the linearized measurement matrix using only the experimental ripple current is:

$$h(x) = I_{DC} = G_A I_A + G_B I_B + G_C I_C \quad \text{Equation 4.3.2.4}$$

Therefore,

$$C_{k+1} = \frac{\partial h(x)}{\partial x}\Big|_{x=\hat{x}_{k+1|k}} = \frac{\partial I_{DC}}{\partial x} = [G_A \quad G_B \quad G_B] \quad \text{Equation 4.3.2.5}$$

Where conduction state G_n can be either 1 or 0. By applying the Equation 4.3.4 it is determined that observability matrix for these vectors does not have complete rank and is unobservable. This means that the ripple current alone cannot be used to estimate the states of the system and EK-SVSF is not possible.

$$\begin{aligned} &Complete\ Observability \\ &= length\left(\begin{bmatrix} 1-\Delta t(L^{-1}R) & 0 & 0 \\ 0 & 1-\Delta t(L^{-1}R) & 0 \\ 0 & 0 & 1-\Delta t(L^{-1}R) \end{bmatrix}\right) \\ &- rank\left(O\left([G_A \quad G_B \quad G_B], \begin{bmatrix} 1-\Delta t(L^{-1}R) & 0 & 0 \\ 0 & 1-\Delta t(L^{-1}R) & 0 \\ 0 & 0 & 1-\Delta t(L^{-1}R) \end{bmatrix}\right)\right) \\ &= False \end{aligned} \quad \text{Equation 4.3.2.6}$$

4.3.3 Observability of System with Phase Currents as Measurements

The ripple current equation is very nonlinear due to the conduction switching states. It is impossible to differentiate the phase currents from this one signal, and the process in Section 4.3.2 proved this. The novel method described in Section 4.4 generates artificial measurements for all the phase currents changing the linearized Jacobian measurement matrix to a much more satisfying result and solves the issue of observability:

$$C_{k+1} = \begin{bmatrix} 1 & 0 & 0 \\ 0 & 1 & 0 \\ 0 & 0 & 1 \end{bmatrix} \qquad \text{Equation 4.3.2.7}$$

Using the system matrix computed in Equation 4.3.2.3 and the new measurement matrix, a new observability matrix can be calculated. With Equation 4.3.4 it is determined that the system is completely observable. The artificially calculated phase currents can be used to estimate the states of the system with EK-SVSF for the alternator model and FDD.

$$Complete\ Observability$$

$$= length\left(\begin{bmatrix} 1-\Delta t(L^{-1}R) & 0 & 0 \\ 0 & 1-\Delta t(L^{-1}R) & 0 \\ 0 & 0 & 1-\Delta t(L^{-1}R) \end{bmatrix}\right)$$

$$- rank\left(O\left(\begin{bmatrix} 1 & 0 & 0 \\ 0 & 1 & 0 \\ 0 & 0 & 1 \end{bmatrix}, \begin{bmatrix} 1-\Delta t(L^{-1}R) & 0 & 0 \\ 0 & 1-\Delta t(L^{-1}R) & 0 \\ 0 & 0 & 1-\Delta t(L^{-1}R) \end{bmatrix}\right)\right) \quad \text{Equation 4.3.2.6}$$

$$= True$$

4.4 Converting Experimental Ripple Current to Phase Currents

The model's system states cannot be estimated with only the measured experimental ripple current as an output. An unobservable system is not sufficient for removing the parametric errors in the model. Likewise, accurate estimation of system variables is essential for the FDD method to function properly. To make the system achieve full rank, and thus observability, it needs measurements for all three phase currents. Due to limitations of the tester and the casing of the alternator, this is not possible. Artificial measurements for the system states must be derived from the sensors available. Using advanced knowledge of alternators, a novel approach is implemented to continuously extract estimated three phase current values from the experimental ripple current signal measured by the D&V Electronics Tester. This developed algorithm solves the issue of observability that is presented by the ripple current described in Section 4.3.2.

4.4.1 Theory

Extracting the three phase currents from the experimental ripple current signal was the only feasible method of obtaining observability with the sensors provided in the scope of this thesis. This idea was conceived by combining knowledge of alternators and modelling equations collected throughout the duration of the project. The ripple current is a summation of the three phase currents, but becomes nonlinear due to the diode conduction switching function that converts the AC signal to a DC signal. Therefore, a system of equations needs to convert the measured DC signal into a three phase AC signal.

As shown in Figure 4-18, Synchronous generators produce sinusoidal waves explained by fundamental principles of electromagnetic inductance. The amount of sinusoidal waves, or phases, produced is equivalent to the number of stator windings on the machine. The automotive alternator in this project is a synchronous generator with three sets of windings and will generate three sinusoidal phases when healthy. In the proposed alternator model the three phase currents are considered to be cosine waves that are 120^{o} electrically separated from each other (see Figure 4-18).

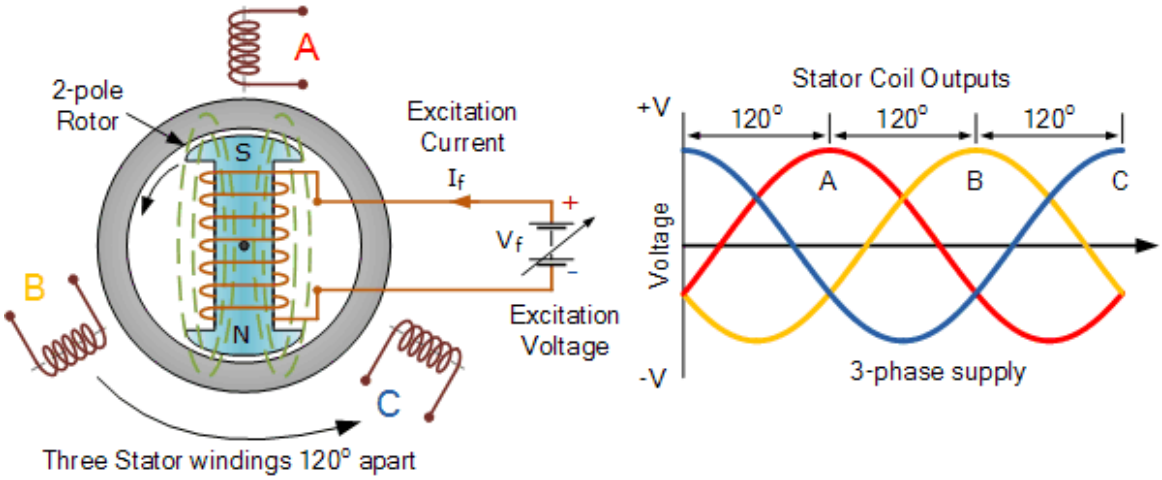

Figure 4-18 3 Phase Synchronous Generator [47]

From Section 4.1.1 it was explained that the model starts from when the first phase turns ON at 270° electrical. This was selected because cosine waves cross zero with a positive derivative at 270° signaling that the phase is going into a positive half cycle. Conversely, the cosine wave begins a negative half cycle at 90°, indicating when the phase turns OFF. It is also important to remember that a cosine wave peaks at 0° and 360°. With this information the phases' diode conduction states can be estimated based on their angle instead of their value. The three phase conduction states are calculated by adjusting Equation 4.1.3.1 as follows:

$$G_n = \begin{bmatrix} \theta_n \geq 90^o \; AND \; \theta_n < 270^o, & 0 \\ else, & 1 \end{bmatrix} \qquad \text{Equation 4.4.1.1}$$

Where G_n is the phase's diode conduction state, θ_n is the phase's shifted rotor angle, and the values 1 and 0 correspond to the phase beginning ON and OFF state respectively. Figure 4-19 displays a cosine wave and its corresponding conduction state calculated by angle. Notice, the graph is identical to Figure 4-11

where the conduction state was calculated by the phase current value.

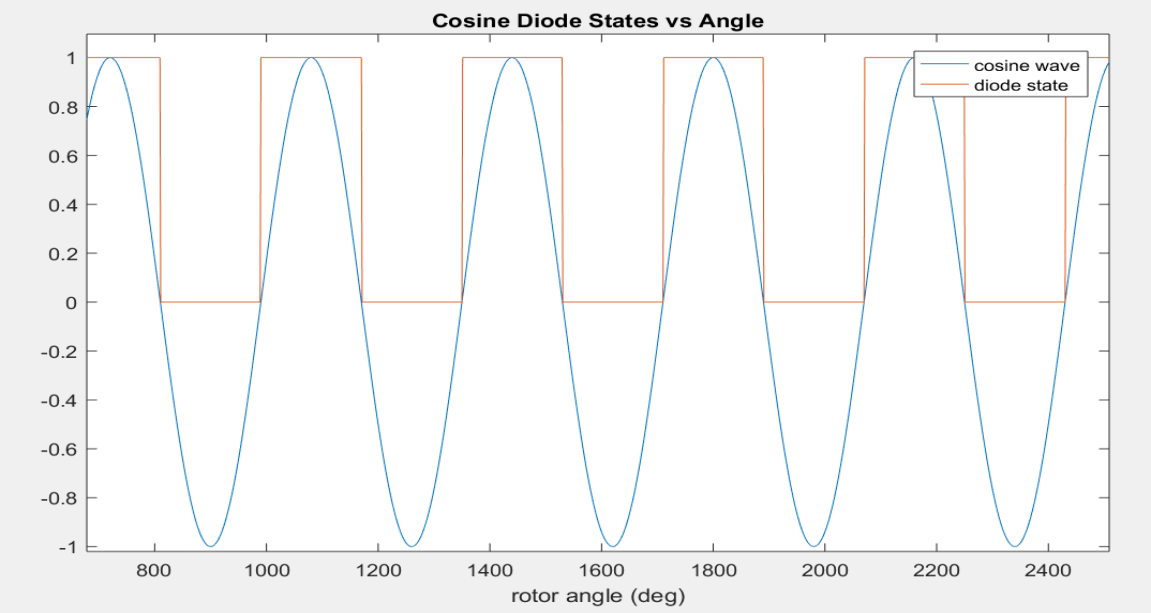

Figure 4-19 The conduction state calculated by angle instead of phase value

In addition to knowing when the phases turn on and off, the phase angles can also approximate where the peaks in the experimental ripple current are. There are two unique events that produce ripple peaks within the alternator current signal. The first event is the result of one ON phase reaching a peak value when one of the rotor poles becomes perpendicular to the ON phase's winding. At this instant, the ON phase is independently contributing to the overall ripple current, as the other two phases are off. Since the three phases are out of phase by 120^{o}, the other two phases are in the negative half cycle and therefore off when the third phase reaches its positive peak. Figure 4-20 depicts three cosine waves that are 120^{o} out

of phase and their corresponding diode states calculated with Equation 4.4.1.1.

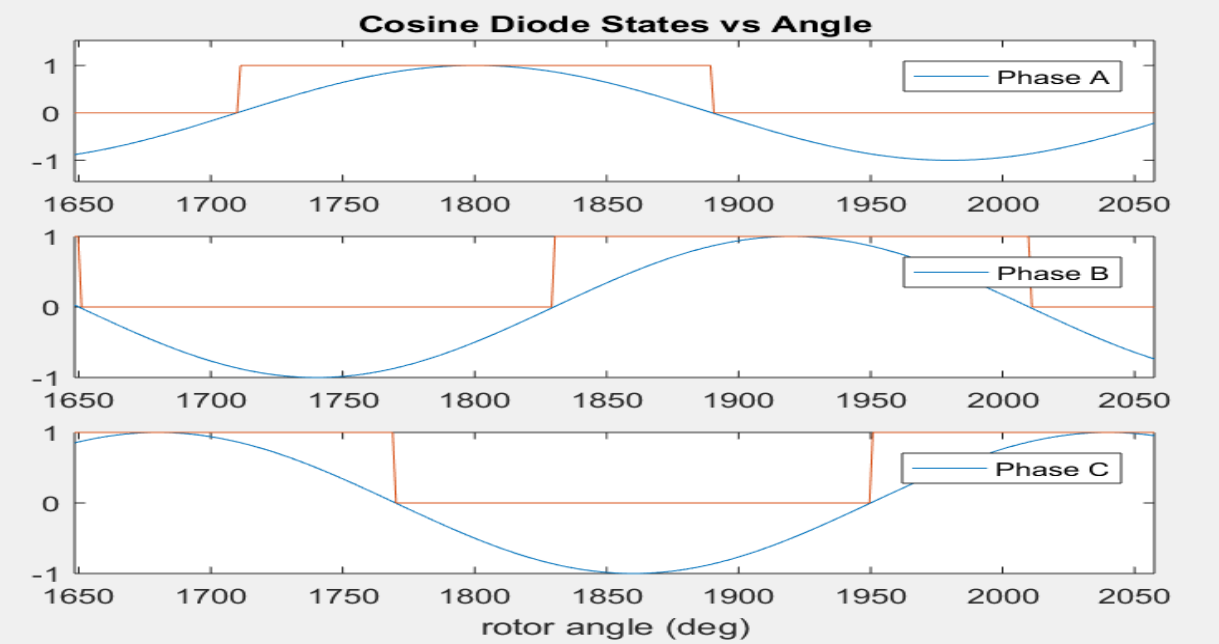

Figure 4-20 Three cosine waves 120 degrees out of phase and their corresponding conduction states

Notice at 1800^{o}, the 50th revolution, the “Phase A” cosine wave reaches its peak and the other two phases are turned off. This event occurs once a revolution per phase with a total of three per revolution for the studied alternator. The second event that causes a ripple peak occurs when one phase is off and the other two phase signals intersect halfway through their respective positive halfcycles. The ripple current is a summation of the three phases; in the instance they intersect each phase has a magnitude of half their peak amplitude. Summing the two values together equates to the peak amplitude of a single phase. This event would happen at 180^{o} in Figure 4-20. Figure 4-21 shows the six ripple peaks that would happen

every revolution in a three phase synchronous generator DC output. Now the ripple current equation (Equation 4.1.3.1) can be used to extract the three phase current signals.

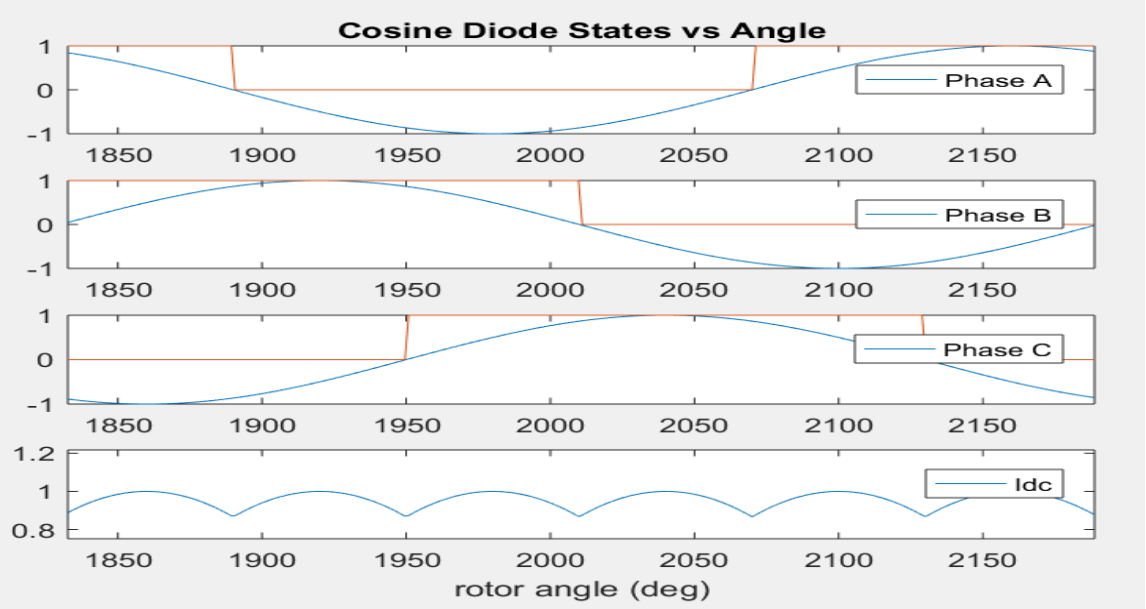

Figure 4-21 Six ripples in every revolution

The three phase current values cannot be calculated at every iteration as there is only one equation for three unknowns (this is what caused the system to be unobservable). Instead, an algorithm is implemented that attempts to identify the three phase currents' peak amplitudes every revolution. As explained before, each phase has one peak per revolution in a healthy alternator. Since the phases are 120^{o} out of phase from each other, there will be a peak every 120^{o} caused by a ON phase working independently with the other phases turned off. This is confirmed in Figure 4-21. Thus, a sample of the ripple current signal is captured

every 120^o along with the phases' angle data. Then, with three approximate peak values and their corresponding angles, simple linear algebra is used to calculate the approximate amplitudes for the phase currents. With three equations and three unknowns three phase current peaks are calculated by solving the following equations every revolution:

$$\begin{bmatrix} G_{A_1} I_{A_{peak}} \cos(\theta_{A_1}) & G_{B_1} I_{B_{peak}} \cos(\theta_{B_1}) & G_{C_1} I_{C_{peak}} \cos(\theta_{C_1}) \\ G_{A_2} I_{A_{peak}} \cos(\theta_{A_2}) & G_{B_2} I_{B_{peak}} \cos(\theta_{B_2}) & G_{C_2} I_{C_{peak}} \cos(\theta_{C_2}) \\ G_{A_3} I_{A_{peak}} \cos(\theta_{A_3}) & G_{B_3} I_{B_{peak}} \cos(\theta_{B_3}) & G_{C_3} I_{C_{peak}} \cos(\theta_{C_3}) \end{bmatrix} = \begin{bmatrix} I_{DC_1} \\ I_{DC_2} \\ I_{DC_3} \end{bmatrix} \quad \text{Equation 4.4.1.2}$$

Where θ_{m_n} and G_{m_n} denotes phase m's shifted angle and conduction state at the n^{th} sample of the current revolution respectively. I_{DC_n} denotes the n^{th} sample of the ripple current and $I_{m_{peak}}$ denotes the amplitude of m^{th}phase's cosine wave of the current revolution. The solved amplitudes are used to generate new cosine waves for the duration of current electrical revolution. The process is repeated for every revolution throughout the entire test in order to capture changes in ripple current due to changes in speed or potential faults.

4.4.2 Extracted Phase Currents Result

The result of the proposed algorithm is demonstrated in Figure 4-22.

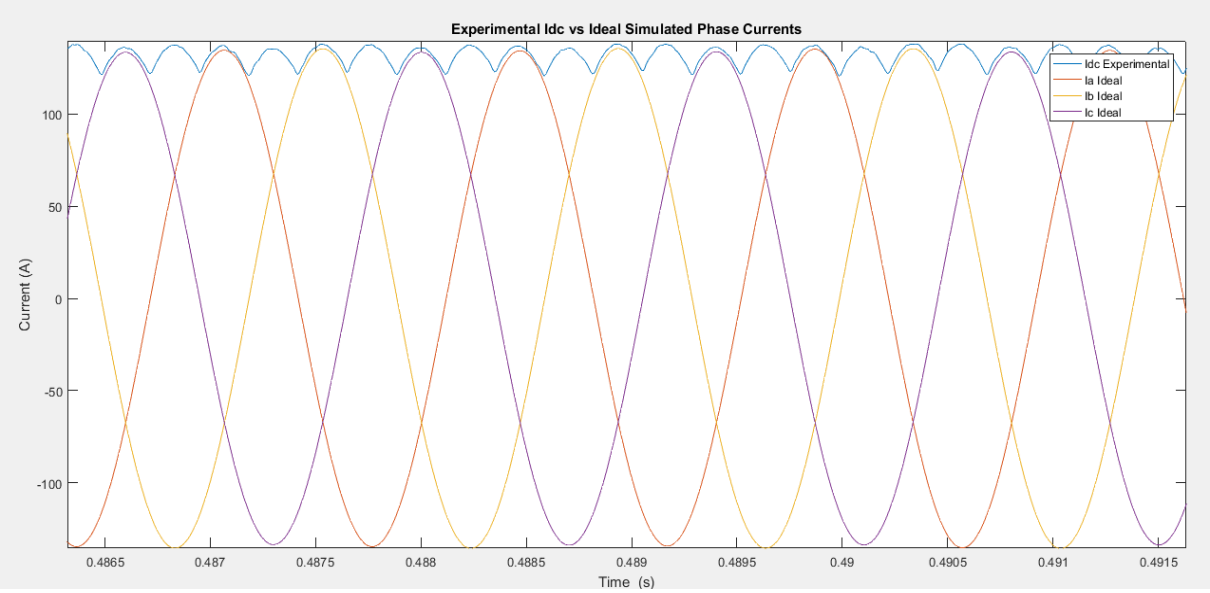

Figure 4-22 Experimental Ripple Current Vs the Simulated Phase Currents

The accuracy of this method can be tested by comparing the experimental ripple current to the summation of the three phase currents with Equation 4.1.3.1. Figure 4-23 compares the experimental data with the simulated ripple current. The proposed algorithm functions well and yields an RMS error of +/-1.05% and a max error of 4.18%.

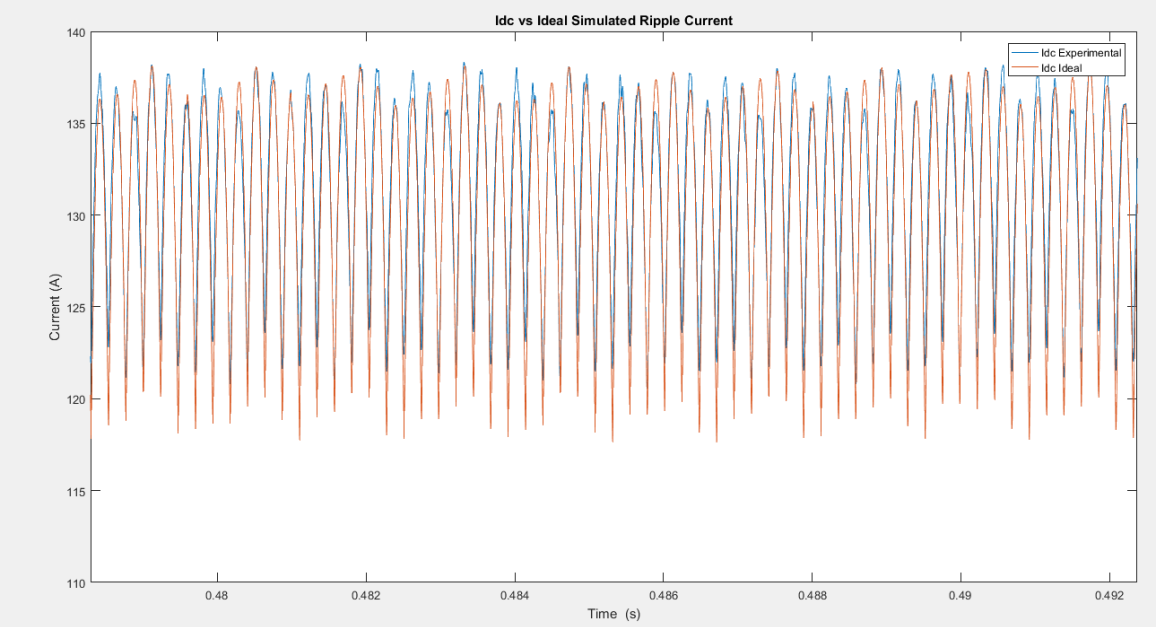

Figure 4-23 Experimental Current Vs Simulated Ripple Current

The artificial measurements for the three phase currents prove to be very accurate and are viable to use as measurements for estimation. With a completely observable system, EK-SVSF can be used for fixing the parametric error of the proposed model and will be used for parameter estimation FDD.

Chapter 5 Results and Discussion

5.1 Model Results

The ideal for this project was to create a model that could be generally used to model and perform FDD on any three phase Lundell alternator placed into the tester machine. This is why the proposed model is a collection of assumptions and simplifications placed on the governing equations used for FEM analysis. However, to use this algorithm on any Lundell alternator a system must be in place to extract values of the system parameters from a healthy sample. Moreover, generalization and lack of information leads to large modelling errors that need to be addressed. This section describes a genetic algorithm used to initialize any Lundell alternator and the comparison of two advanced estimation theories on the proposed alternator model.

5.1.1 Genetic Algorithm Results

In this thesis the parameters to estimate are the stator resistance, R, the stator self inductance, L, and the mutual stator-rotor inductance, M. The first step was to initialize boundaries of the unknown values. Feasible boundaries were successfully constructed from knowledge of alternators and literature. Each parameter was given an initial estimate within their boundaries. Next the population and generation size were initialized to 1000 and 100, respectively. Then, the fitness function, also considered an objective function, was selected. For parameter identification the objective function is targeted at minimizing the error between the model output and

the experimental output. Thus, the chosen objective function was a cumulative sum of the squared error between the model phase current, $\hat{I}$, and the experimental ideal phase current, I, shown in Equation 5.1.1.1.

$$min \int_0^T (I(t) - \hat{I}(t))^2 dt \qquad \text{Equation 5.1.1.1}$$

Initial boundaries and values had to be selected for each parameter before starting the genetic algorithm. Parameter *R* and *L* were able to be approximately measured. All three values (*R*, *L* and *M*) were further validated by comparing their boundaries and their final results to the findings of Dr. Scacchioli [22]. Parameter *R* is related to the resistance of the stator winding and should not generate a lot of power loss, therefore, the lower boundary was 0 and the higher boundary was decided to be 0.5. Parameter *L* is related to the inductance of the stator winding and should be within the µH range, therefore, the lower boundary was 5e-7 and the higher boundary was decided to be 9e-4. Parameter *M* is related to the mutual rotor-stator inductance of the stator winding and varies widely depending on the alternator, therefore, the lower boundary was 0 and the higher boundary was decided to be 6e-4. In this application, the most fit individuals have the smallest fitness value. This procedure is repeated by the total population size every generation. The result is an accurate estimation for the unknown parameters within the system.

5.2 Final Alternator Model with EK-SVSF

Figure 5-1 and Figure 5-2 demonstrate the deviance of the proposed unfiltered model from the extracted phase current and ultimately the experimental ripple current. With no estimation theory, the model yields a RMS error of 5.89% with a max error of 15.70% between extracted phase and modelled phase and RMS error of 2.66% with max error of 12% between ripple current signals. The tuning parameters Υ, ψ, P_{init}, Q, and R were determined through trial and error:

$$\Upsilon = 0.2, \psi = 50, P_{init} = 1e-4, Q = 1e-5, R = 1e-3,$$

Each phase received the same parameters to perform EK-SVSF.

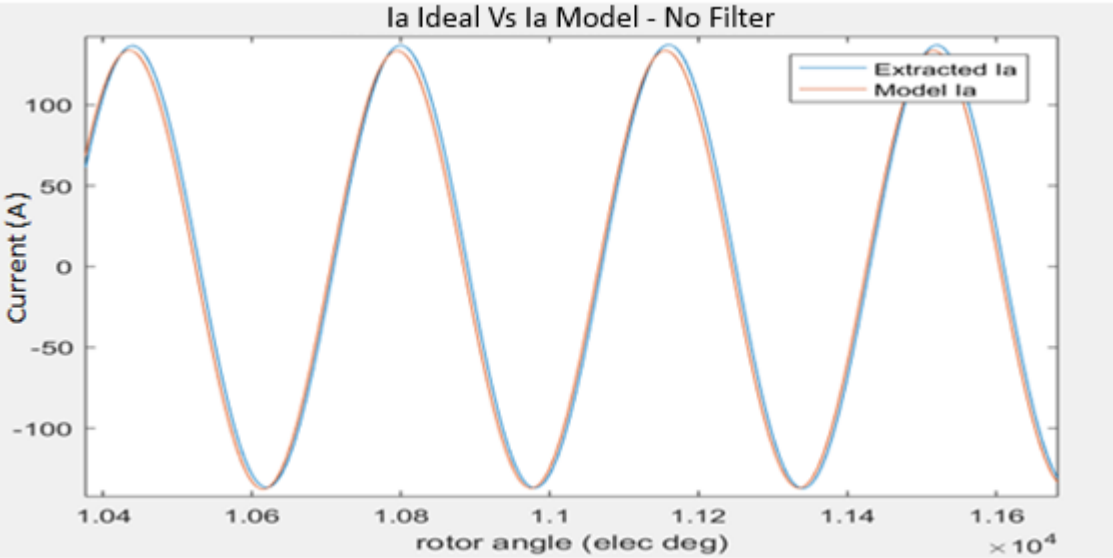

Figure 5-1 Extracted Phase Current Vs The Model Phase Current – No Filter

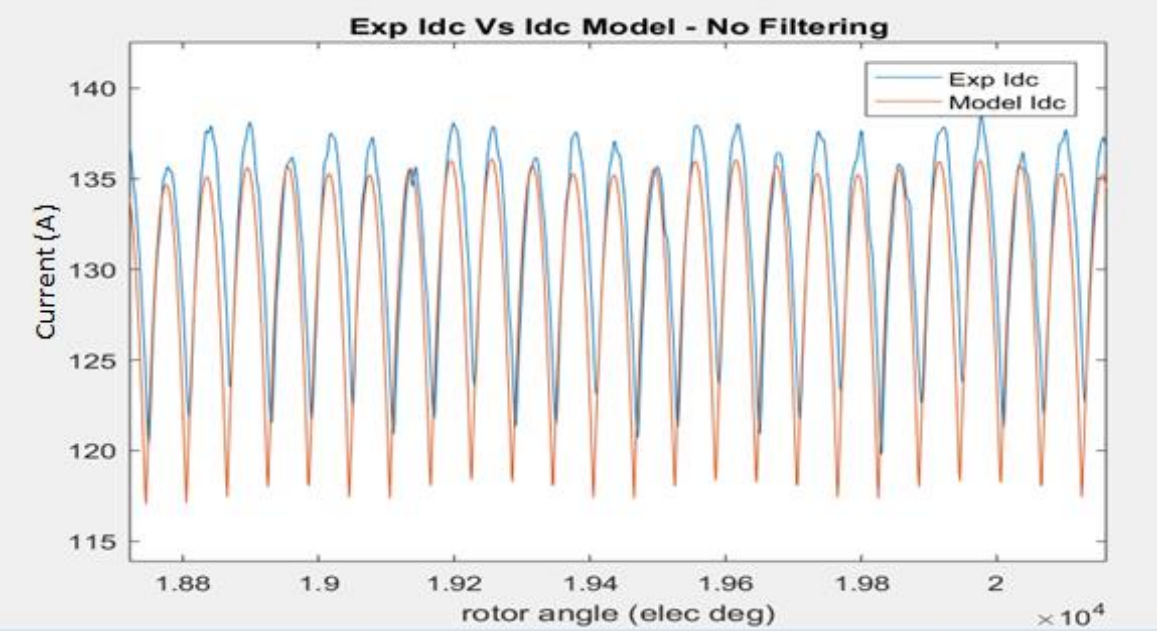

Figure 5-2 Experimental Ripple Current Vs Modelled Ripple Current - No Filter

These results are summarized in Table 3.

Table 3 Summary of Model vs Experimental - No Filter

	Extracted Phase Current Vs Modelled Phase Current	***Experimental Ripple Current Vs Modelled Phase Current***
RMS Error %	**5.89**	**2.66**
Max Error %	**15.70**	**12**

Applying estimation theory to the model allows the measured signals to contribute to the estimation of the system states. This concept is used to remove measurement and process noise from a system. As shown in Figure 5-3 and Figure

5-4, implementing EKSVSF on the proposed model significantly increases accuracy. Between the extracted phase current and model phase current, the RMS error is +/- 1.18% with max error of 1.170%. Comparing the experimental ripple current and the simulated model ripple current obtained an RMS errror of 2.3% with max error of 5.19%. These results are summarized in Table 4.

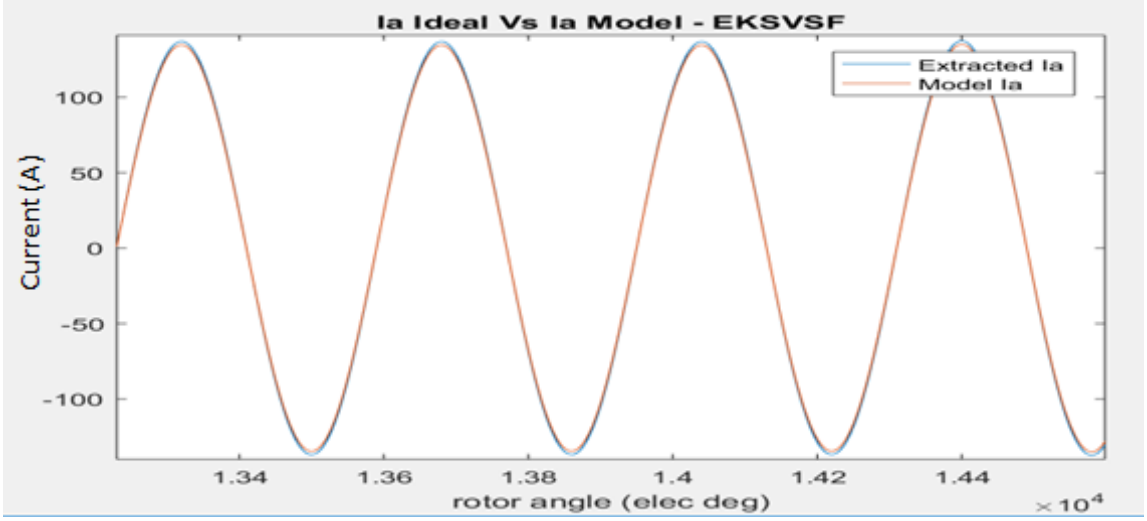

Figure 5-3 Extracted Phase Current Vs Modelled Phase Current with EKSVSF

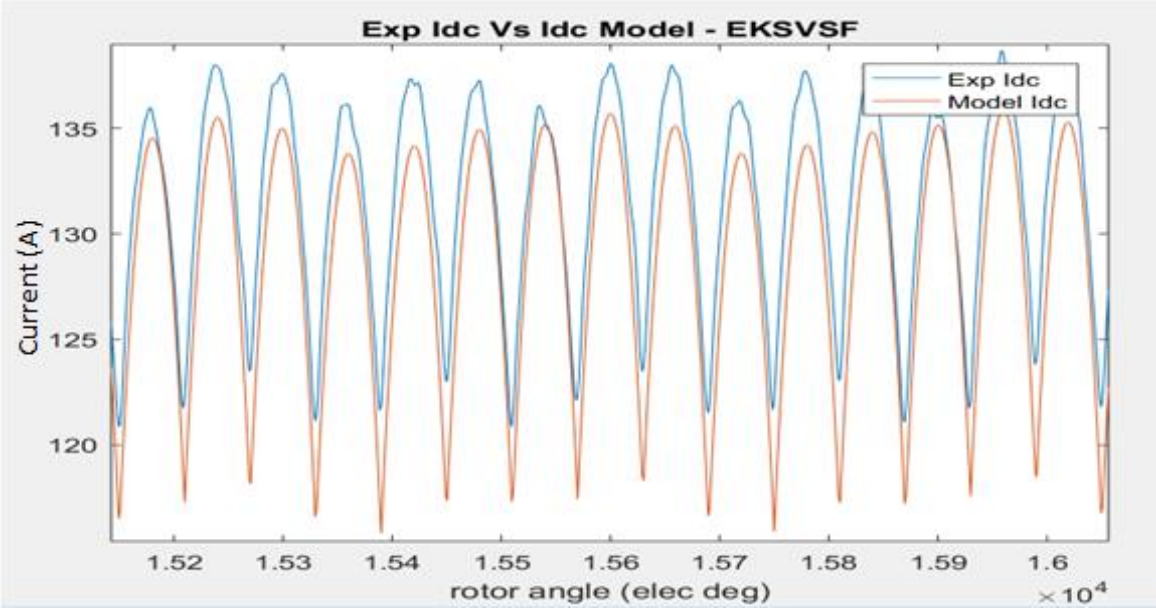

Figure 5-4 Experimental Ripple Current Vs Model Ripple Current with EKSVSF

Table 4 Summary of Model vs Experimental - EKSVSF

	Extracted Phase Current Vs Modelled Phase Current	***Experimental Ripple Current Vs Modelled Phase Current***
RMS Error %	**1.18**	**2.3**
Max Error %	**1.17**	**5.19**

With increased accuracy and robustness, the model can be run on the D&V Tester to provide a visual difference between the experimental and estimated results. An

experienced operator can use this visual to determine the health of the alternator without the use of any FDD.

5.2.1 DEKF Ripple Current Estimation Results

The Dual Extended Kalman Filter (DEKF) was implemented for a comparative analysis against the EK-SVSF model. The fundamental difference between the EK-SVSF and DEKF estimation methods is DEKF's ability to estimate system parameters as well as system states. This advantage allows the model to become increasingly more accurate as the system parameters converge to their true value. Like the EK-SVSF model, each phase current is modelled individually. Therefore, per phase:

$$x = I_n \qquad \text{Equation 5.1.3.1}$$

$$w = [R_n, L_n] \qquad \text{Equation 5.1.3.2}$$

Where x is the system states for estimation, w is the system parameters for estimation and n is the phase. The tuning parameters $Q, R_x, P_{x_{init}}, R_e, R_r, P_{w_{init}}$ were determined through trial and error:

$Q = 1e-5$, $R_x = 1e-3$, $P_{x_{init}} = 1e-4$,

$R_e = 2e-1$, $R_r = \begin{bmatrix} 1 & 0 \\ 0 & 1e-5 \end{bmatrix}$, $P_{w_{init}} = \begin{bmatrix} 1e-4 & 0 \\ 0 & 1e-4 \end{bmatrix}$

Figure 5-5 and Figure 5-6 depict the estimation power the DEKF method possesses. Between the extracted and model phase current, the RMS error is +/- 0.097% with max error of 0.489%; comparing the experimental and model ripple

currents concluded an RMS errror of 1.11% with max error of 3.96%. These results are summarized in Table 5.

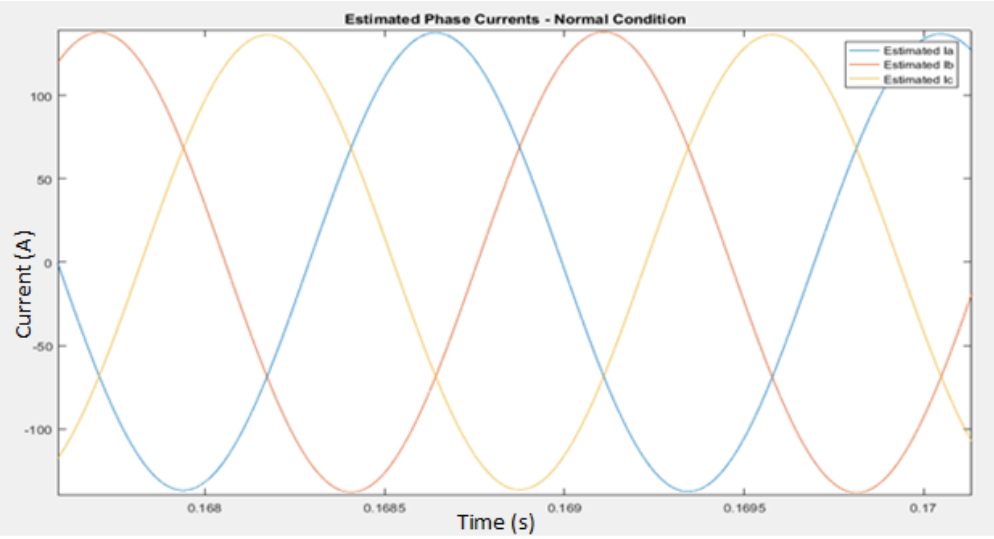

Figure 5-5 Estimated Phase Currents - DEKF

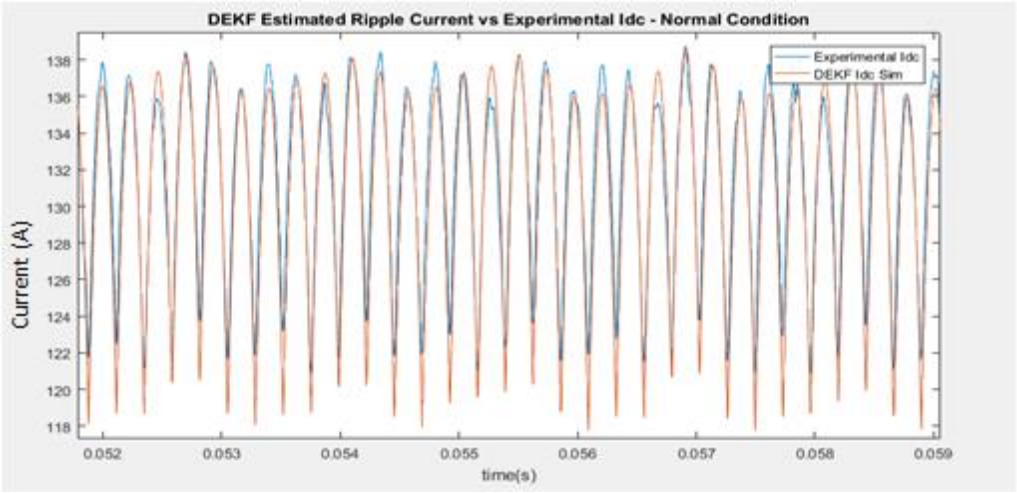

Figure 5-6 Experimental Ripple Current Vs Model Ripple Current with DEKF

Table 5 Summary of Model vs Experimental – Dual Extended Kalman Filter

	Extracted Phase Current Vs Modelled Phase Current	***Experimental Ripple Current Vs Modelled Phase Current***
RMS Error %	**0.097**	**1.11**
Max Error %	**0.489**	**3.96**

Comparing the results from the Section 5.2, DEKF yields a 107.2% better accuracy than the proposed EKSVSF model. Although significant, DEKF's accuracy comes with a large computational cost that makes it unfeasible for End of Line tester and the scope of this project. For this reason, the proposed EKSVSF model will be implemented on the D&V Tester for modelling and FDD functionality. Table 6 compares the results from the two proposed estimation methods.

Table 6 EKSVSF vs DEKF For 3s of Experimental Data

	Model with EKSVSF	***Model with DEKF***
RMS Error %	**2.3**	**1.11**
Computation Time (s)	**0.495**	**15.95**

5.3 Fault Detection and Diagnosis Results

In terms of alternator electrical faults, the most common include the open diode fault, shorted diode fault, and the stator imbalance fault. Section 5.3.1 described the potential threat of these faults and their effect on the overall ripple current outputted by the alternator. These effects are contained in the artificial extracted phase current measurements (see Section 4.4) and consequently will vary the estimation of the system parameters. Therefore, to perform the condition monitoring, the continuous estimation of system parameters is captured. In this research, artificial faults were programmatically simulated based on experimental data and knowledge of the faults. Parameter estimation techniques were implemented to monitor the variation of parameters R_n and L_n on each phase using the extracted phase current signals.

5.3.1 Common Alternator Faults

It is crucial that alternator faults are diagnosed before the alternator is installed in the vehicle. Failure to do so could lead to more problematic failures in the entire Electric Power Generation System (EPGS). The capability of the D&V Electronics tester has a major impact on the type of alternator faults that can be detected considering the addition of sensors is out of the scope for this project. This thesis focuses on common alternator faults that can potentially lead to complete failure including open phase fault, shorted diode fault, and unbalanced loading fault. A healthy alternator's output is displayed in Figure 5-7 as a reference.

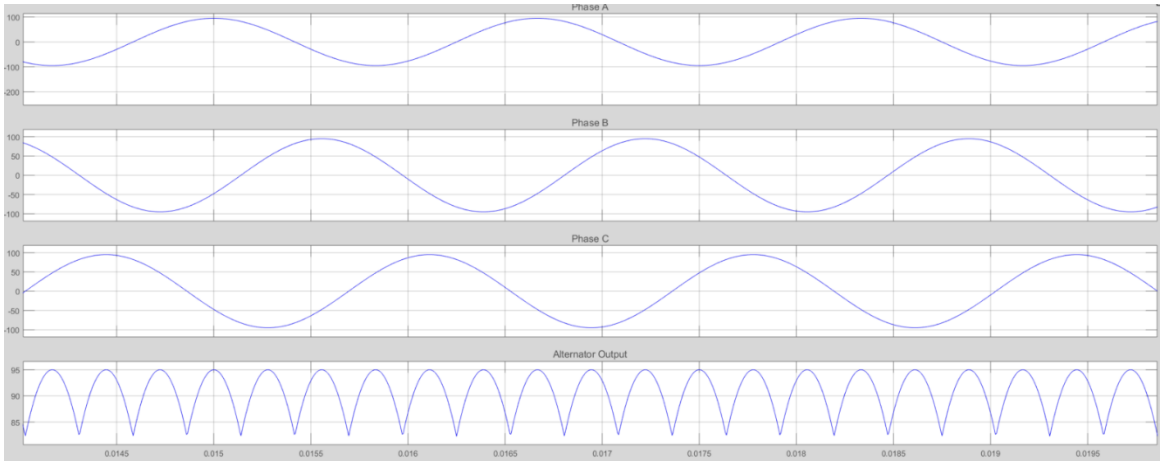

Figure 5-7: Healthy alternator's output generated in Simulink

5.3.1.1 Open Phase Fault

The most common reason for an open phase fault is a failure of diodes in the three phase bridge rectifier. As shown in Figure 5-8, an open diode leads to a loss of a phase and the output ripple current will be unbalanced. This results in a large ripple in the output voltage and current. With inconsistent voltage and the introduction of voltage spikes, the electronic in the system become at risk.

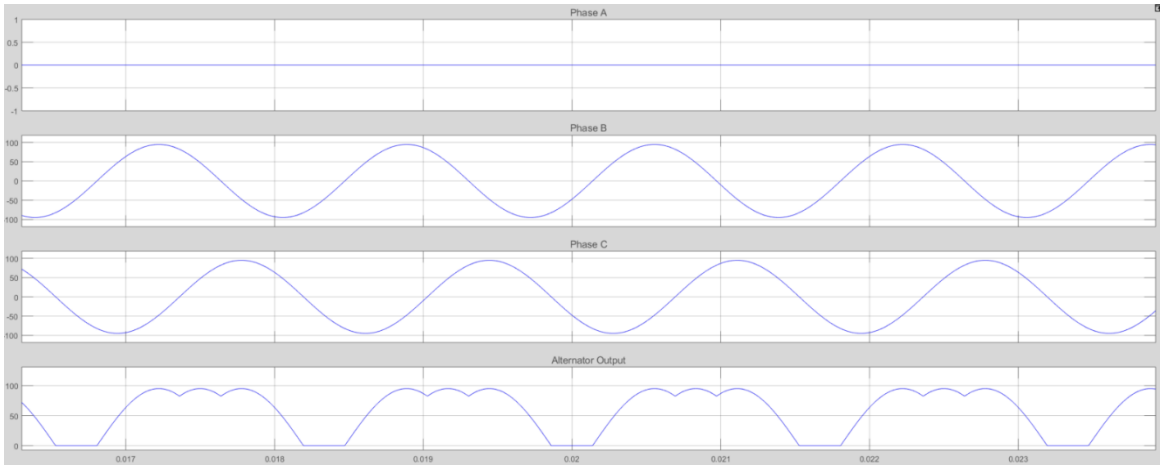

Figure 5-8 Open Diode Fault output signal. Notice the impact from the loss of phase A. Generated in Simulink

5.3.1.2 Shorted Diode Fault

The diodes are tasked with turning the phase off once it has dropped below a certain threshold. When the phase never turns off then the diode is short-circuited. Although similar to the appearance of the open diode fault, this type of diode failure is more dangerous to the EPG system of the vehicle. A shorted diode allows AC current to infiltrate the electrical system [48]. This AC power creates electrical disturbances that can damage electronic modules. In addition, the faulty diode allows current to drain out of the battery when the vehicle is stalled (see Figure 5-9). This introduction of negative power will lead to a dead battery if the vehicle is not being driven.

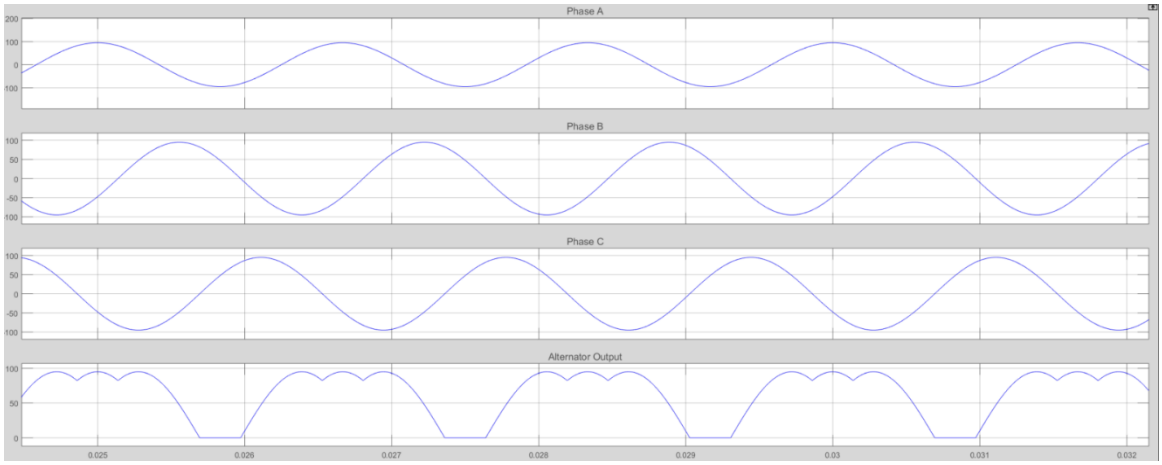

Figure 5-9: Shorted Diode Fault alternator output. Generated in Simulink

5.3.1.3 Unbalanced loading of an alternator

An alternator is considered unbalanced when there are significantly different peak currents in the phases of the alternator. Usually, in a balanced condition, the difference in peak phase current varies +/- 5%. Unbalanced loading is a symptom to other faults such as varying resistances on the stator windings or varying lengths of stator windings. This makes it a helpful indicator of diagnosing a bad alternator. Figure 5-10 shows the effects of 10% unbalanced loading on a faulty alternator output. Similar to the shorted diode fault, the electrical noise introduced in the ripple current can damage the electrical system.

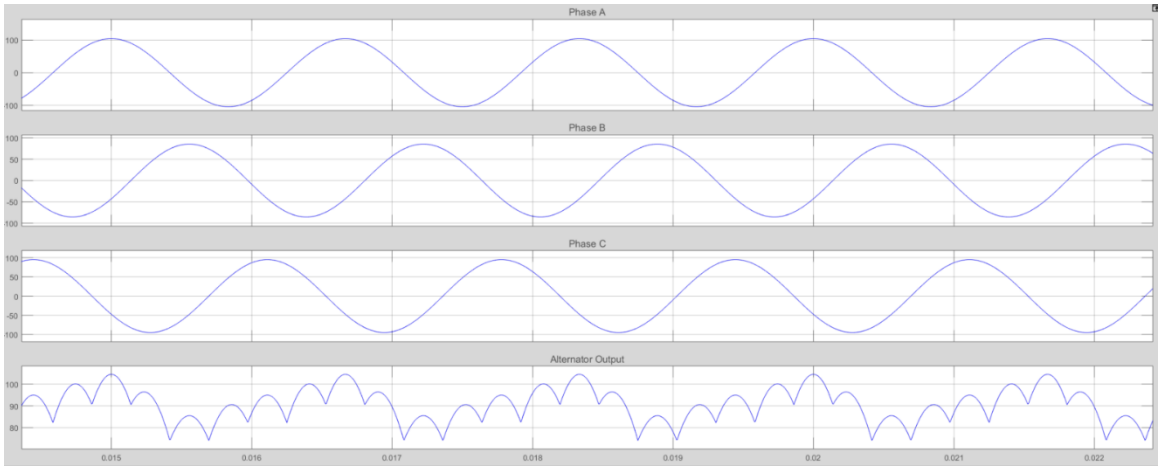

Figure 5-10: 10% Unbalanced Loading Fault. Generated in Simulink

5.3.2 FDD with EK-SVSF Model

To perform parameter estimation, the monitored parameters must become system states. The system states become:

$$x = [I_a, I_b, I_c, R_a, R_b, R_c, L_a, L_b, L_c] \qquad \text{Equation 5.3.1.1}$$

Note the system now has fewer measurements than states. In order to maintain observability, artificial measurements are created for the parameter system states. The artificial measurements are calculated using available systems from the D&V tester and the extracted phase currents to formulate a full measurement matrix; the equations are given as:

$$R_{a_{MN}} = \frac{-M\omega_{e_{MN}} I_{f_{MN}} sin\theta_{a_{MN}} - V_{a_{MN}} - L\frac{dI_{a_{MN}}}{dt}}{I_{a_{MN}}} \qquad \text{Equation 5.3.1.2}$$

$$L_{a_{MN}} = \frac{-M\omega_{e_{MN}} I_{f_{MN}} sin\theta_{a_{MN}} - V_{a_{MN}} - R_a I_{a_{MN}}}{\frac{dI_{a_{MN}}}{dt}}$$ Equation 5.3.1.3

Where MN denotes a range of values around the phase currents peak every revolution. The artificial measurements are filtered to reduce noise. Unfortunately, the artificial measurement of $R_{n_{MN}}$ produced a constant negative value for all three phases. This is can be easily explained by the amount of modelling uncertainty experienced by the proposed model. It is possible that through the defined assumptions and artificial measurements, the value of $R_{n_{MN}}$ has become a lumped parameter for other parameters that have been considered negligible, such as dampening. Likewise, the resistance values of the alternator is very small making it more susceptible to uncertainties. Instead, the absolute value of the $R_{n_{MN}}$ is used for fault detection and diagnosis. An example of $\left|R_{n_{MN}}\right|$ is shown in Figure 5-11. $L_{n_{MN}}$ did not experience the same issue and proves to be a more effective parameter to use for fault detection and diagnosis.

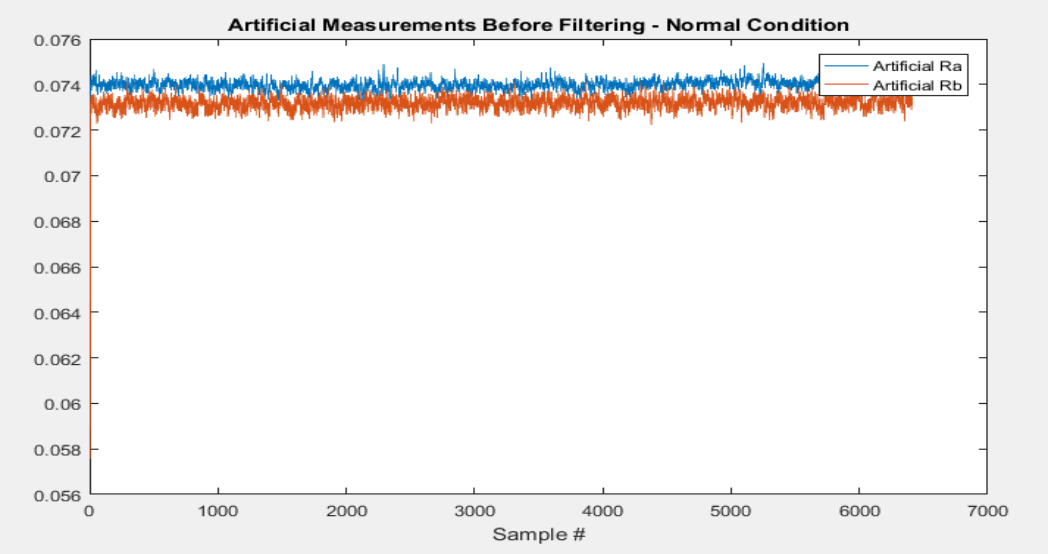

Figure 5-11 Artificial Measurement $|R_{n_{MN}}|$ *Before Estimation*

Estimation Theory is now possible as full rank is achieved with the introduction of artificial measurements. The tuning parameters for EK-SVSF on the new system states were determined through trial and error:

$\gamma = 0.1, \psi = 2,$

$Q = 1e - 8, R = 2e - 1$

These values were used on all three phases for estimating both $R_{n_{MN}}$ and $L_{n_{MN}}$.

First observe the estimated parameters in normal conditions. This to develop a reference for comparing to the faulty conditions. When the alternator is healthy, the estimated system parameters will not vary and each phase's parameters will be of

similar magnitude. Figure 5-12 and Figure 5-13 show $R_{n_{MN}}$ and $L_{n_{MN}}$ under normal condition.

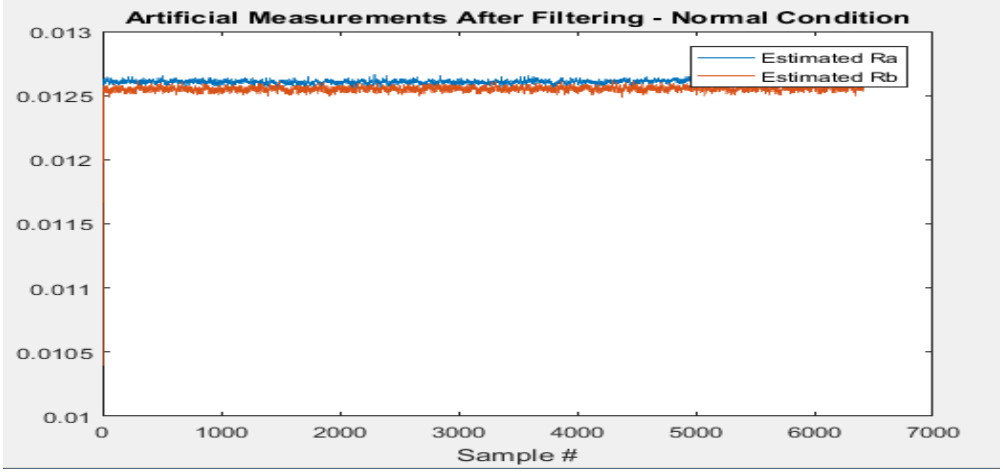

Figure 5-12 EKSVSF Estimated R - Normal Condition

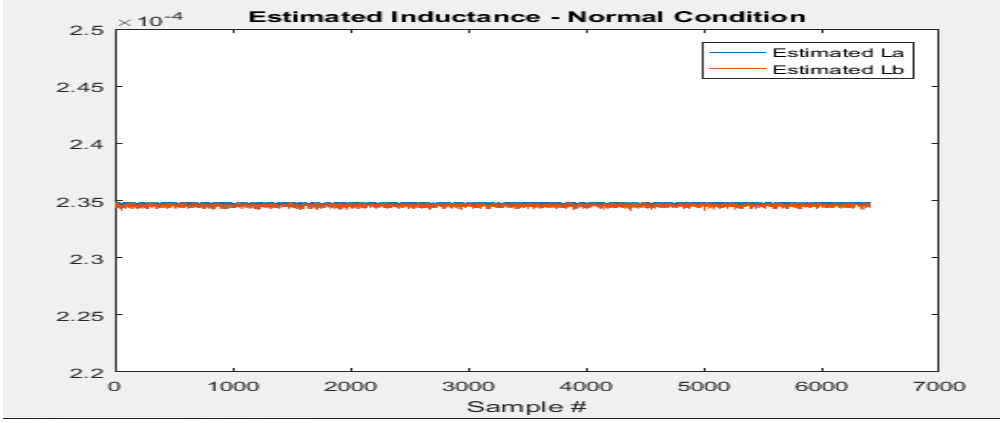

Figure 5-13 EKSVSF Estimated L - Normal Condition

Now, an open diode fault is simulated onto the experimental data. As mentioned previously, the fault is contained in the extracted phase currents and affects the calculation of the system parameter states. Figure 5-14 and Figure 5-15 depicts

the change in the system parameter states when a Phase A open diode fault is introduced to the system.

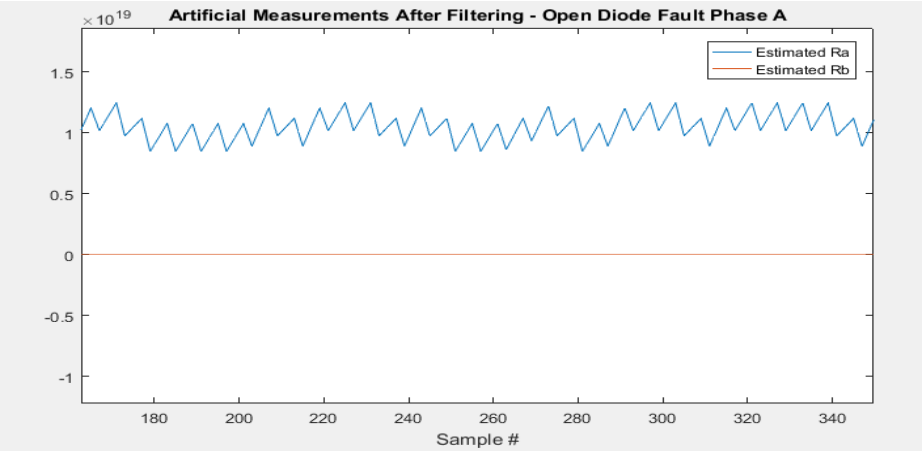

Figure 5-14 EKSVSF Estimated R – Phase A Open Diode Fault

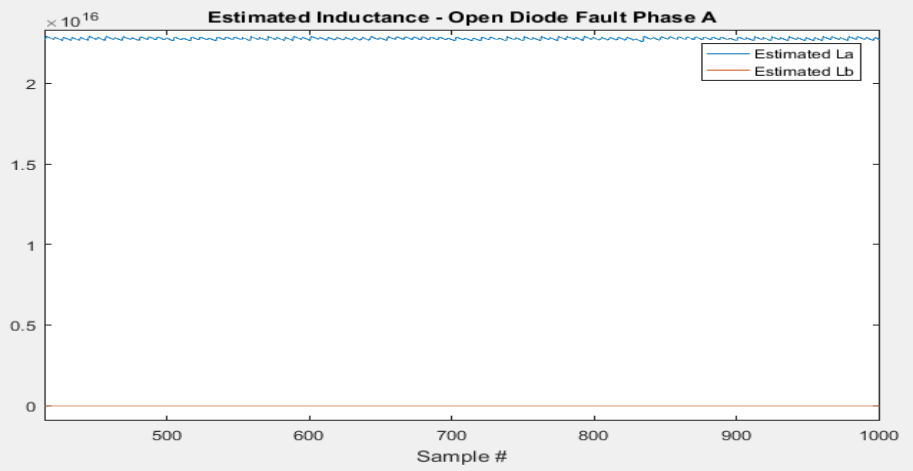

Figure 5-15 EKSVSF Estimated L - Phase A Open Diode Fault

Notice that the Phase A system parameters are significantly larger than those on Phase B running under normal condition. An open diode fault causes the effected phase to produce no current to the summation of the three phases. Thus, the

open circuit causes infinite impedance on the faulty stator winding, making the EKSVSF Phase A parameters increase towards infinity. This concludes that an open diode fault can be detected and diagnosed by the estimation of phase parameters.

The same process is followed to determine if parameter estimation is suitable for FDD on shorted diode faults. Figure 5-16 and Figure 5-17 show the results of the system parameter states when introduced to a simulated Phase A shorted diode fault.

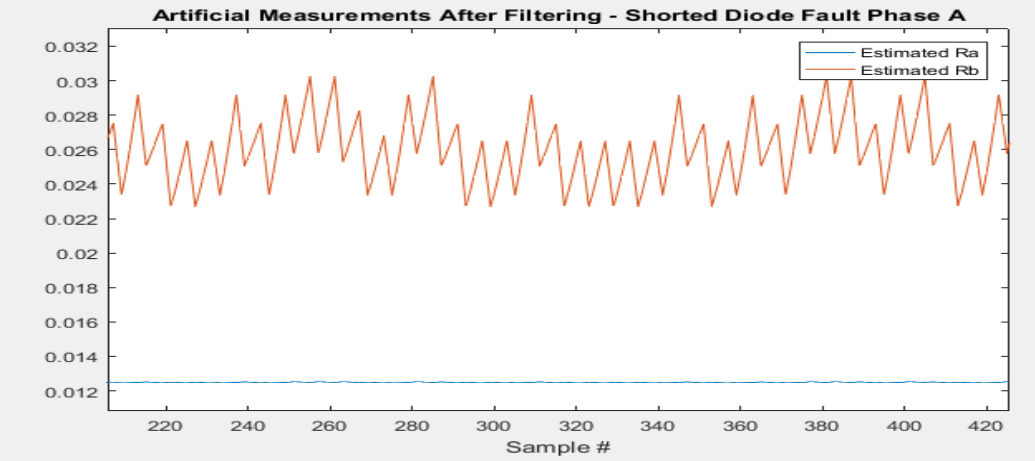

Figure 5-16 EKSVSF Estimated R - Phase A Shorted Diode Fault

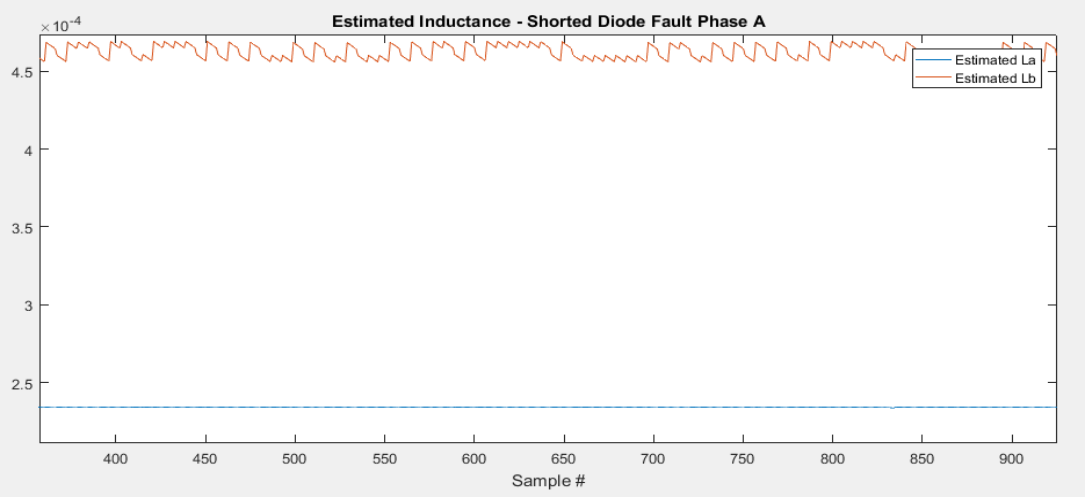

Figure 5-17 EKSVSF Estimated L - Phase A Shorted Diode Fault

Notice that the Phase A system parameters are about twice as large as those on Phase B running under normal condition. A shorted diode fault causes the effected phase to contribute current to the summation of the three phases even when the phase goes negative and the diode is supposed to be shut OFF. Thus, the faulty phase vector subtracts from the other two phases and causes their peaks to be halved. The proposed model will determine that two phases have twice the amount of impedance, making the EKSVSF Phase A parameters seem healthy, while Phase B and C parameters double. This phenomenon indicates that one of the diodes is shorted. This concludes that a shorted diode fault can be detected and diagnosed by the estimation of phase parameters.

Lastly, a stator imbalance fault is simulated to determine if parameter estimation is suitable for FDD on stator imbalance faults. Figure 5-18 and Figure 5-19 show

the results of the system parameter states when introduced to a Phase A 10% stator imbalance fault.

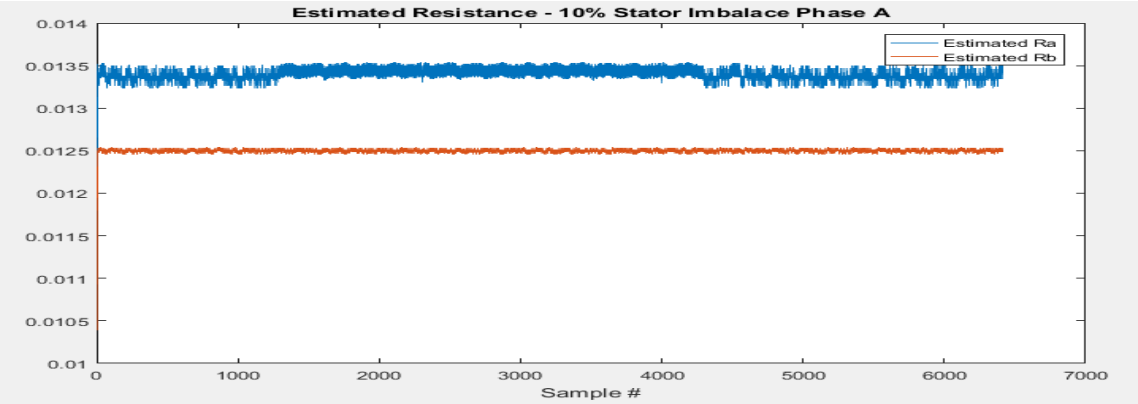

Figure 5-18 EKSVSF Estimated R - 10% Stator Imbalance Phase A

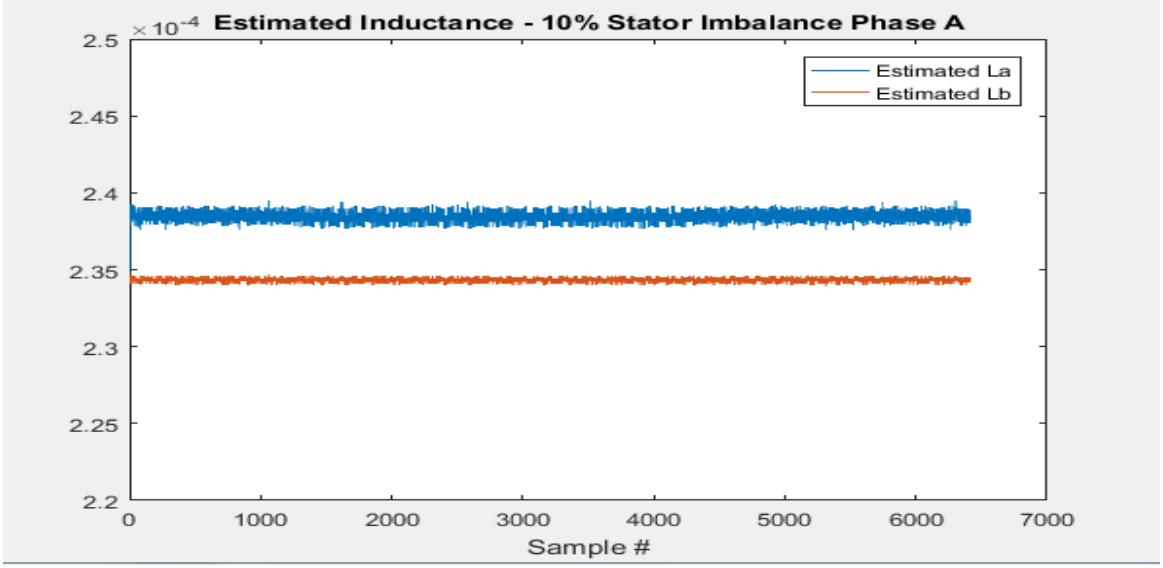

Figure 5-19 EKSVSF Estimated L - 10% Stator Imbalance Phase A

Stator imbalance faults can be caused by a variety of alternator faults that cause the phase peaks to be uneven. This makes it a very important fault to detect for.

A common reason for stator imbalance is when the stator windings of an alternator are not the same length, causing uneven peaks in the ripple current. Notice that the introduction of the fault increases the impedance of Phase A significantly enough to determine that a stator imbalance has effected the system. This slight increase or decrease in impedance, depending how the imbalance occurs, is detected by the estimation capability of the SVSF component of the filter. The EKSVSF filter uses SVSF when the VBL surpasses a boundary and this boundary is tuned to capture the smaller variations caused by a stator imbalance fault. This concludes that a stator imbalance fault can be detected and diagnosed by the estimation of phase parameters with EKSVSF.

5.3.3 FDD with DEKF Model

Initializing FDD for the DEKF model is simpler than the EKSVSF method because the parameters R and L are already calculated at every time step. There is no need for additional artificial measurements. Under normal condition the system parameters due not vary as shown in Figure 5-20 and Figure 5-21.

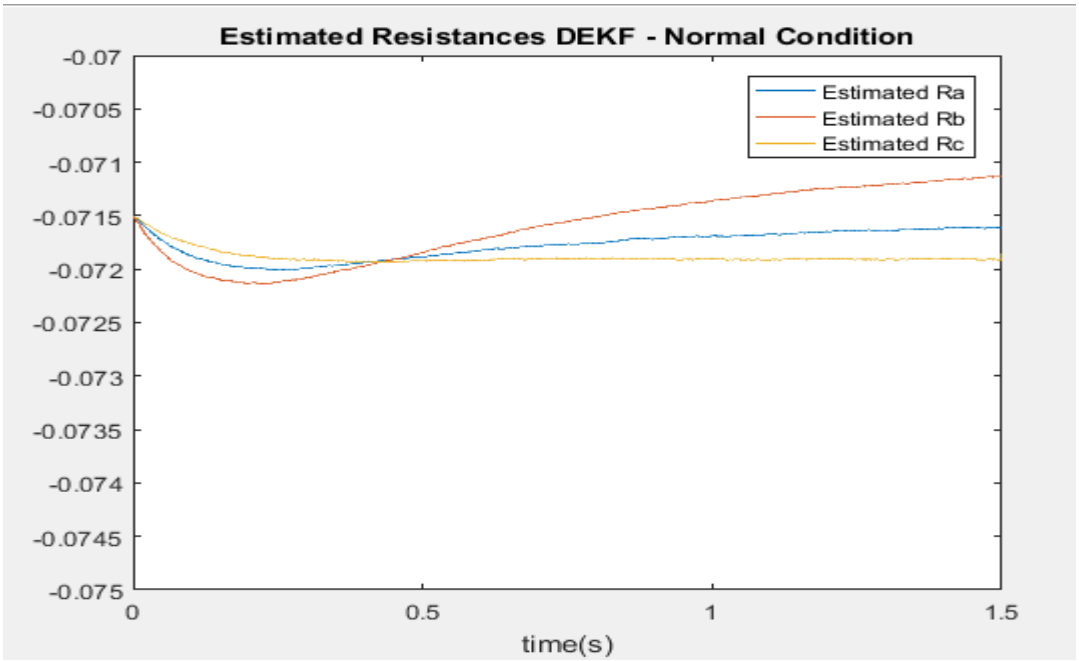

Figure 5-20 DEKF Estimated R - Normal Condition

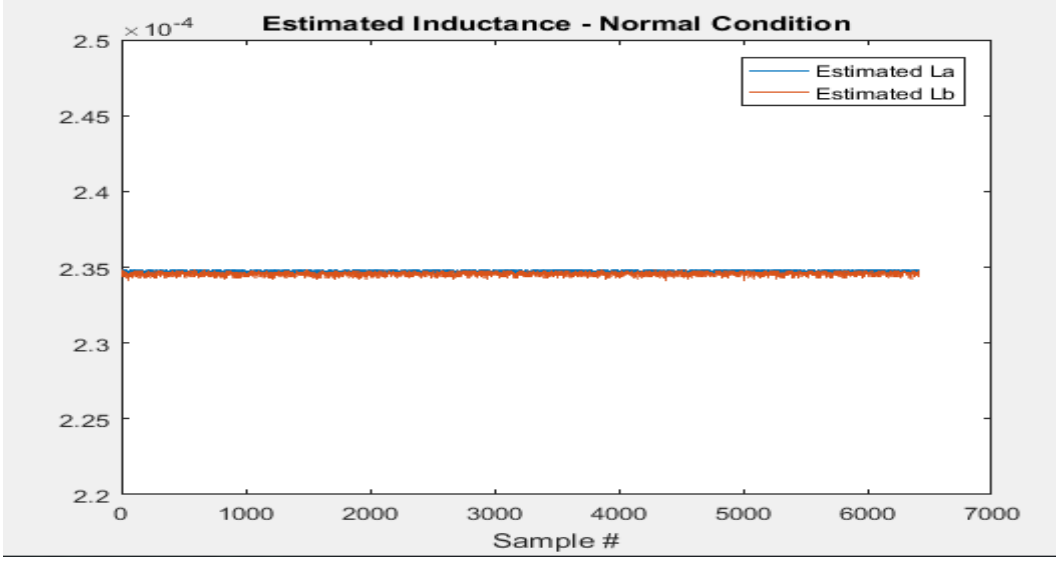

Figure 5-21 DEKF Estimated L - Normal Condition

When an open diode fault is introduced to the system on Phase A, the system parameters attempt to converge to a new value, shown in Figure 5-22 and Figure 5-23.

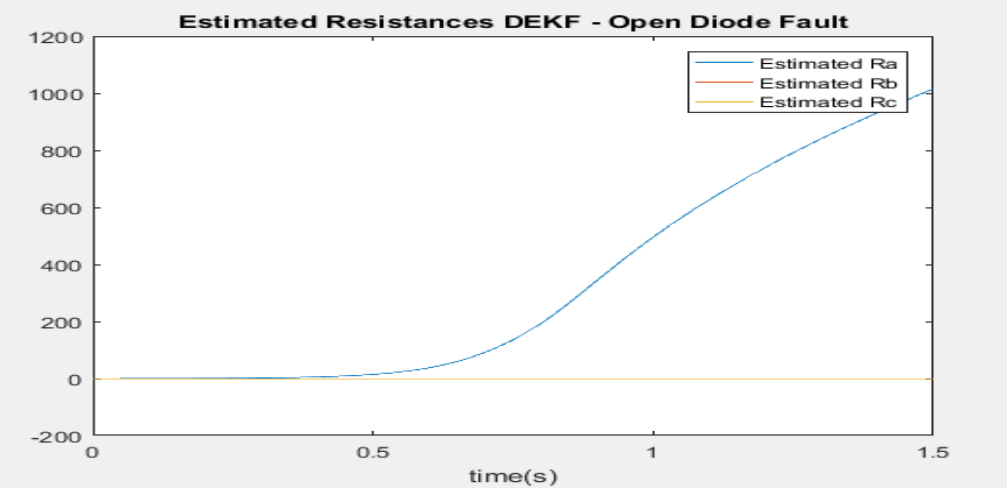

Figure 5-22 DEKF Estimated R – Phase A Open Diode Fault

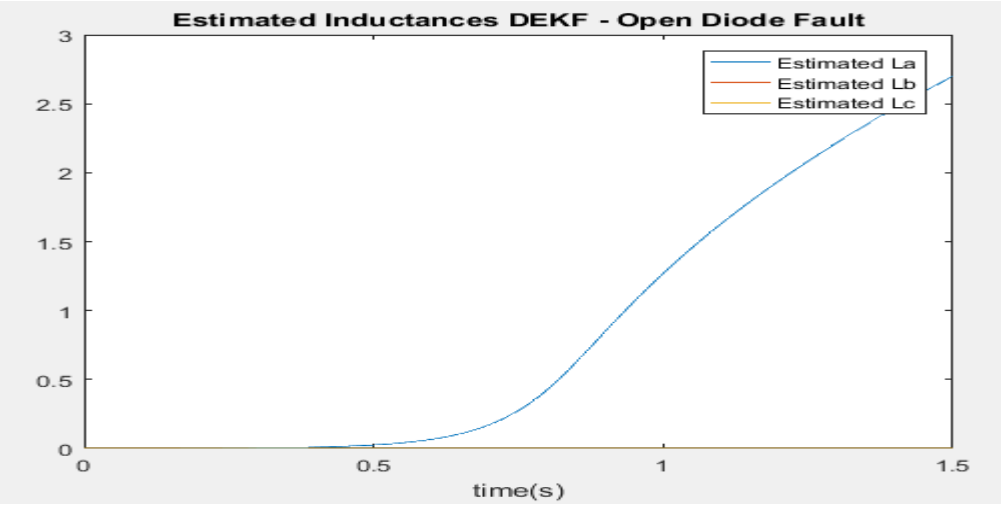

Figure 5-23 DEKF Estimated L – Phase A Open Diode Fault

The Phase A system parameters converge to a significantly larger number in the same manner as the EKSVSF model. Thus, The DEKF model is feasible for detecting and diagnosis open diode faults.

Next, a shorted diode fault is introduced to the system on Phase A. Figure 5-24 and Figure 5-25 depict the results of the system parameters.

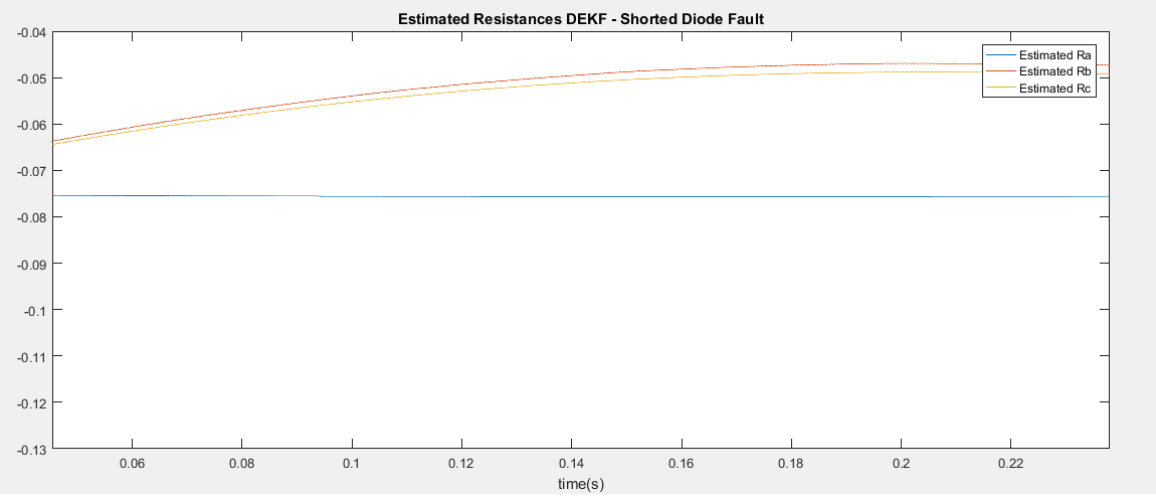

Figure 5-24 DEKF Estimated R – Phase A Shorted Diode Fault

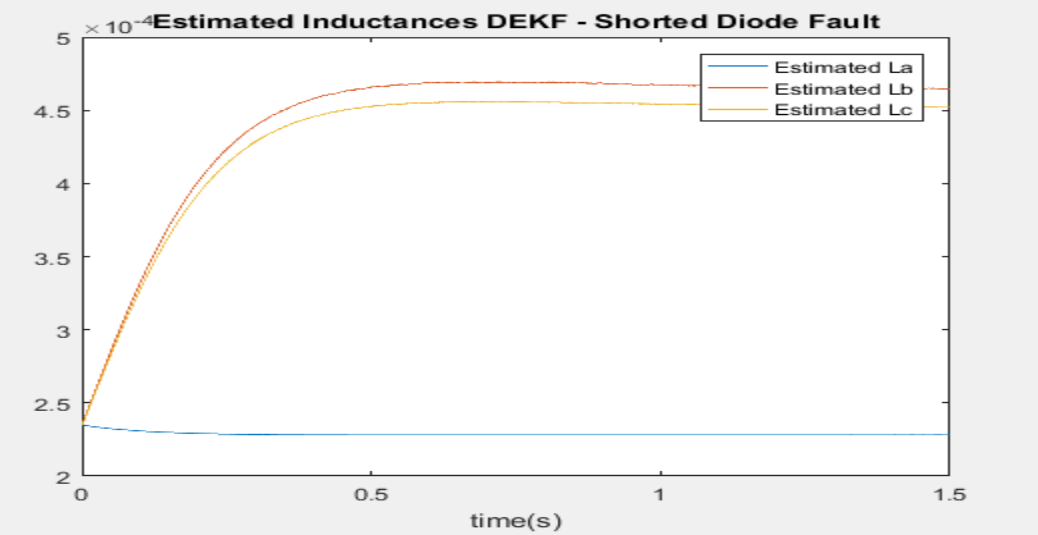

Figure 5-25 DEKF Estimated L – Phase A Shorted Diode Fault

The Phase B and C system parameters converge to a larger impedance similar to the EKSVSF model's response. Thus, The DEKF model is feasible for detecting and diagnosis shorted diode faults.

Lastly, the DEKF model is given a simulated 10% Phase A stator imbalance system to determine feasibility for fault detection and diagnosis. The results, shown in Figure 5-26 and Figure 5-27, demonstrate a significant enough difference to detect the stator imbalance simulated onto the system, similar to the EKSVSF model.

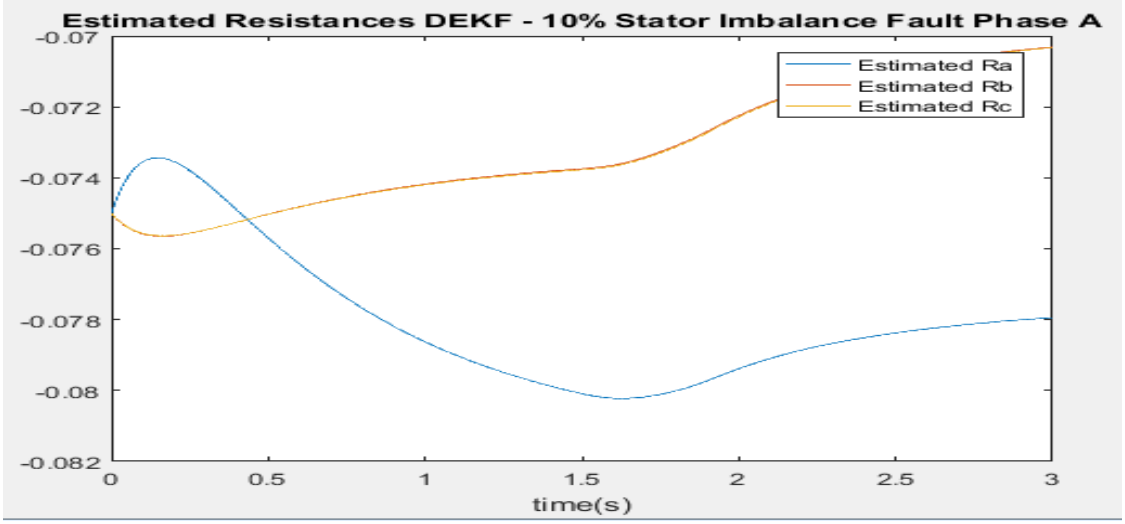

Figure 5-26 DEKF Estimate R R – 10% Stator Imbalance Phase A

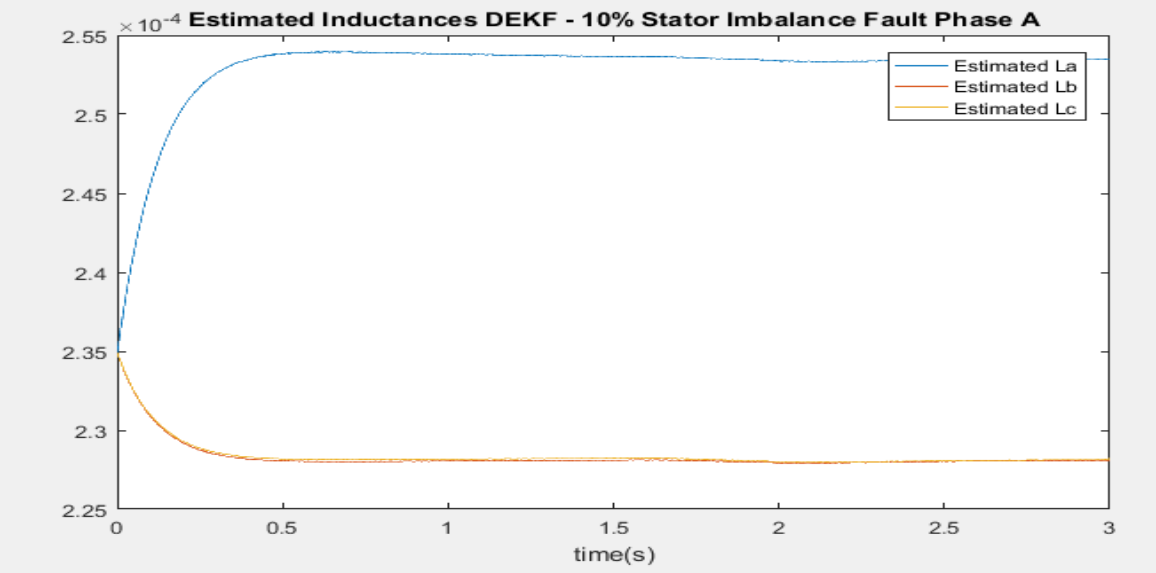

Figure 5-27 DEKF Estimated L – 10% Stator Imbalance Phase A

Notice, that for all faults the DEKF model's system parameters respond in the same fashion as the EKSVSF model. However, the EKSVSF model converges to the new value almost instantly, whereas the DEKF model takes up 1 or more

seconds to stabilize on the new system parameter values. EKSVSF is much faster than DEKF at detecting and diagnosing the fault. Once again, the SVSF component gives an advantage for condition monitoring. As soon as the VBL escapes from the boundary limit, SVSF is able to adjust to the new value the system state parameters are converging to. This quick detection is very useful for End of Line detection, as it reduces the amount of time per test and allows the assembly to increase productivity. Although the EKSVSF is not as accurate as the DEKF, it obtained significantly better accuracy than the alternator model without estimation. In addition, the low computation complexity/time and ability to detect and diagnose faults quickly make the EKSVSF the perfect candidate to implement on the D&V Electronics Alternator testers.

5.4 Proof of Concept Demonstration Application

An offline (after testing) demonstration application was developed to prove the feasibility of the proposed thesis in industry. The software was developed in VB.Net to provide a good graphical user interface. A C++ library was developed to optimize the modelling and estimation theory functionality. In addition, parallel processing was used to speed up computation time. The program covers the entirety of the thesis project without dependency on Matlab including the ability to run the genetic algorithm for parameter tuning, compute of the EK-SVSF alternator model, and perform the EK-SVSF Fault Detection and Diagnosis.

As shown in Figure 5-28, the software consists of a graph and a few buttons. The program loads Common Separated Value (CSV) data outputted from the D&V Electronics ALT-198 after an alternator has been tested. Once the data is loaded, the operator can run the Fault Detection and Diagnosis profile that exists in the software. When the profile is completed, the estimated inductance values, L, are plotted and the health of the alternator is displayed on the screen, as shown in Figure 5-28.

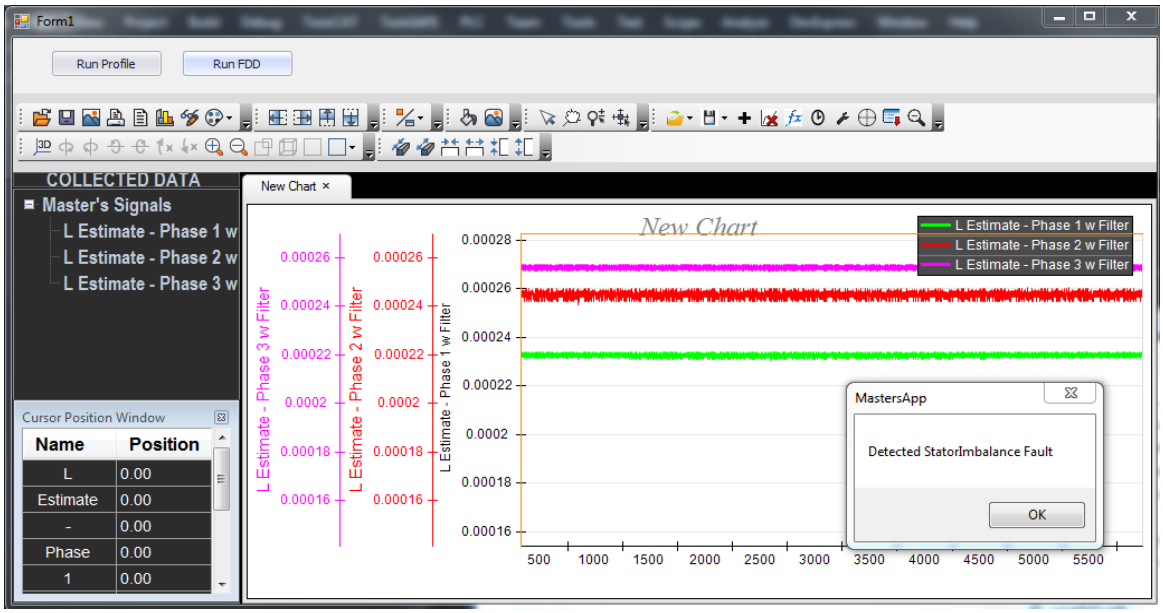

Figure 5-28 Proposed Demo Application Displaying Stator Imbalance Fault

One of the objectives of this thesis was to give a tester operator the ability to visually determine the health of the alternator without a FDD strategy. A trained operator would be able to determine the health of the alternator in Figure 5-28 by looking at the deviations in the estimated inductance values. By adding the FDD

strategy into the software, the trained operator can be more confident about the condition of the alternator during end of line testing.

Chapter 6 Concluding Remarks

6.1 Summary of Thesis

It is crucial for alternators to be properly manufactured before they way into vehicles to ensure quality and safety of the automotive electrical power generation system. The objective of this thesis is to create an efficient fault detection and diagnosis solution for alternators in end of line testing. In this research, a Model-Based Fault Detection and Diagnosis strategy for automotive alternators is developed to capture common defects in their manufacturing. The proposed method uses advanced estimation theory with measurements made available from the D&V ALT198 to successfully model electrical components as well as diagnose Open Diode Faults, Shorted Diode Faults, and Stator Imbalance Faults.

Alternator models are usually developed with the use of FEA software, however, that technology is too computationally expensive and requires extensive information of the alternator that an operator does not possess. The objective is to develop a solution that would generally model any Lundell alternator and report faults in a timely manner. To initialize the model with reduced operator interaction, a genetic algorithm is developed to automatically generate the parameters of the model. To meet these requirements, a simplified version of FEA governing equations is used to construct the proposed model. In addition, algorithms were developed to model the unmeasured electrical rotor angle and

three phase rectifier diode bridge. Introducing assumptions and artificial measurements into the system created modelling uncertainty that caused large modelling errors. To reduce this error, advanced estimation techniques were implemented. Due to the closed casing of the alternator and sensor limitations, the measurement matrix was not full rank for the model and the system was determined unobservable. A novel solution was developed to extract the three phase currents from the D&V Electronics alternator output current measurement. Using knowledge of the three phases' interaction with the rectifier bridge, the phase current signals were calculated with only 1.12% error. The newly generated artificial measurements resulted in full observability and, these were used to fix the modelling uncertainty with estimation theory.

Two estimation theories were considered in this thesis, the EK-SVSF method and the DEKF method. The EK-SVSF is a combination of two nonlinear filters that guarantees the accuracy of the EKF and the robustness of the SVSF. The EK-SVSF method reduced the RMS error of the model by 13% and the max error by 56.8%. The DEKF method uses two EKF to estimate both system state and system weights. Every time step, the two filters work together and use the previous system states, parameters and measurements to compute the next step's system states and parameters. The DEKF method reduced the RMS error of the model by 58.3% and the max error by 67.0%.

Fault Detection and Diagnosis is a key component to the novelty of this thesis project. Defects were discovered based on variations in the system parameters

caused by faulty output signals. In this thesis, faults were simulated on experimental data collected by the D&V Electronics alternator tester. In terms of fault detection and diagnosis, both methods proved successful in detecting and diagnosing the common alternator faults previously mentioned. The EK-SVSF needed extra artificial measurements in order to perform parameter estimation methods for FDD. This method involved rearranging the model equations to recalculate the system parameters based on changes in the alternator output signal. The DEKF method, did not need any additional calculations as the system parameters are already recalculated at every time step. It is important to note that the EK-SVSF model converged almost instantly to the new value caused by the fault whereas the DEKF method took up to 1 second. The EK-SVSF was found to be an excellent indicator of faults when the varying boundary layer would travel outside the defined boundary limit. Although the DEKF method is very accurate, it is unfeasible for this thesis because of its large numerical complexity, excessive computation time, and slow detection of faults. In conclusion, the proposed EK-SVSF model is accurate for tracking modelling uncertainties and uses advanced algorithms to quickly detect and diagnose common alternator faults.

6.2 Future Research

Further studies should involve the investigation of an approach to extract more information out of the alternator in order to produce a more accurate model with less assumptions. In addition, more sensors should be provided to limit the amount of artificial measurements needed to ensure complete observability. This

would reduce the need for using estimation theory for modelling and would give more comprehensive results in the artificial measurements of the parameters during Fault Detection and Diagnosis. Other researchers should use this proposed model to discover other alternator faults that could be detected by variations in the proposed system parameters. Moreover, a signal-based fault detection and diagnosis approach could be combined with this research to produce a more complete analysis of automotive alternators. Changes should be made to optimize the DEKF code and the two EKF should be replaced with two EKSVSF to shorten convergence time when detecting faults. Future work could include developing a strategy to monitor alternator health in moving vehicles to capture faults before they happen. Lastly, it would be very useful to implement the same strategy on Belt Starter Generators (BSGs) as car industries move towards this new technology.

Chapter 7 Appendices

7.1 D&V Electronics Ltd ALT-198

The D&V Electronics Ltd.'s ALT-198 is an end of line alternator tester, shown in Figure 7-1. The tester has up to about 5 seconds to determine the health of the alternator after a experiment finishes. The tester has a built in profile script editor for operators to program their own tests in Visual Basic. The ALT-198 has the ability to run user-defined tests at speeds up to 12,000 rpm and stores the measurements into a CSV file for easy access. The sampling frequencies of the measurements vary up to 200,000Hz. For the purpose of this thesis, custom tests were conducted between 2,000 rpm and 7000 rpm to collect essential measurements such as speed, alternator current, alternator voltage, stator voltages, field current, etc.

Figure 7-1 D&V Electronics ALT-198 [39]

7.2 Experimental Setup

The D&V Electronics Ltd.'s ALT-198, described in Section 7.1, was used to perform the experiments in this thesis. A 12V, 140A rated Lundell alternator is fastened into the machine and secured by the rotating belt. A clamp is attached to the alternator output pins, and a sensor is clipped onto one of the stator windings, shown in Figure 7.2.

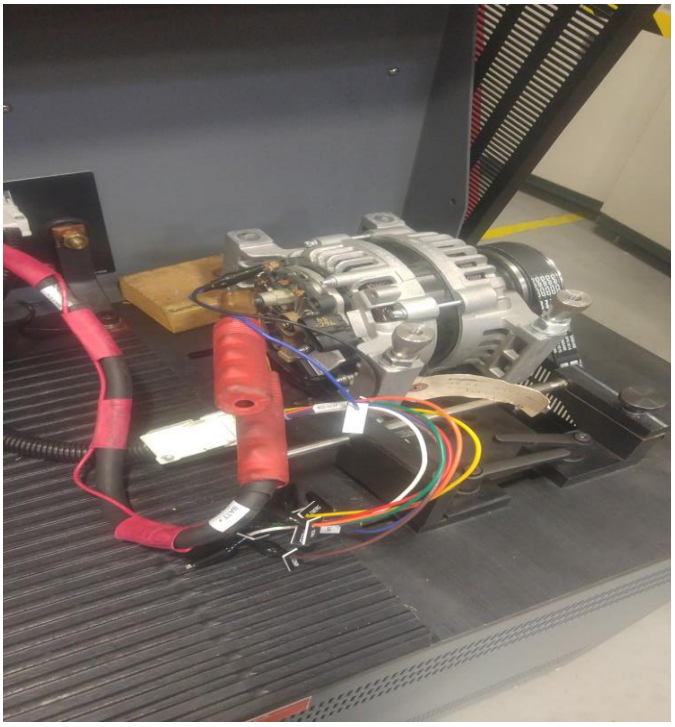

Figure 7-2 Experimental setup of running alternator test

Custom tests were developed to retrieve alternator data versus speed over a wide operating region (between 2000 RPM and 7000 RPM). Multiple alternator tests were conducted to have data for tuning the alternator model, validating the tuned alternator model, and for performing the fault detection and diagnosis. Tests for alternator modelling involved tests with varying speed, while the tests for fault detection and diagnosis were performed at a constant speed. Two alternators were used for the experiments. One was used for tuning, and the other was used for validation, as well as the fault detection and diagnosis. The alternators were run 10-15 times to prove repeatability of the parameter tuning. The genetic algorithm was also run 20-30 times with varying initial values and boundaries to prove it would always converge to approximately the same values.

References

[1] P. Petersen and F. Wilhelm, “Finite Element Analysis of Automotive Alternators Under Any Load,” vol. 24, no. 1, pp. 130–139, 2003.

[2] “Blog | Auto Works Automotive Service.” [Online]. Available: https://www.autoworksmn.com/blog/adam-e2-80-99s-service-tip-3a-charging-system-2falternator-woes. [Accessed: 08-Sep-2018].

[3] Y. B. Danilevicz, P. Drozdowski, W. Mazgaj, T. J. Sobczyk, and Z. Szular, “The influence of failures of a multiphase p.m. synchronous generator and a static voltage converter system on the generator electromagnetic torque,” *2005 IEEE Russ. Power Tech, PowerTech*, no. 1, 2005.

[4] Ibiblio, “Lessons In Electric Circuits -- Volume II,” 2018. [Online]. Available: https://www.ibiblio.org/kuphaldt/electricCircuits/AC/AC_13.html.

[5] AutoSystemPro, “AC Generators.” [Online]. Available: http://autosystempro.com/ac-generators/. [Accessed: 09-Sep-2018].

[6] Kiran Daware, “AC generator (alternator) - construction and working | electricaleasy.com.” [Online]. Available: https://www.electricaleasy.com/2014/02/AC-generator-alternator-construction-working.html. [Accessed: 09-Sep-2018].

[7] M. Das Comunicacoes, “AC (Alternating Current) Generators.” [Online]. Available: http://macao.communications.museum/eng/exhibition/secondfloor/MoreInfo/2_4_1_ACGenerator.html. [Accessed: 09-Sep-2018].

[8] B. Vaseghi, B. Nahid-Mobarakeh, N. Takorabet, and F. Meibody-Tabar, “Modeling of non-salient PM synchronous machines under stator winding inter-turn fault condition: Dynamic model - FEM model,” *VPPC 2007 - Proc. 2007 IEEE Veh. Power Propuls. Conf.*, pp. 635–640, 2007.

[9] “Permanent Magnets vs Electromagnets | Adams Magnetic Products.” [Online]. Available: https://www.adamsmagnetic.com/permanent-magnets-vs-electromagnets. [Accessed: 09-Sep-2018].

[10] A. Mesbahi, M. Khafallah, A. Saad, and A. Nouaiti, “Emulator design for a small wind turbine driving a self excited induction generator,” *Proc. 2017 Int. Conf. Electr. Inf. Technol. ICEIT 2017*, vol. 2018–January, no. 2, pp. 1–6, 2018.

[11] “Advantages and Applications of an Induction Generator - Circuit Globe.” [Online]. Available: https://circuitglobe.com/advantages-and-application-of-

an-induction-generator.html#ApplicationsofanInductionGenerator. [Accessed: 09-Sep-2018].

[12] “Synchronous generator vs. Induction generator | electricaleasy.com.” [Online]. Available: https://www.electricaleasy.com/2014/12/synchronous-vs-induction-generator.html. [Accessed: 09-Sep-2018].

[13] M. Iorgulescu, “Study of T hree- P hase B ridge R ectifier D iagnosis based on O utput V oltage and C urrent A nalysis,” 2013.

[14] L. King, “34 Fantastic 3 Phase Diode Bridge Rectifier Animation,” 2018. .

[15] Z. Kolondzovski and L. Petkovska, “Determination of a Synchronous Generator Characteristics via Finite Element Analysis,” *Serbian J. Electr. Eng.*, vol. 2, no. 2, pp. 157–162, 2005.

[16] C. Ramirez, M. T. Xuan, J. Simond, D. Schafer, and C. Stephan, “Synchronous machines parameters determination using finite elements method.”

[17] P. A. Hargreaves, “of Rotating Electrical Machines,” *Des. Rotating Electr. Mach.*, pp. 1–512, 2012.

[18] J. L. K. Jr., “Electric Machinery,” 2005.

[19] E. Mouni, S. Tnani, and G. Champenois, “Comparative study of three modelling methods of synchronous generator,” *IECON 2006 - 32nd Annu. Conf. IEEE Ind. Electron.*, no. 2, pp. 1551–1556, 2006.

[20] IEEE Standards, *IEEE Guide for Synchronous Generator Modeling Practices and Applications in Power System Stability Analyses*, vol. 2002, no. November. 2003.

[21] A. Scacchioli, G. Rizzoni, and P. Pisu, “Hierarchical Model-Based Fault Diagnosis for an Electrical Power Generation Storage Automotive System,” *Am. Control Conf. 2007. ACC’07*, pp. 2991–2996, 2007.

[22] A. Scacchioli, G. Rizzoni, M. A. Salman, W. Li, S. Onori, and X. Zhang, “Model-based Diagnosis of an Automotive Electric Power Generation and Storage System.,” *IEEE Trans. Syst. Man Cybern.*, vol. 44, no. 1, pp. 72–85, 2014.

[23] A. Hashemi and P. Pisu, “Fault diagnosis in automotive alternator system utilizing adaptive threshold method,” *Proc. Annu. Conf. Progn. Heal. Manag. Soc.*, vol. 29634, 2011.

[24] A. Hashemi, “Model-Based System Fault Diagnosis Utilizing Adaptive Threshold With Application To Automotive Electrical Systems,” 2011.

[25] W. Zhang, “a Fault Detection and Diagnosis Strategy for Permanent Magnet Brushless Dc Motor,” 2012.

[26] T. Lacey, “Tutorial: The Kalman Filter.”

[27] Stanford, “The Kalman Filter.” [Online]. Available: https://stanford.edu/class/ee363/lectures/kf.pdf. [Accessed: 27-Jun-2018].

[28] G. Bishop and G. Welch, “An Introduction to the Kalman Filter.”

[29] G. S.A., “Smooth variable structure filtering: theory and applications,” *Dr. Diss.*, 2011.

[30] M. Akhbari, M. B. Shamsollahi, C. Jutten, and B. Coppa, “ECG denoising using angular velocity as a state and an observation in an Extended Kalman Filter framework,” *Proc. Annu. Int. Conf. IEEE Eng. Med. Biol. Soc. EMBS*, pp. 2897–2900, 2012.

[31] S. Habibi, “The smooth variable structure filter,” *Proc. IEEE*, vol. 95, no. 5, pp. 1026–1059, 2007.

[32] R. Isermann, “Model-based fault detection and diagnosis – status and applications,” *Annu. Rev. Control*, vol. 29, no. 1, pp. 71–85, 2005.

[33] M. Nyberg, *Model Based Fault Diagnosis: Methods, Theory, and Applicationsfile:///C:/Users/ndaquila/Downloads/07793319.pdf*, no. 591. 1999.

[34] “Genetic Algorithm - MATLAB & Simulink.” [Online]. Available: https://www.mathworks.com/discovery/genetic-algorithm.html. [Accessed: 20-Jul-2018].

[35] V. Mallawaarachchi, “Introduction to Genetic Algorithms — Including Example Code.” [Online]. Available: https://towardsdatascience.com/introduction-to-genetic-algorithms-including-example-code-e396e98d8bf3. [Accessed: 20-Jul-2018].

[36] R. Ahmed, “Lecture 4 outline.” 2016.

[37] “Solving the Knapsack Problem with a Simple Genetic Algorithm | DataMiningApps.” [Online]. Available: http://www.dataminingapps.com/2017/03/solving-the-knapsack-problem-with-a-simple-genetic-algorithm/. [Accessed: 09-Sep-2018].

[38] J. McCall, “Genetic algorithms for modelling and optimisation,” *J. Comput. Appl. Math.*, vol. 184, no. 1, pp. 205–222, Dec. 2005.

[39] “ALT Series - Alternator Testers: New ALT-198.” [Online]. Available:

http://www.dvelectronics.com/products/alternator-testers/alt-198.html. [Accessed: 08-Sep-2018].

[40] G. D. Marques, “A simple and accurate system simulation of three-phase diode rectifiers,” *IECON ’98. Proc. 24th Annu. Conf. IEEE Ind. Electron. Soc. (Cat. No.98CH36200)*, vol. 1, pp. 416–421, 1998.

[41] “Synchronous Generators I,” 2011. [Online]. Available: http://www.egr.unlv.edu/~eebag/Synchronous Generator I.pdf. [Accessed: 16-Aug-2018].

[42] “SYNCHRONOUS GENERATORS:THE PHASOR DIAGRAM OF A SYNCHRONOUS GENERATOR | electric equipment.” [Online]. Available: http://machineryequipmentonline.com/electric-equipment/synchronous-generatorsthe-phasor-diagram-of-a-synchronous-generator/. [Accessed: 15-Sep-2018].

[43] J. Seung, D. Lee, and K. Chong, “Parameter Estimation Method for Coupled Tank System using Dual Extended Kalman Filter,” *13th Int. Conf. Control. Autom. Syst. (ICCAS 2013)*, no. Iccas, pp. 1223–1228, 2013.

[44] “A DUAL ESTIMATION APPROACH FOR REMOVING THE SHOW-THROUGH EFFECT IN THE SCANNED DOCUMENTS Sabita Langkam and Alok Kanti Deb Dept. of Electrical Engineering, IIT Kharagpur, West Bengal, INDIA,” pp. 1712–1716, 2017.

[45] M. Dahleh, M. A. Dahleh, and G. Verghese, “Lectures on Dynamic Systems and Control.”

[46] “Observability of GPS Measurements (in an Extended Kalman Filter) | CWRU Cutter Clues.” [Online]. Available: https://cwrucutter.wordpress.com/2012/11/12/observability-of-gps-measurements-in-an-extended-kalman-filter/. [Accessed: 30-Jul-2018].

[47] “Alternative Energy Tutorials is Clean and Green Energy.” [Online]. Available: http://www.alternative-energy-tutorials.com/. [Accessed: 03-Aug-2018].

[48] “Starters and Alternators: Common Misdiagnosis | KnowYourParts.” [Online]. Available: https://www.knowyourparts.com/technical-resources/starting-and-charging/starters-and-alternators-common-misdiagnosis/. [Accessed: 24-Jul-2018].